The Dissertation Committee for Miriam Barquero-Molina
certifies that this is the approved version of the following dissertation:

KINEMATICS OF BIDIRECTIONAL EXTENSION AND COEVAL NW-DIRECTED CONTRACTION IN ORTHOGNEISSES OF THE BIRANUP COMPLEX, ALBANY FRASER OROGEN, SOUTHWESTERN AUSTRALIA

Committee:

_____
Sharon Mosher, Supervisor

_____
William D. Carlson

_____
Mark P. Cloos

_____
James N. Connelly

_____
Catherine V. Spaggiari

_____
Ian M. Tyler

To my parents,

Francisco and Mary Luz,

for their unwavering support and encouragement

KINEMATICS OF BIDIRECTIONAL EXTENSION AND COEVAL NW-DIRECTED CONTRACTION IN ORTHOGNEISSES OF THE BIRANUP COMPLEX, ALBANY FRASER OROGEN, SOUTHWESTERN AUSTRALIA

by

Miriam Barquero-Molina, B.S.; M.S.

Dissertation

Presented to the Faculty of the Graduate School of

The University of Texas at Austin

in Partial Fulfillment

of the Requirements

for the Degree of

Doctor of Philosophy

The University of Texas at Austin

May 2009

Acknowledgements

Faculty, colleagues, friends and family members have helped to complete this dissertation. I would like to express my gratitude to these individuals for their support and assistance during these past five years.

Sharon Mosher has been a remarkably strong and supportive advisor during my time at The University of Texas at Austin. From the start she showed steadfast support, and then some, when I first suggested the idea of carrying out my dissertation work in a far-flung corner of southwestern Australia. She listened to my wishes and slightly "half-cooked" research ideas as an incoming graduate student into the program, helped me to transform them into a full-fledged dissertation proposal, and then happily threw herself to the task of advising and helping me through the following five years. I have always felt the freedom to explore new avenues in my research, because I never doubted that I could count on her unwavering encouragement and incredible professional experience to support me. She always demonstrated faith on my ability to rise to the occasion, and do the necessary work. She had complete confidence in me at times when I had little, and her steady conviction on my success carried me through many a rough patch. In reviewing all my writings and presentations she always offered constructive and effective comments, while always respecting my voice and ideas. Sharon has also helped me immeasurably in my professional development and socialization. She has always been a strong advocate for me; she has made a point to introduce me to other people within our discipline; she has taken the time to write numerous recommendation letters in many different occasions, ranging from grant proposals to academic job applications. She has always shown interest in my present as a graduate student, and my future as a Professor. With her incommensurable help I have been able to have a successful graduate school career.

Deepest thanks to Catherine Spaggiari and Ian Tyler, from the Geological Survey of Western Australia (GSWA). What first appeared to be an inconsequential meeting at a conference in Perth back in 2005, ended up being a pivotal moment that essentially

allowed me to carry out my doctoral dissertation work in Western Australia. When I first met Catherine and Ian I was beginning my third semester as a doctoral student, and all I had to offer were a few ideas and a lot of enthusiasm. Somehow they decided to give me a chance, listened to my research proposal, and after approval from the Directors at GSWA, they formally offered field support for the duration of my dissertation work in Western Australia. Without field support from GSWA I would have simply been unable to carry out my field research in Australia, as I lacked the necessary funds. GSWA provided me with a fully field-equipped four-wheel drive vehicle, plus all necessary field equipment, including HF radio, satellite phone, and fuel card for my two field seasons within their territory, which added up to a total of 11 months. Catherine and Ian were also instrumental in accomplishing the geochronological work in my field area, carried out by two GSWA scientists, Simon Bodorkos and Mike Wingate. Their complete support and willingness to help amazed me then, and still baffles me to this point. Catherine and Ian generously reviewed abstracts for presentations and journal manuscripts, and always encouraged me along the way. They helped finance my travel to the tri-annual meeting of the Geological Society of Australia in Perth in July of 2008, through GSWA support and a travel grant from Geoconferences (WA) Inc., so that I could present the results of my research to a local audience. Catherine and Ian always made a point of introducing me to their colleagues at GSWA and elsewhere in Australia, and fruitful professional relationships sprung from those encounters. They visited me in the field during each of my two field seasons in Australia. During those visits I had the opportunity of exchanging ideas with two experts on the geology of Western Australia while sipping on exquisite Australian wines. Catherine and Ian became my dissertation committee members, my Australian advisors, my collaborators, and my life-long friends.

While on the Australia subject, I wish to give special thanks to Bruce and Louise Bullock, owners and caretakers of Bremer Bay Caravan Park, in Bremer Bay, Western Australia. I spent nearly ten months camping in their park, and they welcomed me in like I was a part of their family. They went out of their way to make my stay as comfortable

as possible, and were always eager to hear about my daily adventures. To me they truly became my Australian family.

Thanks to the faculty of this Department for providing me with an exceptional graduate education. Special thanks to the members of my dissertation committee, Bill Carlson, Mark Cloos and Jim Connelly, for their encouragement and support throughout this past five years. I would specially like to thank them for their time and dedication during the final stretch of completion of this dissertation, and for all their constructive comments and revisions on my dissertation manuscript. They have always shown interest in my progress and eagerness to see me succeed, and have graciously answered my questions and offered guidance when prompted to do so.

Bill Carlson took the time and effort to write recommendation letters for me when applying for academic positions during the last year of my graduate work, and it is with his help that I have been able to find such a position for the future. He was fully supportive throughout the entire job-seeking process, genuinely excited about my success, and was eager to recommend me even though I had not yet completed all of my graduate work.

Grateful thanks also to Mark Helper, for his encouragement during the past five years, his help whenever I sought his advice about research presentations or job interviews, his letters of recommendation during my job-search and all his guidance as I make the transition from graduate student to Professor. I am deeply grateful that he gave me the chance to teach Field Camp in our geology program every year that I have been in this department. That way I discovered my true passion, teaching field geology and teaching geology in the field, and I had the chance to hone in my skills for the future, all while enjoying the scenery of the beautiful western United States, which he knows so well, and we both love so much.

Special thanks to all my past and present graduate student peers in the “Mosher group”. They have been a wonderful source of advice and encouragement at critical points during my graduate school career.

Sarah Collier showed me the meaning of patience, and coped with my occasional neuroses while we shared an office for two and a half years.

John Singleton made for an exceptional conversation partner in topics ranging from metamorphic core complexes to running marathons. John and I share the single-minded focus, doggedness and willingness to trudge of long distance runners.

Jamie Levine was finishing up her Masters work in the department during my first semester as a Ph.D. student, and because of her eternally jovial and pleasing disposition I naturally gravitated towards her when in need of advice or information about the workings of the department. After taking some time off following her graduation, she returned to UT now as a Ph.D. student herself, and rejoined our research group. We picked it up where we left off, and she instantly became one of my closest friends, and a fantastic collaborator to boot, whose scientific ability and know-how I deeply respect. She has helped me maintain my sanity through the last five years, and that is no easy task.

Special thanks also to the administrative and financial staff in the Department of Geological Sciences at the Jackson School of Geosciences. Nicole Evans and Lou Harwell, for cheerfully putting up with my frequent requests for help, particularly during the last stages of my degree. Alice Rentz, Angela Angelo, Dorothy Hight and Tinley Hald, for keeping my payroll straight and my RTA's in check, no easy task. Philip Guerrero, our Graduate Student Coordinator, for being extremely patient, forever obliging, ready to help, and always being happy to go out of his way to lend a hand. Managing the lives of over 150 graduate students is no easy task, but he does it with apparent ease and a jolly disposition, which I always found completely disarming. In five years I have not even seen a glimpse of the almighty "red tape". Philip just made it go away, every time.

I also gratefully acknowledge the institutional support that I have received while working on my dissertation. The Jackson School of Geosciences provided me with financial support as a Teaching Assistant and later Assistant Instructor for the entire ten semesters that I have been a graduate student in this department. The Jackson School of

Geosciences also provided me with financial aid towards my geological field work in Australia, and with extra monetary support to attend national and international professional meetings. The Geological Society of America also granted me financial support for my field research in Australia.

And last, but not least, I would like to thank my parents, Francisco and Mary Luz, and my sister, Susana. My sister, being the eldest, was the ground-breaking sibling, the first one in the family to go to college, the first to pursue further academic education and obtain a Ph.D., the first scientist (albeit a marine biologist, alas, alas), the first to emigrate in chase of opportunities that were denied to us back home. She paved the way.

My parents instilled my passion for the outdoors and the natural sciences and my desire to learn more and better myself. They did not blink an eye when I announced my wish to be a geologist while in junior year in high school. They gave me wings and allowed me to follow my dreams. They stoically watched their second, and last, child pack her few belongings and leave home nearly eight years ago, knowing full well that she would probably never be back to stay. And hard as it was, and still is, they would not have had it any other way.

To all, my deepest thanks.

KINEMATICS OF BIDIRECTIONAL EXTENSION AND COEVAL NW-DIRECTED CONTRACTION IN ORTHOGNEISSES OF THE BIRANUP COMPLEX, ALBANY FRASER OROGEN, SOUTHWESTERN AUSTRALIA

Miriam Barquero-Molina, Ph.D.
The University of Texas at Austin, 2009

Supervisor: Sharon Mosher

Granulite-facies orthogneisses of the Mesoproterozoic Albany-Fraser Orogen from the locality of Bremer Bay, in southwestern Australia, record at least three phases of widespread, pervasive NW- and NE-trending bidirectional extension that alternate with shortening and/or shear related structures. Crustal extension occurred ca. 1180 Ma, based on SHRIMP U–Pb zircon geochronology of melts generated during deformation, which coincided with Stage II (1215-1140 Ma) of the Albany-Fraser Orogeny, a period of NW-directed contraction.

Eight different deformation phases can be recognized in the Bremer Bay area: (1) formation of a pervasive migmatitic fabric, defined by alternating leucosomes and melanosomes, parallel to the main compositional layering, and axial planar to localized isoclinal folds of cm-wide melt bands; (2) first bidirectional extension phase, which formed cm-scale square boudins of mafic layers parallel to the main migmatitic fabric; (3) formation of open to isoclinal, upright to overturned, SW-plunging, NW-verging m-scale folds of early square and rectangular boudins and dominant migmatitic foliation; (4) renewed coeval NE- and NW-directed extension that produced intermediate (< 1 meter to a few meters) boudins of the migmatitic fabric and compositional layering; (5) formation

of regional-scale, NW-verging, SW-plunging overturned folds of all previous structures; (6) third phase of bidirectional extension that formed large, decameter-scale boudins of the migmatitic fabric; (7) late folding phase that resulted in the formation of m-scale open to tight, SW-plunging, upright to moderately overturned, NW-verging folds; and (8) fracturing related to the intrusion of dominantly N-NW- and N-NE-trending intermediate and felsic few cm- to few dm-wide pegmatite veins. Melt generation was concurrent with all stages of deformation.

The Albany-Fraser Orogen is reinterpreted as a diachronous orogen, resulting from the closure of the asymmetrically shaped ocean basin between the West Australian and Mawson cratons, which widens considerably from NE to SW along the length of the orogenic front. Subduction on the western side of the orogen was the driving force for NW-directed collision during Stage II of the orogeny.

Slab breakoff and orogenic collapse following closure of an intracratonic ocean basin could account for the multiple phases of bidirectional extension, granulite facies metamorphism and pervasive partial melting throughout deformation.

TABLE OF CONTENTS

Introduction 1

Chapter 1: Introduction to the Albany-Fraser Orogen: geochronological and structural constraints 4

1.1 Introduction 4

1.2 Tectonic Setting 4

1.3 Northern Foreland 6

1.3.1 Munglinup Gneiss 7

1.3.2 Mount Barren Group 9

1.3.3 Stirling Range Formation 10

1.3.4 Woodline Formation 11

1.4 Biranup Complex 11

1.4.1 Eastern Biranup Complex 12

1.4.1.1 Eastern Dalyup Gneiss 12

1.4.1.2 Coramup Gneiss 13

1.4.2 Western Biranup Complex 14

1.4.2.1 Dalyup Gneiss (Biranup Complex) West of Bremer Bay 14

1.4.2.2 Prior work in the Dalyup Gneiss (Biranup Complex) in Bremer Bay 16

1.5 Nornalup Complex 16

1.5.1 Eastern Nornalup Complex 17

1.5.2 Western Nornalup Complex 18

1.6 Fraser Complex 19

1.7 Summary 21

Figures 22

Chapter 2: Deformation in granulite-facies orthogneisses of the Albany-Fraser Orogen, Bremer Bay, SW Australia: implications for a diachronous Mesoproterozoic orogeny 25
2.1 Abstract 25
2.2 Introduction 26
2.3 Regional Geology 27
2.3.1 Northern Foreland 28
2.3.2 Biranup Complex 29
2.3.3 Nornalup Complex 29
2.3.4 Fraser Complex 30
2.4 Lithologies 31
2.5 Structure and Metamorphism 34
2.5.1 Structural Sequence 34
2.5.2 Interpretation of structures 38
2.6 SHRIMP U-PB zircon geochronology 38
2.6.1 Fisheries Bay 39
2.6.2 Point Henry 39
2.6.3 Short Beach 40
2.6.4 Interpretation of SHRIMP U-Pb zircon geochronology data 40
2.7 Evidence for Stage II contractional/transcurrent motion in the Albany-Fraser Orogen 41
2.7.1 Western Albany-Fraser Orogen 41
2.7.2 Eastern Albany-Fraser Orogen 43
2.7.3 Correlation between deformation in Bremer Bay and elsewhere in the Albany-Fraser Orogen 43
2.8 Discussion 44
2.8.1 Albany-Fraser Orogen as a diachronous collisional Orogen 44
2.9 Conclusions 47
Figures 49

Tables 66

Chapter 3. Bidirectional extension in granulite-facies orthogneisses of the Biranup Complex, Bremer Bay, Western Australia: implications for progressive lithospheric delamination during the Albany-Fraser Orogeny 68

3.1 Abstract 68

3.2 Introduction 69

3.3 Geologic Setting 70

3.4 Metamorphic Conditions 71

3.5 Bidirectional Extension 72

3.5.1 First bidirectional extension phase 72

3.5.2 Second bidirectional extension phase 74

3.5.3 Third bidirectional extension phase 78

3.6 Extension-concurrent Contraction 81

3.6.1 Foliation and early isoclinal folding phase 82

3.6.2 Second folding phase 82

3.6.3 Third folding phase 84

3.8.4 Late folding 85

3.8.5 Shearing 85

3.7 Partial melting during deformation 88

3.7.1 Partial melting during bidirectional extension and contraction 88

3.7.2 Late melts 90

3.8 Discussion 91

3.9 Conclusions 97

Figures 100

Chapter 4. Structural Mapping 126

4.1 Introduction 126

4.2 Lithologies 127
4.3 Structural Petrology 130
4.4 Geologic maps and cross sections of individual headlands 133
4.4.1 Native Dog Beach Headland 135
4.4.2 Blossoms Beach Headland 138
4.4.3 Little Boat Harbour Headland 139
4.4.4 Point Henry Headland 142
4.4.5 Banky Beach Headland 143
4.4.6 Banky Beach East Headland 144
4.4.7 Point Gordon Headland 146
4.4.8 Short Beach Headland 149
4.4.9 Short Beach North Headland 151
4.4.10 Fisheries Bay Headland 153
4.4.11 Back Beach Headland 156
4.4.12 John's Cove Headland 157
Figures 159

Appendix 1. Methods of structural mapping and petrographic work 187
References 193
Vita 205

INTRODUCTION

This dissertation presents the results from a detailed field study conducted on orthogneisses of the Biranup Complex, a lithotectonic unit within the Mesoproterozoic Albany-Fraser Orogen in the locality of Bremer Bay, in southwestern Australia. Field work in southwestern Australia was sponsored by the Geological Survey of Western Australia (GSWA), as part of a comprehensive field research campaign undertaken by GSWA to better understand the structural history, timing of deformation and tectonic relationships of the different lithotectonic units of the Albany-Fraser Orogen and southern-most margin of the Yilgarn Craton of western Australia.

Chapter 1 is a compilation of the most significant published work on the Albany-Fraser Orogen to this date. The aim of this chapter is to provide sufficient geological background information so that the work conducted at Bremer Bay can be placed into tectonic context. This dissertation focuses on the results from structural work done on orthogneisses of the Biranup Complex at Bremer Bay, on the western part of the orogen. However, during my time in southwestern Australia, I also initiated detailed structural work on several outcrops of the Munglinup Gneiss, in the eastern part of the orogen. Initial reconnaissance of rocks from the Munglinup Gneiss during a field trip to the Albany-Fraser Orogen in 2004 revealed structures such as NE-trending, meter-scale boudins, decimeter-scale folds of a migmatitic foliation, and decimeter-scale shear bands, which resembled structures observed in rocks of the Biranup Complex in the Bremer Bay area. Therefore my motivation to work in the Munglinup Gneiss was to evaluate whether it recorded any field structural evidence for bidirectional extension during overall shortening similar to deformation seen in the Bremer Bay area. My own work in the Munglinup Gneiss was interrupted by the effects of a cyclone. However, while working on rocks of the Munglinup Gneiss I had the opportunity to participate in structural reconnaissance and geochronological sampling of this unit with Catherine Spaggiari and Ian Tyler, geoscientists from GSWA. Preliminary results of my field research on the Munglinup Gneiss, together with results and interpretations resulting from work carried

out by GSWA geoscientists in the same unit are included in Spaggiari et al. (in press), of which I am a co-author.

Chapter 2 consists of a manuscript to be submitted for publication to the journal *Precambrian Research*. Chapter 2 gives an overview of the eight different deformation phases that can be recognized in the Bremer Bay area and superposed and crosscutting relationships that provide evidence for relative timing of formation. Deformation includes three phases of bidirectional extension that formed centimeter- to decameter-scale coeval NW- and NE-oriented boudins. Bidirectional extension phases in the Bremer Bay area alternate with up to four shortening and/or shear-related phases, which formed decimeter to kilometer scale NW-verging and SW-plunging folds, and decimeter-scale shear bands. Chapter 2 also presents the results of SHRIMP U–Pb zircon geochronology of melts generated during extension that constrains timing of extension to ca. 1180 Ma. The Albany-Fraser Orogen is currently interpreted to have formed during the collision between the West Australian Craton of southwestern Australia and the Mawson Craton of Eastern Antarctica. Chapter 2 presents a new tectonic model where the Albany-Fraser Orogen is newly interpreted as a diachronous orogen, owing to the closure of the asymmetrically shaped ocean basin between the West Australian and Mawson cratons, which widens considerably from NE to SW along the length of the orogenic front. Bidirectional extension and coeval shortening and/or shear related-structures in Bremer Bay are interpreted to have formed during overall NW-directed orogenic contraction during Stage II (1215-1140 Ma) of the Albany-Fraser Orogeny. NW-directed contraction during Stage II of the orogeny was driven by active subduction on the western-most end of the diachronous orogen.

Chapter 3 is a manuscript to be submitted to the journal *Lithosphere*. Chapter 3 provides a detailed description of structures related to bidirectional extension and concurrent shortening and shearing as well as partial melting and associated granulite-facies metamorphism observed in the Bremer Bay area. Chapter 3 also discusses the relationships between extensional, shortening and/or shear-related structures and partial melting related features seen in the field. Chapter 3 proposes that the two earliest phases

of bidirectional extension recorded in the orthogneisses in the Bremer Bay area were related to breakoff of a subducting slab on the western part of the belt during Stage II of the Albany Fraser Orogeny. Delamination of a subducting slab caused rise of asthenospheric material into higher crustal levels, inducing extensive partial melting and granulite-facies, high-temperature and medium-pressure metamorphic conditions at mid crustal levels represented by orthogneisses of the Biranup Complex in the Bremer Bay area. Upwelling of asthenospheric material produced a bidirectional extensional response in the overlying crust, with (a) extension parallel to the main convergence direction (NW-SE): and (b) coeval extension in the orthogonal direction (NE-SW) due to flow of the asthenosphere around the edges of the detaching slab. Slab breakoff was a catastrophic event, and the extensional response in the overlying crust dissipated over time. Continued active subduction in the western-most part of the orogen resulted in the re-establishment of overall NW-directed convergence, which formed large, kilometer-scale NW-verging folds that fold all previous structures. Regional-scale folds are later boudinaged during a third bidirectional extension phase that forms decameter-scale boudins, which could be associated with orogenic collapse following the complete closure of the intracratonic ocean basin between the West Australian and Mawson cratons.

Chapter 4 is a description of the large-scale structures as shown by the structural mapping and cross sections done in the Bremer Bay area and also includes: (a) a detailed description of the different lithology types described in the orthogneisses in the Bremer Bay area; (b) structural petrology of the orthogneisses, including description of the migmatitic foliation partial melt features, mineral lineation, deformation mechanisms, grain fabrics and other deformation structures observed in oriented petrographic thin sections from rock samples collected in the Bremer Bay area; and (c) detailed field description of the structure, lithology and deformation features of each of the headlands mapped in the Bremer Bay peninsula. Chapter 4 will eventually become part of a Geologic Record report of the work in the Bremer Bay area that will be published by GSWA.

Chapter 1: Introduction to the Albany-Fraser Orogen: geochronological and structural constraints.

1.1 Introduction

The Mesoproterozoic Albany-Fraser Orogen (Figure 1.1) is very little studied. Outcrops are generally limited to narrow coastal exposures, mostly remote and locally of very difficult access. During the past five years scientists of the Geological Survey of Western Australia (GSWA) have undertaken an extensive research campaign in the orogen, where they have conducted widespread geochronological dating and field structural studies. My own dissertation work in southwestern Australia was sponsored by GSWA as part of this effort.

What follows is a compilation of all that is currently known about the Albany-Fraser Orogen, including past work and the results from the first stages of work done by GSWA scientists, notably Catherine Spaggiari, Ian Tyler, Simon Bodorkos and Michael Wingate. It also includes results from my reconnaissance work in the Munglinup Gneiss (Figure 1.1) done in collaboration with GSWA scientists. At present, GSWA is continuing their efforts to unravel the complex geology of the orogen, with ongoing projects in the eastern and northeastern parts of the orogen.

1.2 Tectonic setting

The Albany-Fraser Orogen is a Grenville-aged belt located in southwestern Australia (Figures 1.1 and 1.2), widely believed to have resulted from the collision of the combined West Australian and North Australian cratons and the Mawson Craton, associated with Eastern Antarctica ca. 1.3 Ga (e.g. Myers et al., 1996). Only part of the Albany-Fraser Orogen is exposed in Western Australia, and it is interpreted to be part of the larger Australo-Antarctic Albany-Fraser Wilkes Orogen prior to the breakup of Gondwana (Figure 1.2; Fitzsimons, 2003). The Wilkes Land coast in East Antarctica was part of East Gondwana, and some outcrops of ortho- and paragneisses show similarities with outcrops of the Albany-Fraser Orogen (Fitzsimons, 2003, and references therein).

The Meso- to Neoproterozoic Darling Fault Zone and Pinjarra Orogen truncate the Albany-Fraser Orogen on its western end. To the northeast, the orogen is potentially contiguous with the Musgrave Complex (Figure 1.2; Myers et al. 1996).

U-Pb zircon, monazite and xenotime geochronology have revealed two dominant late Mesoproterozoic tectonothermal events in the Albany-Fraser Orogeny: Stage I, from 1345-1260 Ma, and Stage II, from 1215-1140 Ma (Clark et al., 2000). Bodorkos and Clark (2004a, b) propose the following tectonic model for the Albany-Fraser Orogeny based upon geologic evidence from the eastern part of the belt. Stage I records an entire orogenic cycle. Closure of a restricted ocean basin between the Yilgarn and the Mawson cratons resulted in NW-directed convergence and accretion of the Fraser Complex, a suspected island arc to the southern margin of the Yilgarn Craton. Subsequently, "breakoff" of the subducting slab and possible delamination of overthickened lithosphere resulted in asthenospheric upwelling, causing associated voluminous mafic and felsic plutonism. Further NW-oriented convergence resulted in crustal thickening that was followed by a period of extension that resulted in exhumation of units and sediment deposition. Bodorkos and Clark (2004a, b) proposed that Stage II resulted from renewed intracratonic NW-directed contraction. In the western part of the Albany-Fraser Orogen, structures are consistent with early NW-oriented shortening followed by dextral transcurrent motion, all related to dextral transpression (this dissertation work; Duebendorfer, 2002; Beeson et al., 1995), and geochronological data indicates that deformation occurred during Stage II of the orogeny (this dissertation work; Beeson et al., 1995; Black et al., 1992).

The crustal architecture of the Albany-Fraser Orogen is dominated by NW-vergent (towards the Yilgarn craton) thrust faults and folds at all scales, and to a lesser extent dextral shear zones (e.g. Myers, 1985; Beeson et al., 1988; Myers, 1990a; 1995b; Witt, 1998; Wetherley, 1998; Clark et al., 2000; Bodorkos and Clark, 2004b; Geological Survey of Western Australia, 2007; Spaggiari et al., in press). This crustal architecture has been interpreted as the result of an overall NW-directed shortening regime during Stages I and/or II of the Albany-Fraser Orogeny. Nevertheless extension plays a role

during deformation, as it is seen in rocks of the Biranup Complex in Bremer Bay (Figure 1.1; this dissertation work), which record at least three phases of widespread bidirectional extension that alternate with contractional and/or shear-related structures at mid- to lower crustal levels. Extensional deformation could be more widespread throughout the orogen than currently recognized (Spaggiari et al., in press).

The Albany-Fraser Orogen is subdivided into four main lithotectonic units, largely on the basis of differences in aeromagnetic signature, and more recently based on structural, metamorphic and geochronological work (e.g. Beeson et al., 1988; Myers, 1990; Whitaker, 1992; 1993; Fitzsimons, 2003): Northern Foreland, Biranup Complex, Nornalup Complex and Fraser Complex (Figure 1.1).

1.3 Northern Foreland

The Northern Foreland (Figure 1.1) comprises the part of the Yilgarn Craton that was thermally and tectonically reworked during the Albany-Fraser Orogeny, including the Munglinup Gneiss (Spaggiari et al., in press) and other undifferentiated units, as well as three Paleoproterozoic metasedimentary units, the Mount Barren Group, Stirling Range Formation and Woodline Formation, that were thrust northwards over the Archean gneisses (Myers, 1990; Dawson et al., 2002) (Figure 1.1). Beeson et al. (1998) defined the northern margin of the Northern Foreland by the presence of discontinuous, widely spaced shear zones.

Reworking of the Yilgarn Craton in the Northern Foreland reflects an increase in deformation style and metamorphic grade from north to south, recording greenschist to amphibolite facies, brittle to semi-brittle deformation in the north that progresses to amphibolite to granulite facies, ductile deformation in the south (Beeson et al., 1988; Myers, 1995a; Jones, 2006). The variation in conditions of deformation could reflect either a change in metamorphic grade with increasing distance from the orogenic front, or exhumation of shallower crustal levels of the Northern Foreland towards its northern end (Spaggiari et al., in press). In outcrops of the Pallinup River, north of Pallinup Beach, on the western part of the orogen (PB, Figure 1.1), Beeson et al. (1998) described an

increase of deformation intensity from north to south, with progressive overprinting of regional Archean NNW-trending structures by Mesoproterozoic, Albany-Fraser-related WSW-trending dextral shear zones and gneissic foliations.

A suite of younger dolerite dikes, the E-trending Gnowangerup Dike Swarm, dated at ca. 1210 Ma (Evans, 1999), and the NE-trending Fraser Dike Swarm, dated at ca. 1212 Ma (Wingate et al., 2000), cut through the Northern Foreland. These mafic dikes also show the effects of increased deformation intensity from north to south within the Northern Foreland (Beeson et al., 1988). The mafic dikes preserve magmatic textures and intrusive relationships in the north, whereas towards the south the dikes are metamorphosed and rotated into parallelism with the trend of the Albany-Fraser-related primary gneissic fabric (Beeson et al., 1988).

1.3.1 Munglinup Gneiss

The Munglinup Gneiss (Figure 1.1) was originally defined as a gneissic unit derived from Archean granite, granodiorite, tonalite and pegmatite, included in the Biranup Complex (Myers, 1995b). The Munglinup Gneiss was later interpreted as an allochtonous sliver of Archean and Proterozoic crust accreted to the southern margin of the Yilgarn Craton during the Albany-Fraser Orogeny (Myers et al., 1996). The Munglinup Gneiss has been most recently reinterpreted as a high grade, reworked part of the Yilgarn Craton bound by major faults (Spaggiari et al., in press). Presently it is defined as part of the Northern Foreland (Geological Survey of Western Australia, 2007).

The Munglinup Gneiss contains amphibolite to granulite facies orthogneisses with interspersed metamorphic mafic layers, and minor occurrences of banded chert (jaspilite), amphibolitic schist, serpentinite and metamorphic ultramafic rocks, which have been interpreted as remnants of Archean greenstones (Thom et al., 1997; Beeson et al., 1988; Myers, 1990a). The orthogneisses were derived from Late Archean monzogranitic, monzodioritic, granodioritic and tonalitic protoliths (Nelson et al., 1995; Geological Survey of Western Australia, 2008). Geochronological data indicate at least three phases

of granitic magmatism at ca. 2680, 2660 and 2630 Ma, and these ages are comparable to granite ages of the Yilgarn Craton (Cassidy et al., 2006, and references therein).

Spaggiari et al. (in press) recognized at least three phases of regional-scale folding and localized, outcrop-scale shearing and boudinage in the Munglinup Gneiss. Regional-scale folding is well defined in aeromagnetic imagery, as metamorphic fabrics in the gneisses contain magnetite. Outcrop-scale folds include: (1) early centimeter to decimeter scale hook folds of the gneissic fabric in pavement outcrops(F_1), which in one outcrop on the eastern part of the orogen appear to predate the intrusion of a 2658 ± 21 Ma monzogranite, and are thus interpreted to be Late Archean; (2) N-trending open to tight folds of the gneissic fabric (F_2), which also fold F_1 folds, and (3) E- to NE-trending tight folds of the gneissic fabric, which also fold F_1 and F_2 folds. F_2 and F_3 folds are interpreted as the outcrop-scale counterparts of regional-scale folds observable in aeromagnetic data. Outcrop-scale E-trending dextral and NW-trending sinistral shears postdate the folds and locally contain leucosomes in the shear planes. The Munglinup Gneiss is also locally boudinaged by meter-scale boudins of the migmatitic fabric that trend dominantly NE-SW. Although the relationship between outcrop-scale folds and boudins of the gneissic fabric is unclear, the boudins do not appear to be folded and thus are interpreted to postdate folding.

U-Pb SHRIMP zircon dating of two samples of the Munglinup Gneiss from Powell Point on the eastern part of the Albany-Fraser Orogen (PP, Figure 1.1) gives values of 1195 ± 17 Ma and ca. 1150 Ma for the age of granulite facies metamorphism (Bodorkos and Wingate, 2008a, b), which coincides with Stage II of Clark et al. (2000) for the Albany-Fraser Orogeny. Spaggiari et al. (in press) tentatively suggest that shearing and possibly F_3 folding, with shear zones and axial traces oriented parallel to the regional trend of the orogen, could have formed during Stage II of the orogeny. They also suggest boudinage postdates folding and could have taken place during Stage II. According to Spaggiari et al. (in press), the F_2 folding event is problematic and could be either Late Archean or Mesoproterozoic Stage I or Stage II.

1.3.2 Mount Barren Group

The Mount Barren Group, located NE of Bremer Bay (MBG, Figure 1.1), consists of lower greenschist to upper amphibolite facies Proterozoic metasedimentary rocks that were thrust onto the southern margin of the Yilgarn Craton. This unit has been interpreted as a shallow marine, deltaic sequence (Witt, 1998; Dawson et al., 2002, Vallini et al., 2002; 2005) composed of three main units: (1) Steere Formation, a polymictic thin basal conglomerate interpreted as fluvial or fluvial-deltaic sediments (Thom et al., 1977; Thom et al., 1984; Witt, 1997); (2) Kundip Quartzite, a thickly bedded, pure quartzite, interbedded with mica- and magnetite-bearing quartzites and mudstones and minor lenses of metaconglomerate, interpreted as delta-plain or upper delta-front facies (Thom et al., 1984; Witt, 1997; Vallini et al., 2005); and (3) Kybulup Schist, thinly bedded pelites and psammites (Thom et al., 1984; Witt, 1997), interpreted as a lower delta front. The Mount Barren Group may be part of a much broader group of sedimentary rocks deposited on or near the southern and southeastern margin of the Yilgarn Craton during the Paleoproterozoic, with variable sediment provenance (Hall et al., 2008).

Most studies of the Mount Barren Group have considered it as a NW-verging fold and thrust belt (e.g., Sofoulis, 1958; Thom et al., 1984; Myers, 1990a; Witt, 1998). The amount of overall displacement on the bounding faults is unknown, and there is no agreement on whether the Mount Barren Group is completely allochtonous (e.g. Witt, 1998; Dawson et al., 2002).

Wetherley (1998) described five different contractional deformation phases (D_1 through D_5); D_2 and D_4 effects are widespread throughout the unit, whereas the remaining three are localized. S_2 and S_4 are the primary cleavages observed in the unit and are axial planar to F_2 and F_4 folds, respectively. F_2 folds are tight to isoclinal and plunge steeply to the southwest with steeply southwest-dipping axial surfaces. F_4 folds are closed to tight and plunge moderately to the southwest or to the northeast with axial surfaces that dip moderately to the northwest or southeast. Wetherley (1998) interpreted the folds and associated cleavages as a result of initial N-S contraction and later NW-SE contraction, respectively.

Metamorphic grade changes from low grade, greenschist-facies, chlorite- and sericite- bearing assemblages in the north and west, to high grade, amphibolite-facies, kyanite- and staurolite-bearing assemblages in the south. P-T pseudosections and geothermobarometry indicate that peak assemblages formed just above 600ºC and near 8 kbar (Witt, 1998; Wetherley, 1998). Peak assemblages were produced pre- to syn- D_2 deformation.

SHRIMP U-Pb detrital zircon geochronology gives a maximum depositional age of ca. 1700 Ma for the Mount Barren Group (Nelson 1996a, b). Detrital zircon geochronology suggests a varied provenance, with age clusters from ca. 2.6 to 1.7 Ga (Nelson, 1996a, b; Dawson et al., 2002; Hall et al., 2008). Metamorphic U-Pb ages for xenotime and monazite from kyanite-bearing schists of the Mount Barren Group are 1206±8 Ma and 1194±8 Ma respectively, which Dawson et al. (2003) have interpreted as dating the peak syn-D_2 metamorphic event in the area. Because this age overlaps with the 1210 Ma age of the Gnowangerup and Fraser Dike Swarms (Evans, 1999), Dawson et al. (2003) interpreted metamorphism in the Mount Barren Group, and by extrapolation in the entire Albany-Fraser Orogen, as related to the emplacement of the mafic dike swarms during extension. This interpretation is in contrast to Clark et al. (2002) who postulated the metamorphism was related to early Stage II contractional deformation, which has an overlapping age of 1190-1160 Ma. Nevertheless Dawson et al.'s (2003) interpretation is not consistent with the dominant ages of high-grade metamorphism within the adjacent Biranup Complex, which indicate that granulite facies metamorphism took place at ca. 1180 Ma and post-dated the ca. 1210 Ma mafic dike emplacement (see Fraser Complex section below). The older ages reported by Dawson et al. (2003) could relate to an earlier, less regionally extensive metamorphic event (Spaggiari et al., in press).

1.3.3 Stirling Range Formation

The Stirling Range Formation, located approximately 100 km west of the Mount Barren Group (SRF, Figure 1.1), is a sub-greenschist to lower greenschist-facies metasedimentary unit consisting of quartzite, shale, slate and phyllite (Muhling and

Brakel, 1985). It was interpreted as a shallow marine, tide-dominated sedimentary sequence (Cruse, 1991; Cruse and Harris, 1994). Rasmussen et al. (2004) gave a minimum depositional age of 1800 ± 14 Ma, slightly older than that of the Mount Barren Group, based on an authigenic xenotime of probable diagenetic origin.

1.3.4 Woodline Formation

The Woodline Formation, located approximately 350 km NE of the Mount Barren Group (WF, Figure 1.1), sits unconformably on the Yilgarn Craton and consists of a lower greenschist-facies mature sandstone interbedded with siltstone (Hall et al., 2008). Detrital zircon spectra suggest that the metasedimentary rocks of the Woodline Formation could have been sourced from a Proterozoic Basin in the NE margin of the Yilgarn Craton. The Woodline Formation has a maximum depositional age of ca. 1740 Ma, similar to that of the Mount Barren Group (Hall et al., 2008).

1.4 Biranup Complex

The Biranup Complex was thrust over the southern margin of the Northern Foreland (Myers, 1990) and consists of a suite of ca. 1690-1660 Ma amphibolite- to granulite-facies orthogneisses including the Coramup Gneiss on the eastern part of the belt (near Esperance, Figure 1.1) and the Dalyup Gneiss on the eastern and western parts of the orogen (Spaggiari et al., 2008). Rocks of the Biranup Complex in the western part of the orogen have only recently been identified as part of the Dalyup Gneiss (Spaggiari et al., 2008; Spaggiari et al., in press), partially as a result of the extensive field study conducted during this dissertation. Previously these rocks were mapped as undifferentiated Biranup Complex. Part of the Dalyup Gneiss is complexly interleaved with rocks of the Munglinup Gneiss on the eastern part of the orogen, approximately 100 km NE of Esperance (Figure 1.1). Because of the structural complexity and similarity of rock types in this region, it is difficult to distinguish between Dalyup Gneiss and Munglinup Gneiss rocks. Thus they are shown as undivided in the bedrock geology map of southwestern Australia in Figure 1.1 (Geological Survey of Western Australia, 2007).

1.4.1 Eastern Biranup Complex

The eastern Biranup Complex includes the Coramup Gneiss and rocks of the eastern part of the Dalyup Gneiss (Spaggiari et al., 2008; Spaggiari et al, in press) (Figure 1.1).

1.4.1.1 Eastern Dalyup Gneiss

The Dalyup Gneiss on the eastern part of the Albany-Fraser Orogen (Figure 1.1) is composed of heterogeneous granitic rocks and less abundant mafic rocks, metamorphosed to granulite-facies with little preservation of original igneous textures. Lithologies include granodioritic, monzogranitic, syenogranitic and orthopyroxene-bearing granitic gneisses, as well as quartz-magnetite and mafic gneisses and amphibolite (Beeson et al., 1998, Nelson et al., 1995; Geological Survey of Western Australia, 2007).

The Dalyup Gneiss on the eastern part of the orogen, with crystallization ages of ca. 1680 Ma (Spaggiari et al., in press), was intruded by a 1300-1280 Ma granite during Stage I tectonism, which the interpreted age of pervasive deformation in this unit (Nelson et al., 1995).

1.4.1.2 Coramup Gneiss

The Coramup Gneiss is a fault-bounded package situated between the Dalyup Gneiss and the Nornalup Complex, located on the eastern part of the Albany-Fraser Orogen (Figure 1.1). The Coramup Gneiss is poorly exposed, and most of the previous work has been done on coastal exposures west of Esperance on the eastern part of the orogen (Figure 1.1). It contains both ortho- and paragneisses, with lithologies including granitic, granodioritic and tonalitic gneisses, pyroxene-bearing tonalitic gneisses, interleaved mafic rocks, quart-rich psammites, some migmatitic metapelite and rare lenses of calc-silicate rocks (Bodorkos and Clark, 2004a, b). Previous SHRIMP U-Pb zircon geochronology of the Coramup Gneiss gave an igneous precursor crystallization age of 1700-1600 Ma for a garnet-bearing tonalitic gneiss near Esperance (Figure 1.1;

Bodorkos and Clark, 2004b), consistent with previously reported ages for the Dalyup Gneiss (Nelson et al., 1995).

Deformation during Stage II of the Albany-Fraser Orogeny in the Coramup Gneiss (part of the Biranup Complex) near Esperance (Figure 1.1) was characterized by high-T and lower-P (750-800 °C and 5-6 kbar) metamorphic conditions (Bodorkos and Clark, 2004a). Metamorphism was synchronous with the formation of (1) subvertical, SE-dipping shear zones; (2) shallow SW-plunging mineral stretching lineation; (3) NW-verging, decimeter- to meter-scale tight asymmetric folds to which the main foliation is axial planar; and (4) syn-kinematic pegmatite dike emplacement ca. 1170 Ma (Bodorkos and Clark, 2004b). Kinematic indicators such as shear fabrics, winged porphyroblasts and shear bands in the Coramup Gneiss suggest overall dextral transpression, with a component of pure shear flattening parallel to the main foliation, and dextral simple shear (Bodorkos and Clark, 2004b). As coeval kinematic indicators elsewhere in the orogen indicate that Stage II tectonism was the result of NW-SE oriented convergence, dextral transpression in the Coramup Gneiss is interpreted as the result of oblique contraction resulting from the arcuate geometry of the deformation front (Bodorkos and Clark, 2004b). A series of NNE-striking, subvertical to steeply SE-dipping ductile mylonite zones developed in the Coramup Gneiss ca. 1140 Ma (Bodorkos ad Clark, 2004b). The orientation of these mylonite zones is consistent with overall NNW-oriented contraction, but their origin is unclear. The mylonite zones could represent the last stages of Stage II deformation in the Biranup Complex on the eastern part of the Albany-Fraser Orogen.

New SHRIMP U-Pb zircon geochronology has yielded an igneous crystallization age of 1688 ± 12 Ma for the igneous protolith to an upper amphibolite- to granulite-facies garnet-bearing monzogranitic gneiss from a coastal exposure near Esperance (Figure 1.1; Bodorkos and Wingate, 2008c). This age coincides with igneous protolith ages elsewhere in the Biranup Complex (Spaggiari et al., in press; this dissertation work). Metamorphic zircon rims from the same locality yielded an age of 1224 ± 9 Ma, interpreted as the age for the high-grade metamorphic event that resulted in zircon rim growth (Bodorkos and Wingate, 2008c). An upper amphibolite- to granulite-facies quartzite interlayered with

the garnet-bearing monzogranite described above gave a minimum depositional age of 1757 ± 39 Ma, and a high-grade metamorphic age of 1225 ± 7 Ma (Bodorkos and Clark, 2008d). These ages indicate that both rocks were metamorphosed during the same tectonothermal event, which corresponds to Stage II (Clark et al., 2000) of the Albany-Fraser Orogeny (Spaggiari et al., in press).

Rocks of the Coramup Gneiss consist of ca. 1690 ortho- and paragneisses with comparable ages to other rocks of the Biranup Complex in the western part of the Albany-Fraser Orogen (this dissertation study; Spaggiari et al., in press). Spaggiari et al. (in press) suggest that rocks of the Coramup Gneiss were metamorphosed to granulite-facies conditions and intruded by granites during Stage I of the Albany-Fraser Orogeny, with further high-temperature metamorphism with associated partial melting taking place early during Stage II of the orogeny, ca. 1180 Ma.

1.4.2 Western Biranup Complex

The Western Biranup Complex comprises rocks of the western part of the Dalyup Gneiss (Spaggiari et al., 2008; Spaggiari et al., in press) (Figure 1.1). Rocks of the Dalyup Gneiss in the western Biranup Complex comprise high-grade (up to granulite facies) heterogeneous orthogneisses with interlayered, less abundant mafic rocks. Exposures are intensely deformed, with little preservation of original igneous textures (Beeson et al., 1988; Nelson et al., 1995; Geological Survey of Western Australia, 2007; this dissertation study). Note that previous studies discussed below refer to these rocks as the Biranup Complex, rather than the Dalyup Gneiss.

1.4.2.1 Dalyup Gneiss (Biranup Complex) West of Bremer Bay

For orthogneisses of the Dalyup Gneiss further west of the Bremer Bay area (Groper Bluff, Black Head and Pallinup Beach; GB, BH and PB on Figure 1.1), Beeson et al. (1988) interpreted field structures as evidence for three different, albeit potentially continuous, deformation phases whose absolute timing is unclear. During the first phase they propose early transcurrent shearing that resulted in thrusting of the Biranup Complex

(Dalyup Gneiss) over the Northern Foreland and formation of minor (up to 30 cm long) conjugate dextral (WSW-striking) and sinistral (WNW-striking) cm-wide shear zones. Deformation took place during prograde metamorphism that reached granulite-facies conditions.

The second phase of deformation described by Beeson et al. (1988) consisted of continued NNW-oriented contraction resulting in the uplift of the Biranup Complex (Dalyup Gneiss) along its main bounding thrusts. Antithetic thrusts interpreted on aeromagnetic data formed as subsidiary faults to the main thrust boundary between the Northern Foreland and the Biranup Complex. Thrusting was coeval with minor dextral transcurrent shearing and folding, which resulted in the formation of meter to kilometer-scale, overturned, NW-verging and SW-plunging folds with a well-developed axial planar foliation. Boudins are visible locally on the limbs of meter-scale folds, which Beeson et al. (1988) interpret as a result of extension on the fold limbs during folding. Conjugate dextral (WNW-ESE striking) and sinistral (N-S striking) shears also formed, commonly overprinting earlier shear bands, the dominant foliation, boudins and meter-scale folds. This second phase of deformation was associated with retrograde, amphibolite-facies metamorphism along the northern boundary of the Biranup Complex (Dalyup Gneiss). Beeson et al. (1988) also describe a third deformation phase in which NW-oriented contraction reactivated the thrust boundary between the Biranup Complex (Dalyup Gneiss) and the Northern Foreland and its associated antithetic lineaments within the Dalyup Gneiss. A shallowly (20-35°) E-plunging mineral lineation that developed along the northern boundary of the Biranup Complex (Dalyup Gneiss) was interpreted as the result of dextral-transcurrent movement with a thrust component along this boundary. Deformation took place under amphibolite-facies metamorphic conditions.

Black et al. (1992) conducted SHRIMP U-Pb zircon geochronology on a granulite-facies pegmatite from the locality of Groper Bluff (GB, Figure 1.1), west of Bremer Bay, which they interpreted as intruding the host granulite-facies felsic gneiss at an early stage during its structural history. They reported igneous crystallization ages of 1196 ± 8 Ma and 1165 ± 28 Ma for this granulite-facies pegmatite. Spaggiari et al. (in

press) considered 1165 ± 28 Ma as a more conservative estimate for the crystallization age of the pegmatite. This age indicates deformation of these Dalyup Gneiss (Biranup Complex) rocks during Stage II of the Albany-Fraser Orogeny.

1.4.2.2 Prior work in the Dalyup Gneiss (Biranup Complex) in Bremer Bay

At Fisheries Bay Headland in the Bremer Bay area (Figure 1.1), Pisarevsky and Harris (2001) and Harris et al. (2002) attribute meter- to decameter- scale boudins and associated listric shear bands to NW-SE extension related to orogenic collapse, lithospheric delamination or rebound of a thickened crustal root (also see Harris, 2003). The same authors claim that renewed NW-SE directed convergence took place after extension in this area and was manifested by what they interpreted as a steeply dipping NE-striking foliation in pegmatites and mafic dikes that intruded along normal shear zones and by the formation of upright to inclined folds within the gneisses that display axial planar cleavage subparallel to that within the pegmatites and mafic dikes.

Prior to this dissertation study, the only timing constraints for deformation in the Bremer Bay area were a Rb-Sr age of 1140 ± 40 Ma for a granulite-facies pegmatite in a normal-sense shear zone (Black et al., 1992) and a paleomagnetic pole, obtained from country rock (granulite facies tonalitic gneiss and mafic granulite) and intruding metadolerite dikes, that fits the ca. 1.2 Ga part of the Precambrian Australian apparent polar wander path (Pisarevsky and Harris, 2001).

1.5 Nornalup Complex

The Nornalup Complex is the southernmost of the lithotectonic units differentiated within the Albany-Fraser Orogen (Figure 1.1). The complex was apparently thrust onto the southern margin of the Biranup Complex (Myers, 1990) and consists of a number of ortho- and paragneisses on the eastern and western part of the belt.

1.5.1 Eastern Nornalup Complex

The Nornalup Complex on the eastern part of the Albany-Fraser Orogen (Figure 1.1) includes the Malcolm Gneiss, the Recherche Granite (more prevalent in the Nornalup Complex, although it also intrudes into the Biranup Complex), the Esperance Granite, the metasedimentary rocks of the Mount Ragged Formation, and the Salisbury Gneiss (Myers, 1995b; Clark, 1999). The oldest unit exposed is the Malcolm Gneiss, dominated by siliciclastic metasedimentary rocks and orthogneiss with interlayered mafic amphibolitic schist, paragneiss and minor calc-silicate rocks (Nelson et al., 1995; Clark, 1999). Low-pressure, high-temperature metamorphism (4-5 kbar, 750-800ºC) of the Malcolm Gneiss is coeval with the intrusion of early stage ca. 1330 Ma monzogranites and granodiorites belonging to the ca. 1330-1280 Ma Recherche Granite during Stage I of the Albany-Fraser Orogeny (Clark, 1999). Stage I tectonism continued with the formation of NW-verging folds that are cut by ca. 1313 intrusive bodies (Clark et al., 2000) and culminated with NW-directed thrusting of the Nornalup Complex over the Coramup and Dalyup gneisses prior to the intrusion of late-stage (ca. 1300-1280) Recherche Granite plutons (Clark et al., 1999; 2000; Bodorkos and Clark, 2004b). Intrusion of the late-stage plutons was followed by the deposition of the Mount Ragged Formation (MRF, Figure 1.1), which comprises upper greenschist- to lower amphibolite-facies metasedimentary rocks (Clark, 1999). Clark et al. (2000) interpreted detrital zircon ages from the Mount Ragged Formation of ca. 1320 Ma to suggest the unconformably underlying Recherche Granite as a source for the sediment. Clark et al. (2000) obtained an age of 1154 ± 15 Ma for the growth of rutile in the Mount Ragged Formation, which they interpreted as an indication of burial and metamorphism of the metasedimentary rocks during Stage II of the Albany-Fraser Orogeny. In view of this geochronological data, Clark et al. (2000) suggested that the eastern Nornalup Complex was uplifted and eroded between Stages I and II of the Albany-Fraser Orogeny.

The Salisbury Gneiss that occurs in the eastern Nornalup Complex is exposed on several islands offshore to the southeast of Esperance (Figure 1.1; Myers, 1995b; Clark et al., 2000). The gneiss includes varied lithologies, including ortho- and paragneisses and

metamorphic mafic rocks, and records medium-pressure granulite-facies metamorphic conditions (800ºC and >5 kbar; Clark, 1999; Clark et al; 2000). SHRIMP U-Pb zircon geochronology gave a crystallization age for the Salisbury Gneiss of 1214 ± 8 Ma, and a high-grade metamorphic age of 1182 ± 13 Ma, which coincides with Stage II of the Albany-Fraser Orogeny (Clark et al., 2000). The depositional age of the Salisbury Gneiss is unknown, but Clark (1999) interpreted the lack of isotopic evidence for Stage I deformation as suggesting that deposition of the protholith for the Salisbury Gneiss postdated Stage I of the orogeny, and thus the unit would be genetically distinct from the Malcolm Gneiss.

Stage II tectonism in the eastern Nornalup Complex produced syntectonic pegmatites within spaced, NE-trending ductile shear zones with dip-slip kinematics in the Malcolm Gneiss and Recherche Granite (Clark et al., 2000). One of those pegmatites intruded in the Malcolm Gneiss yielded a SHRIMP U-Pb monazite crystallization age of 1165 ± 5 Ma. The end of Stage II tectonism in the eastern Nornalup Complex was marked by the intrusion of the ca. 1140 Ma porphyritic Esperance Granite (Myers, 1995b; Nelson et al., 1995), which is probably coeval with late felsic dykes that intrude the Mount Ragged Formation (Myers, 1995b; Clark, 1999).

1.5.2 Western Nornalup Complex

The Nornalup Complex on the western part of the Albany-Fraser Orogen (Figure 1.1) consists of garnet-sillimanite-bearing migmatitic paragneisses, quartzites and intrusive rocks (Clark, 1995; Love, 1999). SHRIMP U-Pb geochronology on migmatitic paragneisses from two localities near Albany (Figure 1.1) gave a maximum depositional age of ca. 1360 Ma for the sedimentary precursor to the paragneisses (Love, 1999). Limited evidence for Stage I magmatism exists for intrusive rocks in outcrops near the town of Albany with crystallization ages of ca. 1289, 1296, and 1302 Ma (Pidgeon, 1990; Love, 1999). The same rocks gave high-grade metamorphic ages of 1314 ± 5 Ma and 1304 ± 3 Ma (Clark, 1995; Love, 1999), which coincides with the timing of Stage I of the Albany-Fraser Orogeny, and could be a result of result of metamorphism related to the

magmatism, or could have occurred outboard of the Biranup complex prior to final closure of the intracratonic ocean basin in the western part of the orogen. The western Nornalup Complex was intruded by the voluminous porphyritic Burnside Granite between 1190-1170 Ma (Black et al., 1992), during Stage II of the Albany-Fraser Orogeny (Clark et al., 2000). Intrusion of the Burnside Granite triggered a metamorphic event recognizable by the growth of metamorphic zircon rims in the Nornalup Complex paragneisses 1169 ± 7 Ma (Clark et al., 1995).

In paragneisses of the Nornalup Complex east of Albany (Figure 1.1), Duebendorfer (2002) identified four different deformation phases. He interprets the first deformation phase, which results in a subhorizontal foliation and recumbent folds associated with granulite-facies metamorphism, as a consequence of NW-SE contraction. The second phase, which resulted in the formation of upright, NW-verging folds and a subvertical, NE-striking foliation, is associated with dextral transpression. The third phase is observable in mylonitic to cataclastic conjugate WNW-striking dextral and NNE-striking sinistral shear zones. He interpreted the prevalence of dextral over sinistral shears as evidence of overall tectonic dextral transpression. The fourth phase is brittle deformation that resulted in conjugated joint sets. According to Duebendorfer (2002) all these features are similar in geometry and kinematics to structures near Albany, dated at 1190-1170 Ma (Black et al., 1992), and coeval with Stage II deformation, and to structures east of Esperance associated with Stage I deformation (Clark et al., 2000).

1.6 Fraser Complex

Mafic rocks of the Fraser Complex (Figure 1.1) are interpreted to represent part of a large layered intrusion (Myers, 1985). Condie and Myers (1999) reinterpreted the Fraser Complex as remnants of multiple oceanic magmatic arcs, based on trace element data that indicated a subduction-related source for the mafic magma. Exposures are best towards the south and southwestern part of the unit.

Myers (1995) distinguished five different metamorphic mafic units in the Fraser Complex, with lithologies including metamorphosed gabbro, anorthosite, norite,

gabbronorite and ultramafic lithologies. The five mafic units are structurally interlayered with thin fault-bound slivers of paragneiss, quartzite, metagranite and pegmatite (Wilson, 1969; Doepel and Lowry, 1970; Myers, 1985; Clark et al., 1999). Granite and pegmatite also intrude the mafic rocks and appear later deformed and metamorphosed (Myers, 1985; Clark et al., 1999).

Rocks of the Fraser Complex display a NE-trending, steeply NW- to SE-dipping, pervasive foliation, and moderately NE- to SW- plunging mineral lineations and fold axes (Myers, 1985; Clark et al., 1999). Myers (1985) interpreted the tectonic boundaries between the different units in the complex as major thrust faults that interleaved thin slivers of basement gneiss and metasedimentary rocks with the mafic rocks. He also interpreted the NW-verging Fraser Fault, which is the northern-most fault that separates the Fraser Complex from the Biranup Complex and Munglinup Gneiss to the north (Figure 1.1), as the leading thrust of the package.

In the southern part of the Fraser Complex, Clark et al. (1999) defined three phases of deformation (D_1-D_3), two phases of metamorphism (M_1-M_2) and four episodes of recrystallization (M_{1a}-M_{2b}). They interpreted: (1) D_1 and $M_{1a/b}$ to reflect pyroxene-bearing granulite facies conditions; (2) D_2 and M_{2a}, which reflect retrogression to garnet-amphibolite facies (lower temperature, higher pressure than $M_{1a/b}$), to result from burial of the Fraser Complex, crustal thickening and tectonic interleaving; and (3) D_3, which was marked by development of mylonites and further retrogression to lower amphibolite-greenschist facies assemblages, to result from exhumation of the Fraser Complex along the Fraser Fault.

Published Sm-Nd and SHRIMP U-Pb geochronology has focused on the better exposed, southern part of the Fraser Complex, with reported igneous crystallization ages for the metamorphic mafic units of ca. 1300 Ma (Fletcher et al., 1991; Clark et al., 1999; De Waele and Pisarevsky, 2008). Fletcher et al. (1991) also reported a Rb-Sr cooling age of 1268 ± 20 Ma from a metamorphic olivine-bearing gabbronorite from the Fraser Complex. Wingate and Bodorkos (2007) reported a maximum depositional age of 1466 ±

17 Ma and a metamorphic age of 1304 ± 7 Ma for a metasedimentary rock interleaved between two of the mafic units of the Fraser Complex.

Limited geochronological data from the Fraser Complex suggest a short time span for igneous crystallization, granulite-facies metamorphism, retrogression and cooling (Spaggiari et al., in press). The data also point to tectonothermal activity taking place in the Fraser Complex during Stage I (1345-1260 Ma; Clark et al., 2000) of the Albany-Fraser Orogeny (Fletcher et al., 1991; Clark et al., 1999).

1.7 Summary

The Albany-Fraser Orogen, with an exposed length along the southwestern Australian coast of approximately 1200 km, is a complex Mesoproterozoic orogen that records tectonothermal activity spanning nearly 200 million years, from 1345 to 1140 Ma. The following chapters focus on the area near Bremer Bay in the western portion of the orogen, where results of detailed structural mapping and analysis are used to provide constraints on tectonic models for the Albany-Fraser Orogeny and on the processes associated with bidirectional extension during overall contraction in mid-crustal levels.

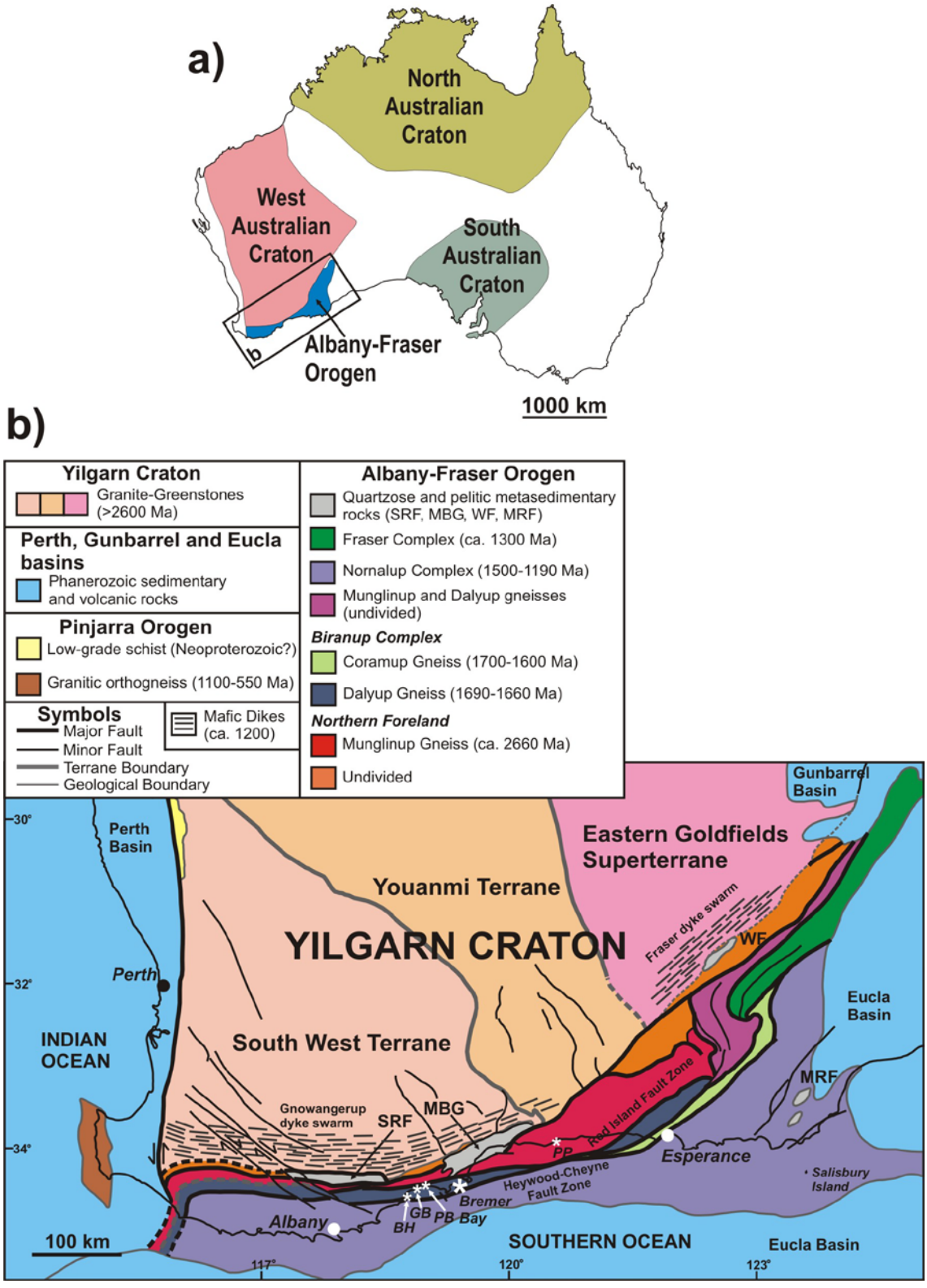
a)
North Australian Craton
West Australian Craton
South Australian Craton
Albany-Fraser Orogen
b
1000 km
b)
Yilgarn Craton
Granite-Greenstones (>2600 Ma)
Perth, Gunbarrel and Eucla basins
Phanerozoic sedimentary and volcanic rocks
Pinjarra Orogen
Low-grade schist (Neoproterozoic?)
Granitic orthogneiss (1100-550 Ma)
Symbols
Major Fault
Minor Fault
Terrane Boundary
Geological Boundary
Mafic Dikes (ca. 1200)
Albany-Fraser Orogen
Quartzose and pelitic metasedimentary rocks (SRF, MBG, WF, MRF)
Fraser Complex (ca. 1300 Ma)
Nornalup Complex (1500-1190 Ma)
Munglinup and Dalyup gneisses (undivided)
Biranup Complex
Coramup Gneiss (1700-1600 Ma)
Dalyup Gneiss (1690-1660 Ma)
Northern Foreland
Munglinup Gneiss (ca. 2660 Ma)
Undivided
Gunbarrel Basin
Eastern Goldfields Superterrane
Perth Basin
Youanmi Terrane
YILGARN CRATON
Fraser dyke swarm
WF
Perth
INDIAN OCEAN
South West Terrane
Eucla Basin
MRF
Gnowangerup dyke swarm
SRF
MBG
Red Island Fault Zone
PP
Esperance
Heywood-Cheyne Fault Zone
Salisbury Island
Bremer
GB
PB
Bay
BH
Albany
100 km
SOUTHERN OCEAN
Eucla Basin
30°
32°
34°
117°
120°
123°

Figure 1.1. (Previous Page). Geology of southwestern Australia, modified from Spaggiari et al. (in press). Abbreviated metasedimentary units in the Albany-Fraser Orogen include: **MBG**, Mount Barren Group; **MRF**, Mount Ragged Formation; **SRF**, Stirling Range Formation; **WF**, Woodline Formation. Abbreviated locations in the Albany-Fraser Orogen include: **BH**, Black Head; **GB**, Groper Bluff; **PB**, Pallinup Beach; **PP**, Powell Point.

Figure 1.2. (Next Page). Crustal elements of eastern-most Gondwana (after Fitzsimons, 2003, and Spaggiari et al., in press). Where paler and darker shades of the same color are shown, the paler shade indicates large areas without outcrop where the crustal element is inferred. **AG**, Terre Adélie-King George V Land; **BH**, Bunger Hills; **CC**, Curnamona Craton; **DG**, Denman Glacier region; **DML**, Dronning Maud Land; **M-F-W**, Madura, Forrest and Waigen Complexes (undivided, concealed by the Gunbarrel, Officer and Eucla Basins); **MR**, Miller Range; **PB**, Prydz Bay; **SPCM**, southern Prince Charles Mountains; **SR**, Shackleton Range; **WI**, Windmill Islands.

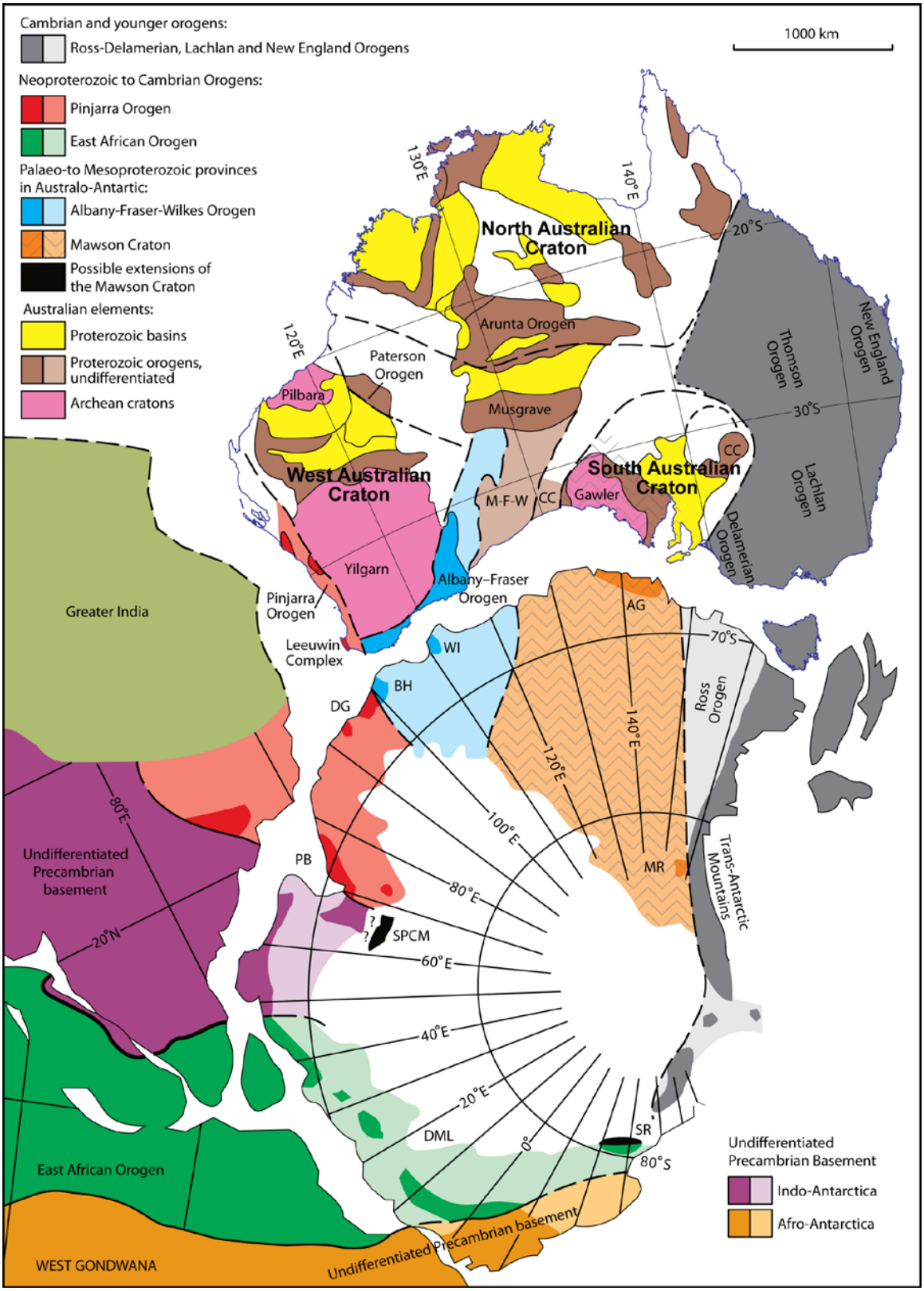
Cambrian and younger orogens:
Ross-Delamerian, Lachlan and New England Orogens
Neoproterozoic to Cambrian Orogens:
Pinjarra Orogen
East African Orogen
Palaeo-to Mesoproterozoic provinces in Australo-Antartic:
Albany-Fraser-Wilkes Orogen
Mawson Craton
Possible extensions of the Mawson Craton
Australian elements:
Proterozoic basins
Proterozoic orogens, undifferentiated
Archean cratons
1000 km
North Australian Craton
West Australian Craton
South Australian Craton
Arunta Orogen
Paterson Orogen
Pilbara
Musgrave
M-F-W
CC
Gawler
Yilgarn
Albany–Fraser Orogen
Pinjarra Orogen
Leeuwin Complex
WI
BH
DG
PB
AG
Ross Orogen
MR
Trans-Antarctic Mountains
Thomson Orogen
New England Orogen
Lachlan Orogen
Delamerian Orogen
Greater India
Undifferentiated Precambrian basement
SPCM
DML
SR
East African Orogen
WEST GONDWANA
Undifferentiated Precambrian basement
Undifferentiated Precambrian Basement
Indo-Antarctica
Afro-Antarctica
130°E
140°E
120°E
20°S
30°S
70°S
80°S
80°E
100°E
120°E
140°E
60°E
40°E
20°E
0°
20°N

Chapter 2. Deformation in granulite-facies orthogneisses of the Albany-Fraser Orogen, Bremer Bay, SW Australia: implications for a diachronous Mesoproterozoic orogeny.

2.1 Abstract

Granulite-facies rocks from the Bremer Bay area of the Mesoproterozoic Albany-Fraser Orogen, in southwestern Australia, record at least three phases of widespread, pervasive bidirectional extension that alternate with shortening and/or shear related deformation. Crustal extension occurred ca. 1180 Ma, based on SHRIMP U–Pb zircon geochronology of melts generated during deformation, which coincides with Stage II (1210-1140 Ma) of the Albany-Fraser Orogeny, a period of NW-directed contraction. Up to eight different deformation phases can be recognized in the Bremer Bay area: (1) formation of a pervasive migmatitic fabric, defined by alternating cm-wide leucosome and residuum bands, which is locally axial planar to early tight to isoclinal folds of layer-parallel, cm-wide, leucosome bands within the orthogneisses; (2) first bidirectional extension phase that resulted in the formation of NW- and NE-trending, foliation-parallel, cm-scale, blocky boudins of mafic layers parallel to the compositional layering, coeval with partial melting of the country rock; (3) second folding phase that formed open to isoclinal, upright to overturned, SW-plunging, NW-verging m-scale folds of early square boudins and dominant migmatitic fabric; (4) second bidirectional extension phase that formed NW- and NE- trending m-scale boudins of migmatitic fabric and earlier folds; (5) third folding phase that resulted in km-scale, NW-verging, SW-plunging, strongly asymmetric, overturned folds, which fold all earlier structures; (6) third bidirectional extension phase that formed NW- and NE- trending decameter-scale boudins of the migmatitic fabric, which are visible only on the shallow S- to SW-dipping limbs of km-scale folds; (7) late folding phase that resulted in the formation of m-scale open to tight, SW-plunging, upright to moderately overturned, NW-verging folds; and (8) fracturing related to the intrusion of dominantly N-NW and N-NE trending intermediate and felsic few cm- to few dm-wide pegmatite veins. Structures observed in the orthogneisses in the

Bremer Bay area indicate that deformation took place under overall NW-directed orogenic convergence during Stage II of the orogeny. The Albany-Fraser Orogen is reinterpreted as a diachronous orogen, resulting from the closure of an asymmetrical ocean basin between the West Australian and Mawson Cratons, which was considerably wider to the southwest. Subduction on the western part of the orogen was the driving force for NW-directed collision during late Stage I and Stage II of the orogeny.

2.2 Introduction

The Albany-Fraser Orogen is a collisional Mesoproterozoic belt located along the southern margin of the Archean (3.7 – 2.6 Ga) Yilgarn Craton in western Australia (Figure 1.1 in Chapter 1). The belt is currently interpreted to be the result of collision between the West Australian Craton, which includes the Yilgarn Craton of southwestern Australia, and the Mawson Craton of eastern Antarctica at ca. 1.3 Ga (Myers et al., 1996; Clark et al., 2000; Dawson et al., 2002; Fitzsimons, 2003). The Albany-Fraser Orogeny consists of two distinct tectonothermal events, based upon structural, petrographic and geochronological (SHRIMP U–Pb zircon, monazite and rutile) analysis: Stage I, between 1345-1260 Ma, and Stage II, between 1215-1140 Ma (Clark et al., 2000). Stage I has been defined as a period of NW-directed convergence during the collision of the West Australian and Mawson Cratons, and Stage II as a stage of renewed NW-directed convergence (Clark et al., 2000; Bodorkos and Clark, 2004 a&b). Bodorkos and Clark (2004b) give a detailed tectonic evolution for Stage I of the Albany-Fraser Orogeny: (1) closure of an ocean basin between the West Australian and Mawson Cratons during NW-directed convergence was followed by (2) lithospheric thickening in the vicinity of the now “jammed” subduction zone as a result of continued NW-directed collision, which resulted in (3) breakoff of the subducted slab and delamination of overthickened lithosphere, with upwelling of asthenospheric mantle and possible extension of the middle crust. Delamination was followed by (4) crustal thickening due to continued NW-directed convergence towards the end of Stage I. Following Stage I (1280-1215 Ma) the belt was exhumed through extension and erosion. Bodorkos and Clark (2004b) define

Stage II as a period of intracratonic reactivation of the orogen as a result of renewed NW-directed convergence. A question that is not addressed by the current tectonic model for the Albany-Fraser Orogen is the nature of the driving force behind NW-directed convergence that led to Stage II after complete closure of the ocean basin between the West Australian and Mawson Cratons during mid- to late Stage I.

This chapter reports the results of a detailed field study of the Albany-Fraser Orogen in the locality of Bremer Bay, Western Australia (Figure 1.1 in Chapter 1 and Figure 2.1). Granulite-facies orthogneisses in the Bremer Bay area display field evidence for three phases of widespread, bidirectional extension during overall orogen-wide contraction at ca. 1180 Ma, during Stage II of the Albany-Fraser Orogeny. Extensional deformation produced three generations of boudins of progressively increasing size, from centimeter to decameter-scale. Extensional deformation alternated with shortening and/or shear-related folding phases, which resulted in the formation of meter- to kilometer-scale folds. The deformational and metamorphic history of orthogneisses in the Bremer Bay area is compared to previous detailed field studies conducted in the Albany-Fraser Orogen (Beeson et al., 1988; Wetherley, 1998; Clark et al., 2000; Duebendorfer, 2002; Bodorkos and Clark, 2004 a&b) and it is suggested that the orogen was diachronous. Subduction on the western part of the belt was coeval with collision on the eastern part and acted as the driving force for continued NW-directed convergence during the orogeny, requiring modification to the current tectonic models for the region.

2.3 Regional Geology

The Albany-Fraser Orogen comprises four lithotectonic domains, defined on the basis of different structural styles inferred from aeromagnetic data, which from inboard to outboard are: the Northern Foreland, the Biranup Complex, the Fraser Complex (which occurs only in the eastern half of the belt), and the Nornalup Complex (Myers, 1990; Myers, 1995b) (Figure 1.1 in Chapter 1). The Biranup, Fraser and Nornalup Complexes are bounded by thrusts and are interpreted as having been sequentially thrust northwards onto the southern margin of the Yilgarn Craton, forming the Northern Foreland, during

Stage I of the Albany-Fraser Orogeny (Beeson et al., 1988; Myers, 1990; Clark et al., 2000). The Biranup and Nornalup Complexes are considered as exotic terranes unrelated to the West Australian Craton, although their origin is still debated (Nelson et al., 1995; Spaggiari et al., in press). The Fraser Complex has been interpreted as an oceanic island arc (Condie and Myers, 1999). Overall, Stage II is observed along the length of the orogen, whereas Stage I is only recorded in the eastern half of the orogen. A brief overview of the lithotectonic domains follows.

2.3.1 Northern Foreland

The Northern Foreland comprises tectonically reworked Archean (ca. 2660 Ma) rocks of the southern margin of the Yilgarn Craton, including the Munglinup Gneiss (Beeson et al., 1988; Nelson et al., 1995; Spaggiari et al., in press), and two Paleoproterozoic metasedimentary units, the Mount Barren Group and the Stirling Range Formation, all of which have been thrust northwards over the Yilgarn Craton (Myers, 1990; Dawson et al., 2002) (Figure 1.1 in Chapter 1). The imprint of the Albany-Fraser Orogeny on the southern margin of the Yilgarn Craton resulted in amphibolite- to granulite-facies recrystallization, and formation of spaced dextral and sinistral shear zones, which increase in intensity towards the southern edge of the craton, near the boundary with the Biranup Complex (Central Domain of Beeson et al., 1988). Coupled with this, a suite of dolerite dykes, the ENE- trending Gnowangerup Dyke Suite dated at ca. 1210 Ma (Figure 1.1 in Chapter 1; Evans, 1999), is progressively deformed within the Northern Foreland (Beeson et al., 1988), indicating Stage II deformation. On the eastern part of the belt, the NE-trending Fraser Dyke Suite, which was coeval with the Gnowangerup Dyke Suite and has been dated at ca. 1212 Ma (Wingate et al., 2000), cuts across major Proterozoic faults and shear zones near the craton boundary (Spaggiari et al., in press). Both metasedimentary formations located on the western part of the belt were polydeformed during Stage II, but at different metamorphic grades. The Stirling Range Formation is a poly-deformed, sub-greenschist to lower-greenschist metasedimentary sequence (Muhling and Brakel, 1985), deposited at ca. 1800 Ma

(Rasmussen et al., 2004). This sequence was intruded and metamorphosed by dolerite dykes of the ca. 1210 Ma Gnowangerup Dyke Suite (Rasmussen et al., 2002; Rasmussen and Fletcher, 2004), with deformation taking place after emplacement of the dykes. The Mount Barren Group comprises lower greenschist- to upper amphibolite-facies metasedimentary units that have undergone up to five different deformation phases (Wetherley, 1998), with peak metamorphism occurring at ca. 1200 Ma, during Stage II of the Albany-Fraser Orogeny (Dawson et al., 2003).

2.3.2 Biranup Complex

The Biranup Complex was thrust over the southern margin of the Northern Foreland (Myers, 1990) and consists of a suite of ca. 1600–1700 Ma amphibolite- to granulite-facies orthogneisses, including the Dalyup and Coramup Gneisses (Figure 1.1 in Chapter 1). The Biranup Complex was intruded by ca. 1300-1280 Ma Recherche Granite during Stage I tectonism, the interpreted age of pervasive deformation in the Dalyup Gneiss (Nelson et al., 1995). The Dalyup Gneiss, with crystallization ages of ca. 1690–1660 Ma, extends from at least the southern end of the Fraser Complex in the east (Nelson et al., 1995), and has now been recognized as far west as Bremer Bay (this study, Spaggiari et al., in press). The Coramup Gneiss, with protolith crystallization ages of 1700-1650 Ma, was deformed during Stages I and II of the Albany-Fraser Orogeny (Nelson et al., 1995; Bodorkos and Clark, 2004a, b). Granulite-facies orthogneisses of the Dalyup Gneiss at Bremer Bay on the western part of the belt have protolith crystallization ages of ca. 1680 Ma (this study, Spaggiari et al., in press) and show evidence for Stage II deformation (this study, Spaggiari et al., in press). No record of Stage I deformation has been documented in the Biranup Complex on the western part of the Albany-Fraser Orogen (Clark et al., 2000; this study).

2.3.3 Nornalup Complex

The Nornalup Complex was thrust onto the southern margin of the Biranup Complex (Myers, 1990) and consists of a number of different units on the eastern and

western parts of the belt (Figure 1.1 in Chapter 1). On the eastern part the Nornalup Complex includes the 1330-1288 Ma Recherche Granite (which also intrudes into the Biranup Complex), the ca. 1500-1400 Ma Malcolm Gneiss (dominantly paragneiss) (Nelson et al., 1995; Myers, 1995b), and the Mount Ragged Formation, a metasedimentary unit that is interpreted to unconformably overlie the Recherche Granite (Clark et al., 2000). The Nornalup Complex also includes the 1140 Ma Esperance Granite, which intruded the Mount Ragged Formation and the paragneisses of the Nornalup Complex. The Recherche Granite and the Malcolm Gneiss exhibit Stage I deformation (Clark et al., 2000), which was followed by deposition of the Mount Ragged Formation. These three units underwent Stage II deformation at ca. 1160 Ma (Clark et al., 2000; Bodorkos and Clark, 2004b), followed by the emplacement of the late-tectonic Esperance Granite into the sequence at ca. 1140 Ma (Nelson et al., 1995).

On the western part of the orogen, the Nornalup Complex comprises undifferentiated paragneisses (Duebendorfer, 2002) extensively intruded by late-tectonic, Stage II granites of the 1190-1170 Ma Burnside Batholith (Pidgeon, 1990; Black et al., 1992). Limited evidence for Stage I magmatism exists for intrusive rocks in outcrops near the town of Albany with crystallization ages of ca. 1289, 1296, and 1302 Ma (Pidgeon, 1990; Love, 1999). Stage I metamorphic zircon ages of ca. 1304 and 1314 Ma exist for metasedimentary rocks also near Albany (Clark, 1995; Love, 1999) (Figure 1.1 in Chapter 1), one of which contains a second generation of metamorphic zircon dated at ca. 1160 Ma (Clark, 1995), coincident with Stage II tectonism.

2.3.4 Fraser Complex

The Fraser Complex, restricted to the eastern half of the orogen, is a thrust package of granulites of mainly gabbroic composition derived from at least three different mantle sources and with geochemical anomalies consistent with an oceanic arc origin (Myers, 1985; Condie and Myers, 1999). Fletcher et al. (1991) obtained an igneous crystallization age of ca. 1291 Ma for a relatively unmetamorphosed gabbro, but it is unlikely to be representative of the entire complex. The Fraser Complex only shows

isotopic evidence of Stage I deformation. Granulite-facies metamorphic assemblages are pervasive throughout the complex and postdate intrusion of a ca. 1300 Ma charnockitic orthogneiss (Clark et al., 1999). Retrograde amphibolite-greenschist assemblages formed prior to emplacement of ca. 1288 Ma aplite dykes (Clark et al., 1999). Exhumation of the complex, with associated retrograde upper greenschist-facies metamorphism along the northern margin of the complex, was over by ca. 1250 Ma (Fletcher et al., 1991).

2.4 Lithologies

Rocks in the Bremer Bay area (Figure 2.1) are granulite-facies, felsic to intermediate, migmatitic orthogneisses, which have commonly been partially to completely retrograded to amphibolite-facies assemblages. The gneisses display a well-developed compositional banding (migmatitic fabric), defined by alternating leucosome-rich and residuum-rich layers, commonly 1-5 cm wide (Figure 2.2). The rocks exposed on the Bremer Bay peninsula can be grouped into eight different lithologies, on the basis of their relative mineral percentages and presence or absence of diagnostic peak-metamorphism mineral phases.

1. Orthopyroxene-clinopyroxene-biotite quartz monzonite orthogneiss

Orthopyroxene-clinopyroxene-biotite quartz monzonite orthogneiss is the most common lithology in the Bremer Bay area, and it appears on most of the headlands mapped on the peninsula (Figure 2.1). The orthogneiss is medium-grained and displays a light to moderate green hue that becomes darker with increasing percentage of mafic minerals, which make up from 7% to 30% of the overall rock volume. On some headlands on the eastern side of the Bremer Bay Peninsula, particularly along Banky Beach East, Point Gordon, Fisheries Bay and Back Beach headlands, this lithology appears segregated into centimeter-wide, foliation-parallel, felsic-enriched and mafic-enriched compositional bands.

Two slightly different mineral assemblages occur within this rock type: (1) the mafic assemblage is orthopyroxene (up to 2%), clinopyroxene (up to 1%), biotite (up to 3%), and magnetite (less than 1%); the rock is light gray to green and commonly

medium-grained, although locally coarse-grained; (2) the mafic minerals include hornblende (10-20%), orthopyroxene (up to 3%), clinopyroxene (up to 1%), biotite (up to 5%), and magnetite (less than 1%). Hornblende replaces orthopyroxene + clinopyroxene. The rock is dark green and typically medium-grained, with local coarse-grained to porphyritic layers.

2. Hornblende-biotite quartz monzonite orthogneiss

Hornblende-biotite quartz monzonite orthogneiss appears mainly in two localities in the Bremer Bay area, Blossoms Beach and Little Boat Harbour headlands (Figure 2.1). This unit is medium- to coarse-grained, locally porphyritic, dark grey to dark green, with a mafic mineral content of 10-15% comprising biotite (up to 5%) and hornblende (up to 15%). This unit is texturally very similar in thin section to the one described above, and the different mineral assemblage could indicate that this is a retrograde, amphibolite-facies equivalent of the former.

3. Hornblende-orthopyroxene-clinopyroxene monzodiorite orthogneiss

The hornblende-orthopyroxene-clinopyroxene monzodiorite orthogneiss is medium- to coarse-grained, dark green to almost black in color, with a mafic mineral content of 40-65% comprising hornblende (up to 40%), clinopyroxene (from 10 to 15%), orthopyroxene (quite variable, from 1% to 10%), and biotite (less than 1%). This unit is common across the entire field area and appears in two distinct ways: (1) as discrete layers from a few centimeters up to one meter in thickness; and (2) as broken up and disarranged parts of formerly discrete layers, locally showing evidence of prior deformation and floating in a leucocratic matrix of monzogranitic orthogneiss. These layers usually display very variable thickness and commonly are not laterally continuous.

4. Garnet-biotite quartz monzonite orthogneiss

The garnet-biotite quartz monzonite orthogneiss is a medium-grained, quite leucocratic unit that occurs on four of the twelve headlands on the Bremer Bay peninsula: Point Henry, Banky Beach, Short Beach and Fisheries Bay headlands (Figure 2.1). This unit appears either as discrete, several meters to decameters wide layers, or thin, few meter wide, irregular slivers within a different host lithology. Mafic mineral contents

range from 5% to 30%, including garnet (5-15%), biotite (5-10%), hornblende (rare, less than 2%) and opaque minerals (mostly magnetite) up to 5%.

5. Orthopyroxene-garnet quartz monzonite orthogneiss

Orthopyroxene-garnet quartz monzonite orthogneiss appears as a discrete layer less than 10 meters thick only in one locality, Banky Beach East Headland (Figure 2.1). The unit is medium-grained, dark in color, and contains 20-25% mafic minerals, including orthopyroxene (about 10%), garnet (up to 5%), biotite (about 5%), and magnetite (less than 2%).

6. Leucocratic granodiorite orthogneiss with pink felsic veins

The leucocratic granodiorite orthogneiss is a medium- to coarse-grained white granitic unit with pink felsic veins and is common throughout the field area. The unit bears no mafic minerals, except rare biotite (less than 2%) in some samples. The pink felsic veins are medium- to coarse-grained, commonly thin (up to a few centimeters wide), straight to anastomosing and subparallel to the foliation, and are mostly composed of potassium feldspar and quartz.

7. Magnetite-granodiorite orthogneiss

Magnetite-granodiorite orthogneiss appears exclusively on Banky Beach Headland (Figure 2.1) as relatively laterally continuous, 5 to 40 meter wide layers. It is grey in color, coarse-grained, and granitic in composition, comprising quartz, plagioclase and potassium feldspar, biotite (up to 3%), magnetite (up to 5%), and accessory hornblende and chlorite.

8. Charnockite orthogneiss

The charnockite orthogneiss is a leucocratic unit, which is only present on the southern end of Fisheries Bay Headland (Figure 2.1). The unit contains quartz, plagioclase, some potassium feldspar, variable amounts of orthopyroxene, and accessory biotite. This lithology is segregated into decimeter-wide white layers, with less than 3% orthopyroxene, and cm-wide dark gray layers, with up to 20% orthopyroxene.

2.5 Structure and metamorphism

2.5.1 Structural sequence

Orthogneisses of the Biranup Complex in the Bremer Bay area display a complex structural history comprising up to three different phases of bidirectional boudinage (extension in two orthogonal directions), which alternate with phases of folding. Deformation was ductile and took place at high temperatures as shown by the dynamothermal granulite-facies metamorphism. Pegmatitic material resulting from partial melting and associated with deformation at Bremer Bay yields temperatures from 800 to 1000^{o} C (Black et al., 1992). Different melts were generated and emplaced during all stages of ductile deformation and continued to migrate through the country rock after deformation ceased (this work). Mapping at a scale of 1:500, along 12 km of coastline (Figure 2.1), reveals a complex superposition history of structures. Below is a summary of structures observed in the field in the order in which they formed. A more detailed description and analysis of all structures is provided in Chapters 3 and 4 of this dissertation.

1. Foliation and early isoclinal fold phase

A very pervasive migmatitic (gneissic) foliation is present throughout, defined by both a compositional segregation and parallel alignment of tabular and platy minerals (mainly amphibole and biotite) (Figure 2.2). The compositional banding forms alternating centimeter scale leucosome bands (dominantly felsic) and residuum bands (dominantly mafic).

Small (less than a meter in amplitude) isoclinal folds that fold centimeter-wide leucosome-rich bands are present throughout, although they appear only locally. The migmatitic foliation is axial planar to these folds, indicating that they were coeval. The leucosome bands associated with these folds are different from the leucosomes defining the migmatitic foliation; they are laterally continuous, discrete layers, with well defined boundaries (Figure 2.3).

2. First bidirectional extension phase

Small, centimeter to decimeter blocky boudins of mafic-rich layers parallel to the dominant migmatitic fabric are present throughout the entire field area (Figure 2.4). These boudins appear concurrently with two orthogonal directions, NW-SE and NE-SW (Figure 2.4a). Leucosomes (former melt) are localized in the neck areas of these small boudins, and locally along the boudinaged layers as well (Figure 2.4b).

3. Second folding phase

Open to isoclinal, upright to recumbent folds (Figure 2.5) of the migmatitic foliation fold the boudinaged mafic layers described above. The folds are a few centimeters up to a meter in amplitude, plunge shallowly to moderately (from 3° to nearly 40°) to the SW, typically contain axial-planar leucosomes, and are common throughout the entire field area. Locally they lie in zones almost parallel to the overall foliation and show a progression from overturned to recumbent suggesting zones of non-coaxial shear.

4. Second bidirectional extension phase

Intermediate-scale (less than a meter to a few meters in scale) boudins of the migmatitic foliation and locally, compositional layering (defined by alternating bands of slightly different lithologies within the country rock) occur throughout the entire field area (Figure 2.6). These boudins occur in two orthogonal orientations, NW-SE and NE-SW, and show no crosscutting relationships or changes in style or overall size. Leucosomes are commonly observed concentrated in the necks of the boudins. The intermediate-scale boudins also boudinage the open to isoclinal folds of mafic square boudins and migmatitic foliation described above (Figure 2.6).

5. Third folding phase

Regional, km-scale, asymmetric, NW-verging, SW-plunging overturned folds with long shallowly-dipping limbs occur throughout the area (Figure 2.7a). Continuous exposure along Banky Beach East Headland shows both limbs and the hinge region of one of the regional antiforms (Figure 2.7b). These regional-scale folds are evident across the Bremer Bay area by the migmatitic foliation map pattern: (1) exposures of NE-striking and moderately to steeply SE-dipping foliation (corresponding to steeply dipping

overturned limbs of km-scale folds) versus (2) areas of NW-striking and shallowly SW- to S-dipping foliation (corresponding to upright, shallow-dipping limbs of km-scale folds) (Figure 2.7a). The stereonet of poles to foliation in Figure 2.8 shows that the regional fold axes trend 219° and plunge 19° to the SW.

6. Third bidirectional extension phase

Large, decameter-sized boudins of the migmatitic foliation and compositional layering, which occur in orthogonal NW-SE and NE-SW orientations, are present in the Bremer Bay area (Figure 2.9). They are visible only in areas with NW-trending, shallow SW-dipping migmatitic foliation and not on the steeply dipping overturned limbs of the regional folds. As observed for boudins from the two previous extension phases, former melts have intruded in the neck areas of these two sets of boudins. On Fisheries Bay Headland (Figure 2.1), decameter-size boudins are offset by normal sense shear zones, one of which has been intruded by a felsic (white) pegmatitic melt (Figure 2.9).

As a result of the interference of NW and NE-trending boudin sets on the surface, topography has a “hummocky” appearance, with domes and troughs corresponding to the top of boudins and boudin neck areas respectively (Figure 2.10). Trains of domes and troughs can be followed in NW and NE directions, and no given set is seen clearly disrupting the other. Felsic material representing previous melt is found in the boudin neck areas.

7. Late folding phase

The rocks in the Bremer Bay area display meter-sized folds that appear to have formed after the last bidirectional extension phase that resulted in the formation of large boudins. They fold the foliation, are slightly asymmetric, open, SW-plunging, generally upright to moderately overturned, and dominantly NW-verging (Figure 2.11). The folds occur only locally throughout the field area and are only visible on the shallow-dipping limbs of the large, kilometer-scale overturned folds. Their style of deformation is different from other folds seen in the field area with less flow of the folded layers and no associated axial-planar leucosomes.

The style of deformation observed in these folds suggests that they could have formed at lower temperatures than other folds in the field area, and thus could potentially be the result of a younger folding phase.

8. Late melt structures

Discrete, undeformed, few centimeter- to few decimeter-wide, late pegmatites cut through all other structures in the Bremer Bay area (Figure 2.12a). These pegmatites are dominantly of two distinct chemistries: (1) intermediate to mafic composition (green in color) and (2) felsic composition (reddish pink to pale pink in color). Intermediate (green) pegmatites dominantly strike N-NW and N-NE (Figure 2.12a, b) and cut through all structures previously described. Felsic (pink) pegmatites dominantly strike NW and locally NE (Figure 2.12a, c) and cut through the intermediate to mafic composition pegmatites as well as all other structures observed in the field.

Other structures

1. Mineral Lineation

A weak mineral grain lineation is observed on foliation planes, defined by alignment of acicular and platy minerals, principally pyroxene, and locally hornblende and biotite. The lineation appears locally throughout the field area; the mean orientation is 227° with a plunge of 21° SW (Figure 2.8).

The attitude of the mineral lineation coincides with that of fold axes of small folds of the migmatitic fabric (and early cm-scale boudins) formed during the second folding phase in the Bremer Bay area. Small folds of the gneissic fabric in one outcrop display a weak mineral lineation parallel to the fold axes, which suggests that the mineral lineation could have formed as a result of extension in a NE-SW direction along the fold axes during the second folding phase in the Bremer Bay area.

2. Shear bands

Shear bands, from a few centimeters up to a few meters in length, are found throughout the field area. Both left-lateral and right-lateral shears occur with or without leucosomes (former melt) present on the shear plane. Shear bands are observed to offset the migmatitic foliation, early square boudins of foliation-parallel mafic layers, folds of

the foliation and early square boudins, intermediate boudins of the migmatitic foliation, and locally, some of the large, decameter-sized boudins (Figures 2.9 and 2.13).

From field relationships I have been unable to decipher whether all shear bands are the result of the same phase of shearing, or whether there have been several discrete phases of shearing during the entire deformation history in the Bremer Bay area. Shear bands rarely interact in the field, and thus there are no clear cross-cutting relationships from which one can draw relative timing constraints.

2.5.2 Interpretation of structures

For each of the three generations of orthogonal boudins, the boudins in NE-SW and NW-SE orientations are interpreted as having formed coevally as the result of biaxial extension. In each case the similar-aged boudins are similar in size and style and lack cross-cutting relationships with the boudins in the orthogonal orientation. The last generation also shows interference patterns formed by the trains of orthogonal boudins that suggest they formed in the same strain field. The earliest and smallest orthogonal boudins are folded by outcrop-scale folds, and those folds are in turn boudinaged. This second set of intermediate size boudins is folded by regional scale folds. The largest, decameter scale boudins are found only on the shallow limbs of these folds, indicating folding occurred prior to this last phase of boudinage. Thus each of the three generations of boudins are interpreted as the result of a separate phase of bidirectional extension with the magnitude of boudinage increasing with time. Folding as a result of shortening and/or shearing occurred before and after each phase of extension.

2.6 SHRIMP II U-Pb zircon geochronology

SHRIMP U–Pb zircon geochronology analyses were conducted on country rock and boudin neck-melt samples from three different headlands in Bremer Bay: Fisheries Bay, Point Henry and Short Beach (Figure 2.1; Tables 1-3). This work was undertaken at the geochronology facilities in the John de Laeter Centre of Mass Spectrometry housed at Curtin University of Technology in Perth, Western Australia. Complete ion microprobe

analytical results, and cathodoluminescence (CL) images and descriptions of the zircons from each of the six samples dated are given in Bodorkos and Wingate (2008e, f, g, h, i, j).

Prior to this study, the only timing constraints for deformation in the Bremer Bay area were a Rb-Sr age of 1140 ± 40 Ma for a granulite-facies pegmatite in a normal-sense shear zone (Black et al., 1992) and a paleomagnetic pole, obtained from country rock (granulite facies tonalitic gneiss and mafic granulite) and intruding metadolerite dykes, that fits the ca. 1.2 Ga part of the Precambrian Australian apparent polar wander path (Pisarevsky and Harris, 2001).

2.6.1 Fisheries Bay

The country rock sampled is a medium to coarse-grained orthopyroxene-clinopyroxene-biotite quartz monzonite orthogneiss with well developed compositional layering. Magmatic zircon cores yielded an age of 1680 ± 7 Ma, which corresponds to the crystallization of the igneous protolith to the orthogneiss (sample GSWA 184311) (Table 1). The age of a high-grade metamorphic event affecting the orthogneiss is constrained by a very coarse-grained leucocratic granodiorite that intrudes the neck area of a decameter-size NW-SE trending boudin set (Figure 2.14), which gave an igneous crystallization age and best estimate of synchronous high-grade metamorphism of 1178 ± 3 Ma (sample GSWA 184310) (Table 1).

2.6.2 Point Henry

Zircon cores from a medium- to coarse-grained leucocratic quartz monzonitic orthogneiss yielded a minimum age of crystallization for its protolith of 1670 ± 12 Ma (sample GSWA 184119) (Table 2). Metamorphic zircon rims produced an age of 1178 ± 4 Ma for the high-grade metamorphic event responsible for zircon rim growth.

A pegmatitic granodiorite located in the neck of an intermediate, meter-sized NE-SW trending boudin train (Figure 2.15) gave an igneous crystallization age, from magmatic zircon cores, of 1187 ± 5 Ma, and an age of 1172 ± 16 Ma for a high-grade

metamorphic event responsible for the formation of thick zircon rims that mantle magmatic cores, and also new growth of discrete zircons (sample GSWA 184307) (Table 2). The date of 1172 ± 16 Ma attributed to high-grade metamorphism of the pegmatitic granodiorite is indistinguishable from the date of 1178 ± 4 Ma ascribed to high-grade metamorphism of the host monzogranitic gneiss.

2.6.3 Short Beach

Magmatic zircon cores from a medium-grained leucocratic granodiorite, from which yielded an igneous crystallization age of 1689 ± 11 Ma for the granodioritic precursor to the orthogneiss (sample GSWA 184312). Metamorphic zircon rims and discrete grains produced an age of 1154 ± 25 Ma, considered as the best estimate for the timing of high-grade metamorphism (Table 3).

An unmetamorphosed coarse-grained leucogranite intruded in the neck of a meter-sized NW-SE trending boudin set (Figure 2.16) gave an igneous crystallization age of 1148 ± 9 Ma (sample GSWA 184326) (Table 3).

2.6.4 Interpretation of SHRIMP U-Pb zircon geochronology data

Protolith ages from orthogneisses in the Bremer Bay area obtained in this study are the first published ages to be obtained for rocks from the Biranup Complex on the western part of the Albany-Fraser Orogen. The three protolith samples from Fisheries Bay, Point Henry and Short Beach Headlands (Tables 1-3) all gave igneous crystallization ages of ca. 1680 Ma, which correlate with crystallization ages of orthogneisses of the Biranup Complex that occur in the central part of the Albany-Fraser Orogen (Nelson et al., 1995). The origin of the Biranup Complex remains unknown, and is presently interpreted as a large piece of ca. 1680 Ma exotic crust representing a fragment of a Paleoproterozoic orogenic belt accreted to the Archean Yilgarn Craton during Stage I of the Albany-Fraser Orogeny (Nelson et al., 1995; Spaggiari et al., 2008; Spaggiari et al., in press).

High-grade metamorphic ages of orthogneisses at Point Henry and Short Beach headlands are 1178 ± 4 Ma and 1154 ± 25 Ma respectively (Tables 2, 3). Crystallization ages for granitic bodies intruded into boudin necks of different generations and orientations at Fisheries Bay and Point Henry are 1178 ± 4 Ma and 1187 ± 5 Ma respectively, with high-grade metamorphic ages of the same melts in these two locations being 1178 ± 4 Ma and 1172 ± 16 Ma respectively (Tables 1, 2). These ages indicate that intrusion of melts into boudin necks as well as high-grade metamorphism of the country rock protoliths and boudin neck melts in the Bremer Bay area took place during Stage II (1245-1140 Ma) of the Albany-Fraser Orogeny (Clark et al., 2000).

The crystallization age of 1148 ± 9 Ma obtained from an unmetamorphosed granite intruded into a meter-sized boudin neck at Short Beach Headland (Table 3) is significantly younger than the igneous crystallization ages obtained from boudin neck melts from Fisheries Bay and Point Henry headlands. The unmetamorphosed character of the leucogranite suggests that this melt could have been emplaced into a preexisting boudin neck at a later time, after the high-grade metamorphic event that affected the rocks in the Bremer Bay area.

2.7 Evidence for Stage II shortening/transcurrent motion in the Albany-Fraser Orogen

In both the eastern and western parts of the Albany–Fraser Orogen, most structural studies have concluded that NW- to NNW-directed contraction and dextral transpression appear to be the dominant deformation regimes (see below). However, this study shows that shortening and/or shear-related deformation alternated with bidirectional extension in orthogneisses of the Biranup Complex in the Bremer Bay area (Figure 1.1 in Chapter 1).

2.7.1 Western Albany-Fraser Orogen

For orthogneisses of the Biranup Complex to the west of Bremer Bay (Groper Bluff, Black Head and Pallinup Beach) (Figure 1.1 in Chapter 1), Beeson et al. (1988)

proposed an early phase of granulite-facies transcurrent shearing that resulted in thrusting of the Biranup Complex over the Northern Foreland and formation of minor (up to 30 cm long) conjugate dextral (WSW-striking) and sinistral (WNW-striking) cm-wide shear zones. This deformation dated at 1190-1170 Ma occurred during Stage II (Black et al., 1992). Continued NNW-oriented contraction resulted in amphibolite-facies thrusting coeval with minor dextral transcurrent shearing and folding, which formed meter- to kilometer-scale, overturned, NW-verging and SW-plunging folds with a well-developed axial planar foliation. Boudins are visible locally on the limbs of meter-scale folds, which Black et al. (1992) interpret as a result of extension on the fold limbs during folding. Conjugate dextral (WNW-ESE striking) and sinistral (N-S striking) shears also formed, commonly overprinting earlier shear bands, the dominant foliation, boudins and meter-scale folds.

In the metasedimentary rocks of the Mount Barren Group NE of Bremer Bay (Figure 1.1 in Chapter 1), Wetherley (1998) described five different shortening deformation phases (D_1 through D_5). He interpreted the resulting folds and associated cleavages as a result of initial N-S contraction and later NW-SE contraction respectively. No extensional features have been described. Wetherley (1998) obtained THERMOCALC temperature and pressure estimates of 560-675ºC and 7-12.4 kbars for the metasedimentary rocks of the Mount Barren Group.

Dawson et al. (2003) obtained metamorphic U-Pb ages for xenotime and monazite from kyanite-bearing schists of the Mount Barren Group of 1206±8 Ma and 1194±8 Ma respectively, which they interpreted as dating the peak syn-D_2 metamorphic event in the area. These ages are consistent with major deformation taking place in the western Albany–Fraser orogen during Stage II.

In paragneisses of the Nornalup Complex east of Albany (Figure 1.1 in Chapter 1), Duebendorfer (2002) identified four different deformation phases: (1) formation of a subhorizontal foliation and recumbent folds associated with granulite facies metamorphism as a consequence of NW-SE contraction; (2) formation of upright, NW-verging folds and a subvertical, NE-striking foliation, associated with dextral

transpression; and (3) formation of mylonitic to cataclastic conjugate WNW-striking dextral and NNE-striking sinistral shear zones, as a result of overall tectonic dextral transpression. According to Duebendorfer (2002) all these features are similar in geometry and kinematics to structures near Albany, dated at 1190-1170 Ma (Black et al., 1992), which is consistent with Stage II deformation, and to structures east of Esperance associated with Stage II deformation (Spaggiari et al., in press).

2.7.2 Eastern Albany-Fraser Orogen

Deformation during Stage II of the Albany-Fraser Orogeny in the Coramup Gneiss (part of the Biranup Complex) near Esperance (Figure 1.1 in Chapter 1) was characterized by high-T and low-P (750-800 °C and 5-6 kbar) metamorphic conditions (Bodorkos and Clark, 2004a). Metamorphism was synchronous with the formation of (1) subvertical, SE-dipping shear zones; (2) a shallow SW-plunging mineral stretching lineation; (3) NW-verging, decimeter- to meter-scale tight asymmetric folds to which the main foliation is axial planar; and (4) syn-kinematic pegmatite dyke emplacement at ca. 1170 Ma (Bodorkos and Clark, 2004b). Kinematic indicators in the Coramup Gneiss suggest overall dextral transpression, with a component of pure shear flattening parallel to the main foliation, and dextral simple shear (Bodorkos and Clark, 2004b).

2.7.3 Correlation between deformation in Bremer Bay and elsewhere in the Albany-Fraser Orogen

The Stage II shortening structures observed in the Bremer Bay area are compatible with those described in both the Biranup and Nornalup Complexes elsewhere in the orogen, including those absolutely dated as Stage II. Thus Stage II of the Albany–Fraser Orogeny was dominated by widespread NW-vergent folding and dextral transpression during NW- to NNW-directed contraction. However, from the structural relationships observed at Bremer Bay, it is clear that extension has also played a role, but perhaps has been more difficult to recognize in other localities.

2.8 Discussion

This study represents the first detailed field study and determination of the absolute timing of deformation and metamorphism in the western Biranup Complex, therefore allowing tectonism of this unit to be placed within the context of the Albany-Fraser Orogeny. Progressive deformation at granulite-facies conditions in the Bremer Bay area took place at ca. 1180 Ma during Stage II of the Albany-Fraser Orogeny. The progressive deformation includes three phases of bidirectional extension, three either shortening or perhaps shear-related phases of folding, and shearing, with partial melting and granulite facies metamorphism occurring during all phases of deformation.

2.8.1 Albany-Fraser Orogen as a diachronous collisional orogen

The most current tectonic model for the Albany-Fraser Orogeny has been proposed by Bodorkos and Clark (2004b), and modified after Giles et al. (2004). This model suggests that the present-day configuration of the North Australian, West Australian and Mawson Cratons was reached to a large extent by ca. 1500 Ma, based on paleomagnetic data from Wingate and Evans (2003), who demonstrated that all post-1500 Ma paleopoles for these three cratons lie on the same apparent polar wander path. According to Giles et al. (2004) and Bodorkos and Clark (2004b), the paleomagnetic data of Wingate and Evans (2003) do not rule out the possibility of rotations between neighboring Australo-Antarctic cratons, particularly during the early Mesoproterozoic. Thus, Giles et al. (2004) suggested that the North Australian and the Mawson Cratons were indeed adjacent by ca. 1500 Ma, but that the Mawson Craton was rotated nearly 52º counterclockwise from its present day orientation. This reconstruction creates sufficient space for an ocean basin between the southeastern margin of the West Australian Craton and the western margin of the Mawson Craton (Bodorkos and Clark, 2004b). Giles et al. (2004) envisioned post-1500 Ma clockwise rotation of the Mawson Craton with respect to the North Australian and Western Australian Cratons, with overall transtension and rifting on the northern margin and overall transpression and convergence on the western margin of the Mawson Craton during the Albany-Fraser Orogeny (Figure 2.17).

Bodorkos and Clark (2004b) picture the process of closure of the ocean basin between the Mawson and the West Australian Cratons as a clockwise asymmetric motion towards the West Australian Craton of an E-dipping subduction zone located along the western margin of the Mawson Craton.

Stage I, from 1345-1260 Ma, comprises the closure of the ocean basin between the West Australian and Mawson Cratons during overall NW-directed convergence (Clark et al., 2000, Bodorkos and Clark, 2004b). Bodorkos and Clark (2004b) proposed that complete closure of the ocean basin was achieved by ca. 1300 Ma, and was followed by lithospheric thickening near the now "jammed" subduction zone, with subsequent breakoff of the relict subducting slab and delamination of an overthickened lithosphere at ca. 1290 Ma, followed by upwelling of the asthenosphere, extension of the middle crust, and high-T, low-P metamorphism. These tectonic events were followed by renewed NE-directed cratonic convergence, which resulted in crustal thickening and high-P metamorphism at mid-crustal levels at ca. 1280 Ma. According to Bodorkos and Clark (2004b), Stage I concluded with tectonic exhumation of mid-crustal units via extensional reactivation, based on relationships of a major bounding fault (the Heywood Fault), decompression metamorphic assemblages, and deposition of sediments into intracratonic basins. Extensional tectonics dominated until the beginning of Stage II of the orogeny which marked a period of renewed NW-directed contraction from 1215 to 1140 Ma, which resulted in intracratonic reactivation of major structures within the orogen (Bodorkos and Clark, 2004b).

Rocks of the Albany-Fraser Orogen display ample isotopic evidence of Stage I and Stage II deformation on the eastern part of the belt. However, evidence for Stage I deformation of the Biranup Complex is conspicuously absent on the western part of the orogen. Stage I metamorphic ages recorded in the western Nornalup Complex near Albany (Figure 1.1 in Chapter 1; Clark, 1995; Love, 1999) could be the result of metamorphism related to the magmatism, and could have occurred outboard of the Biranup complex prior to final closure of the intracratonic ocean basin in the western part of the orogen. This study shows that deformation and high-grade metamorphism in rocks

of the Biranup Complex in the Bremer Bay area took place during Stage II of the orogeny at ca. 1180 Ma. Although the rocks in the Bremer Bay area record three phases of bidirectional extension, these phases alternate with shortening and/or shear-related folding phases, and deformation has been interpreted as taking place in a NW-directed shortening environment. Thus, deformation along the orogen was the result of NW- to NNW-directed contraction and in some areas dextral transcurrent motion.

Bodorkos and Clark (2004b) suggested that complete closure of the ocean basin between the West Australian and the Mawson Cratons could have culminated at ca. 1300 Ma, during Stage I of the orogeny. It was proposed that NW-directed orogenic contraction continued during the latter parts of Stage I and again during Stage II. Bodorkos and Clark (2004b) indicated that continued convergence and localized oblique collision between the West Australian and the Mawson Cratons took place during Stage II, as was evident by ca. 1170 Ma shearing along the Coramup Fault. However, it is now evident that Stage II in the western Biranup Complex was a much hotter and more pervasive tectonothermal event than previously recognized, and the presence of granulite-facies metamorphism, pervasive partial melting and multiple phases of bidirectional extension requires explanation.

The Albany-Fraser is interpreted as a diachronous orogen (Figure 2.17). Stage I of the orogeny recorded the collision between the West Australian and Mawson Cratons on the eastern part of the orogen, while subduction was ongoing on the western part of the orogen. This difference along strike of the orogen would explain the existence of field and isotopic evidence for Stage I shortening deformation on the eastern part of the belt, and the absence of such evidence on the western part in the Biranup Complex. Additionally, Stage II records the collision between the West Australian and Mawson Cratons on the western part of the orogen, which represents the final closure of the ocean basin between these two cratons. Such progressive closure of the ocean basin could also explain the occurrence of dextral transpression. Thus the driving force for NW-directed convergence post ca. 1300 Ma during Stage I and during Stage II of the orogeny was ongoing subduction on the western part of the belt. The diachronous character of the

Albany-Fraser Orogen is explained by the asymmetric, NW-directed motion towards the West Australian Craton driven by subduction retreat of the E-dipping subduction zone located on the western margin of the Mawson Craton, as was shown by Bodorkos and Clark (2004b) and Giles et al. (2004).

2.9 Conclusions

(1) This detailed field study has revealed that granulite-facies orthogneisses of the Biranup Complex on the western part of the Albany-Fraser Orogen in the Bremer Bay area, SW Australia, underwent a complex deformation history at ca. 1180 Ma, during Stage II of the Mesoproterozoic Albany-Fraser Orogeny, interpreted as a period of NW-directed convergence.

(2) Progressive deformation recorded in the orthogneisses in the Bremer Bay area includes three phases of bidirectional extension that alternate with shortening and/or shear-related folding phases, shearing, and melt generation throughout deformation. Progressive deformation recorded in the Bremer Bay area took place under overall NW-directed orogenic convergence.

(3) The driving force for NW-directed orogenic convergence during Stage II of the Albany-Fraser Orogeny was subduction on the westernmost end of the orogen during the final stages of the closure of an ocean basin between the West Australian and Mawson Cratons.

(4) The Albany-Fraser Orogen behaved as a diachronous orogen. The closure of the ocean basin between the West Australian and Mawson Cratons was asymmetric, allowing for NW-directed cratonic collision to propagate from NE to SW, along an arcuate collision zone.

(5) The diachronous nature of the Albany-Fraser Orogen resulting from the asymmetric closure of an ocean basin explains the isotopic-age distribution of shortening structures along the strike of the belt. The eastern part of the belt records high temperature deformation events during Stage I (1345-1260 Ma) and Stage II (1215-1140 Ma), both interpreted as resulting from NW-directed contraction, whereas the

Biranup Complex in the western part of the belt only contains evidence of high temperature deformation for Stage II. Complete closure of the ocean basin between the two cratons would result in Stage II deformation, recorded both on the western and eastern parts of the belt.

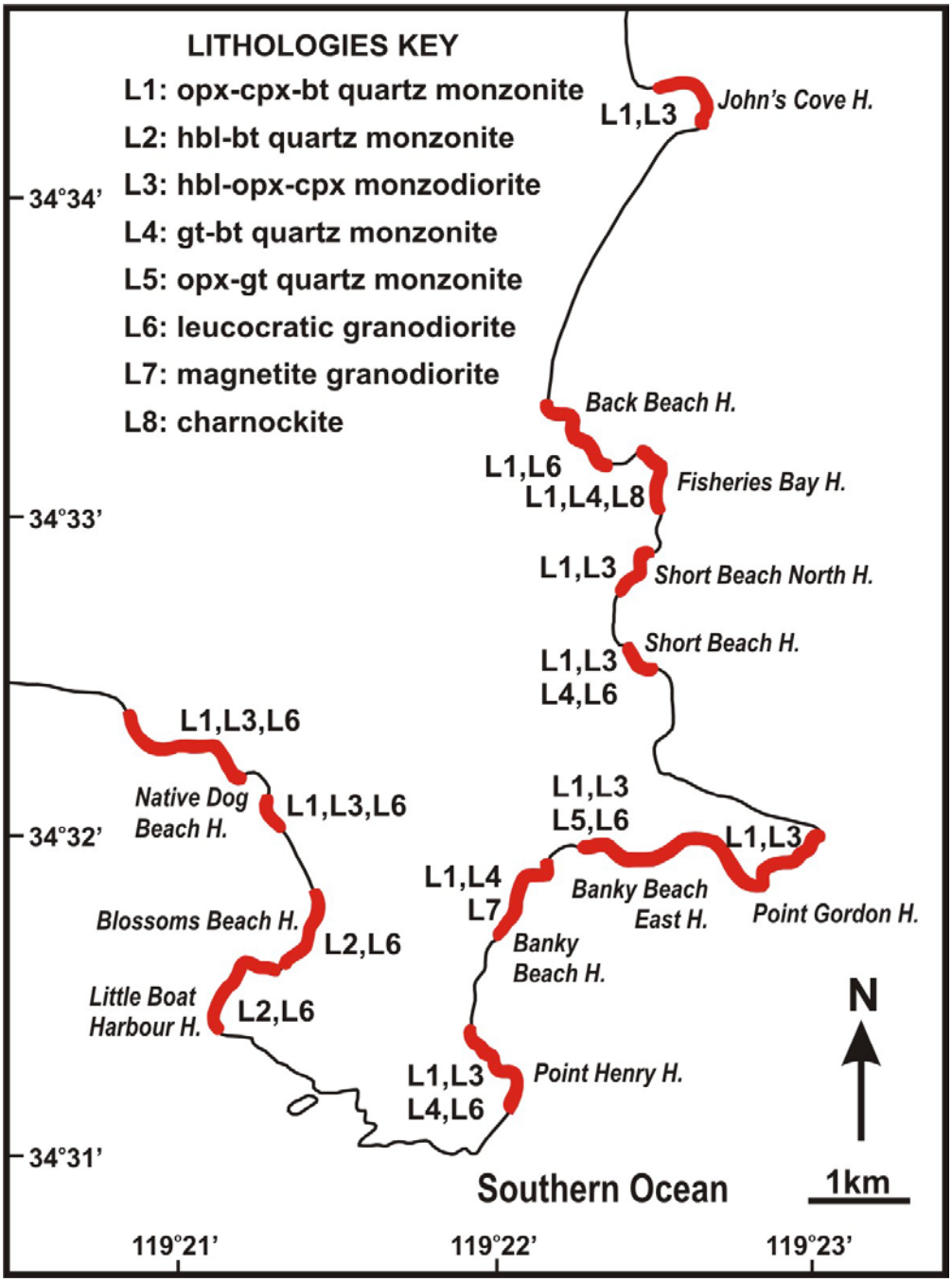

Figure 2.1. Map of the Bremer Bay peninsula, highlighting the 13 headlands mapped in this study, and the distribution of the main lithologies throughout the field area. The extent of the area mapped for each headland is highlighted in red.

Figure 2.2. Pervasive migmatitic fabric present in orthogneisses at Bremer Bay, defined by 1-5 cm wide leucosomes and residuum layers. Chisel for scale is 20 cm long.

Figure 2.3. Small isoclinal fold of a centimeter-wide leucosome-rich band at Native Dog Beach Headland. Pencil (12 cm) near the hinge area parallels the attitude of the axial planar migmatitic fabric.

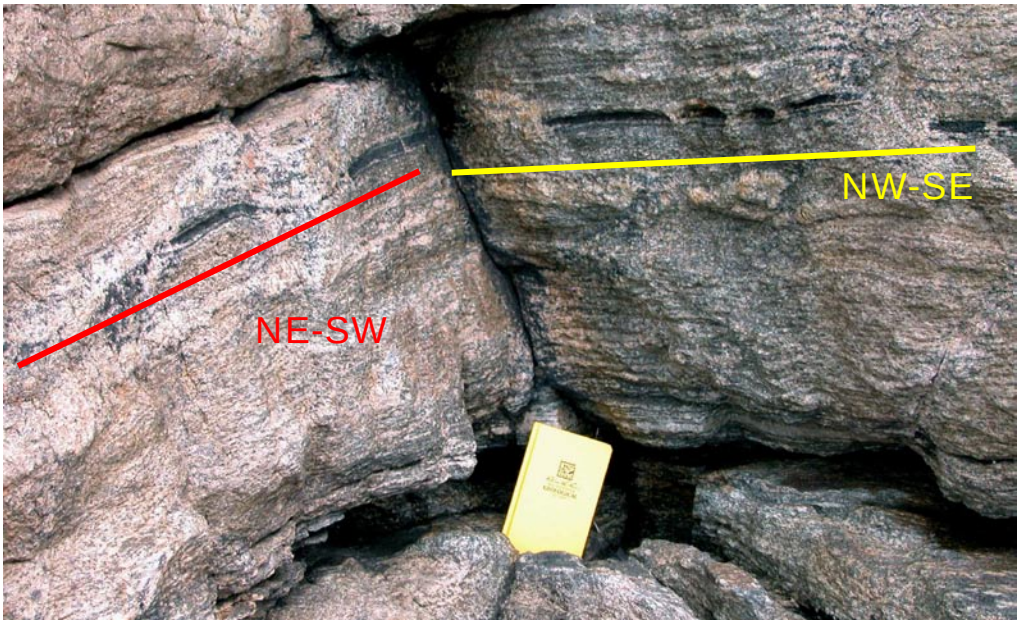

Figure 2.4a. Centimeter-sized blocky boudins of a mafic layer parallel to the migmatitic fabric at Fisheries Bay Headland; extension in two orthogonal directions, NW-SE and NE-SW. Field book for scale is 19 cm long.

Figure 2.4b. Centimeter-sized blocky boudins of mafic layers parallel to the migmatitic fabric at Fisheries Bay Headland, with leucosomes localized in the neck areas of the boudins and along the boudinaged layer. Note upper layer has been later boudinaged by the second phase of extension. Compass for scale is 10 cm long.

Figure 2.5a. Open to isoclinal, SW-plunging antiformal folds of migmatitic foliation and foliation-parallel boudinaged mafic layers at Fisheries Bay Headland. Field book for scale is 19 cm long.

Figure 2.5b. Inclined (NW-verging) and recumbent folds of migmatitic foliation and foliation-parallel boudinaged mafic layers at Point Gordon Headland. Field book for scale is 19 cm long.

Figure 2.6a. NE-SW trending boudin (outlined green) of a meter-wide tight fold of the migmatitic foliation (hinge area outlined red) in Banky Beach Headland. Compass for scale is 10 cm long

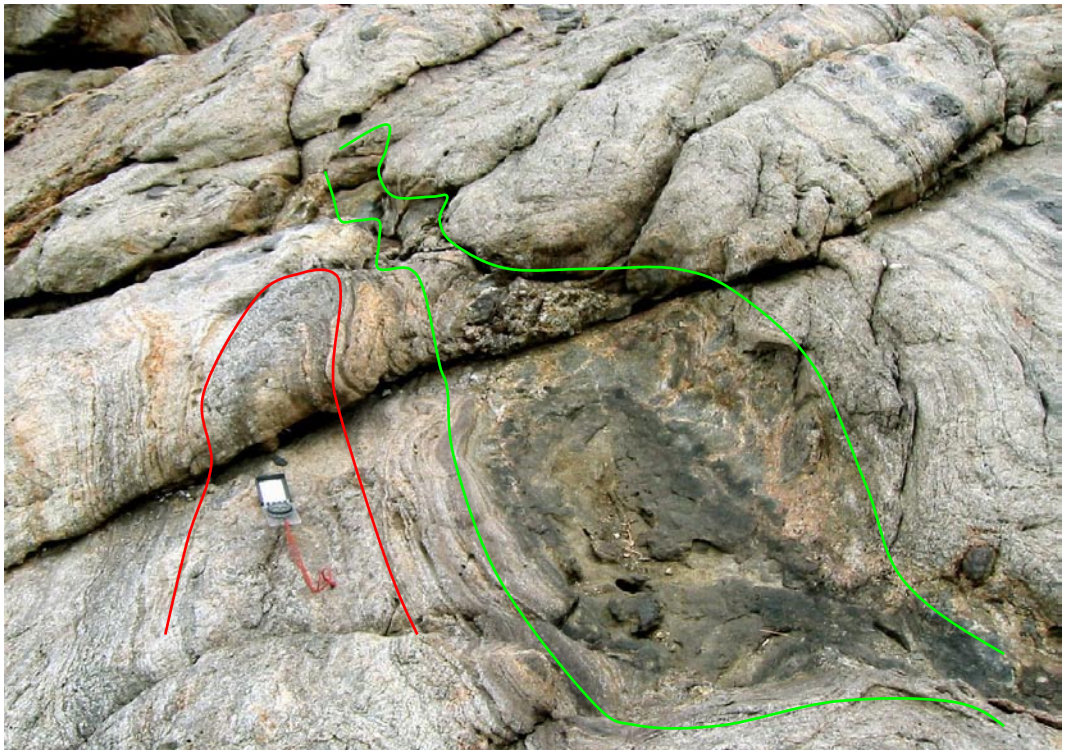

Figure 2.6b. NW-SE trending meter-wide, boudinaged mafic layer (now partially eroded) parallel to the main migmatitic foliation, outlined by green line in Fisheries Bay Headland. An earlier isoclinal fold of the migmatitic fabric and compositional layering (outlined by red line) appears “drawn into” the neck area between two boudins in the boudinaged mafic layer. Compass for scale is 10 cm long.

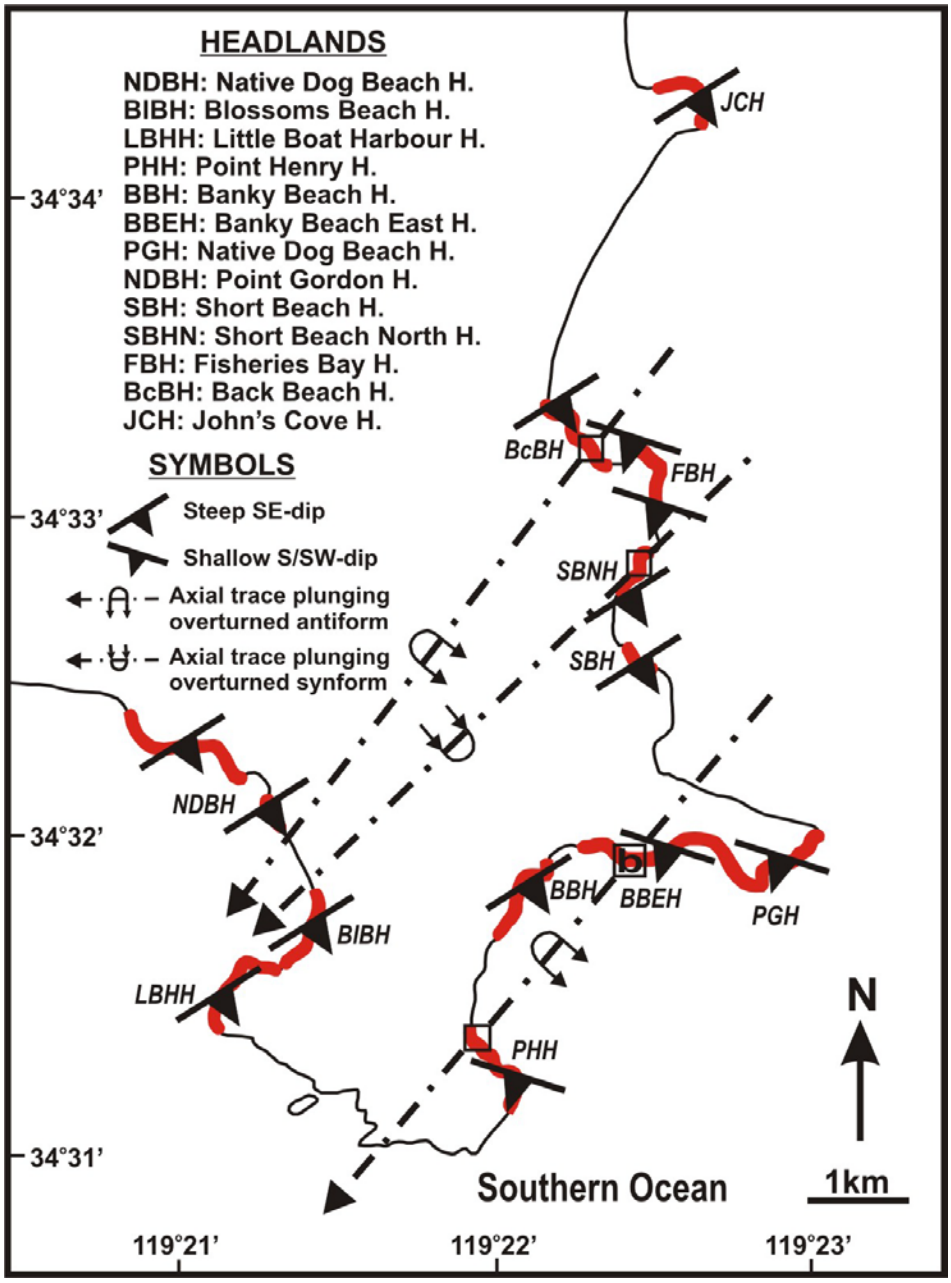

Figure 2.7a. Location of axial traces for three regional, kilometer-scale, asymmetric, NW-verging, SW-plunging, overturned folds of the migmatitic foliation. Two antiformal traces, exposed in the field area, and one hypothetical synformal trace have been drawn. The pattern of the migmatitic foliation: (a) NE-trending and moderately to steeply SE-dipping; and (b) NW-trending and shallow SW- to S-dipping, is represented for the areas mapped along the peninsula. Three boxed areas in Point Henry, Banky Beach East (see Figure 2.7b) and Back Beach headlands represent areas where more or less continuous outcrop exposes the limbs and/or the hinge region of the two regional antiforms. Mapped headlands are highlighted in red.

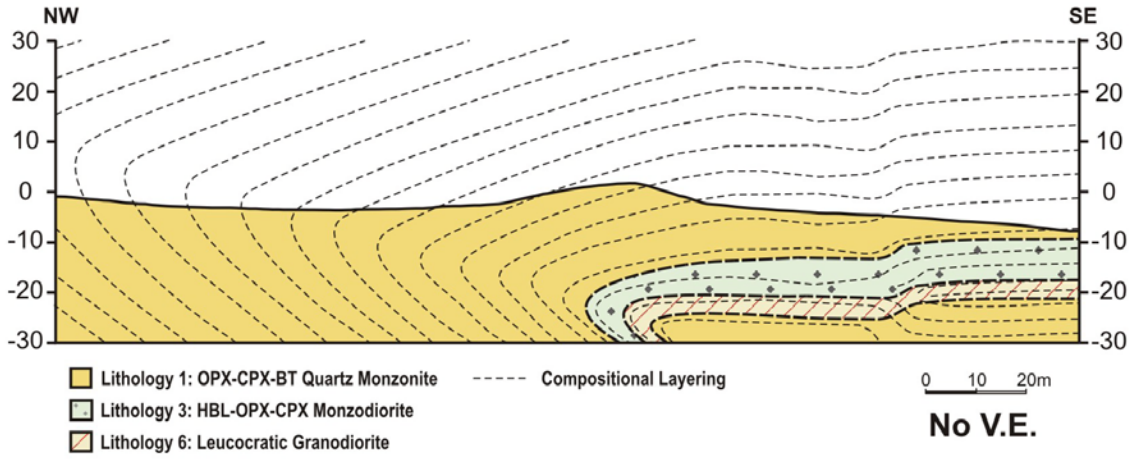

Figure 2.7b. NW-SE geologic cross-section across the northern end of Banky Beach East Headland (see boxed area labeled with "b" along Banky Beach East Headland in Figure 2.7a), where continuous outcrop exposes both limbs and the hinge region of the southernmost regional antiform in the Bremer Bay Area.

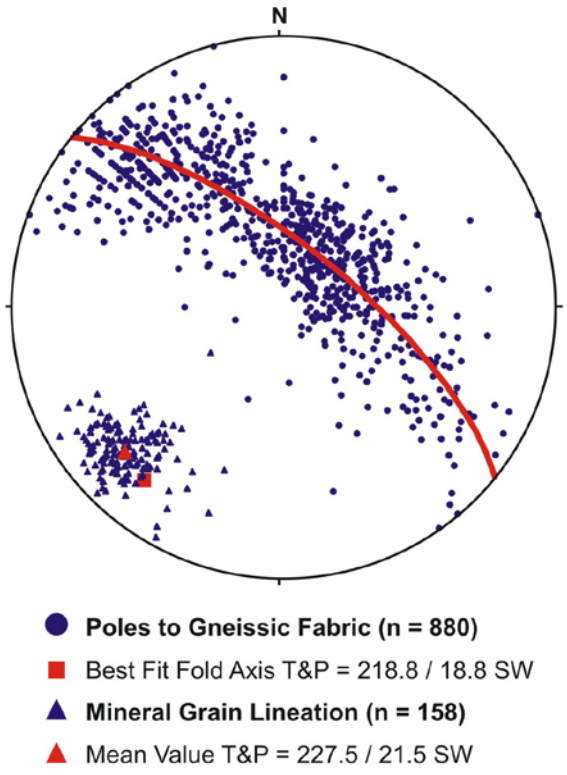

Figure 2.8. Lower hemisphere, equal area stereonet of poles to the migmatitic foliation and mineral grain lineation. The average orientation of the fold axes that fold the migmatitic foliation trends 219 and plunges 19° to the SW. The average mineral grain lineation trends 227 and plunges 21° to the SW.

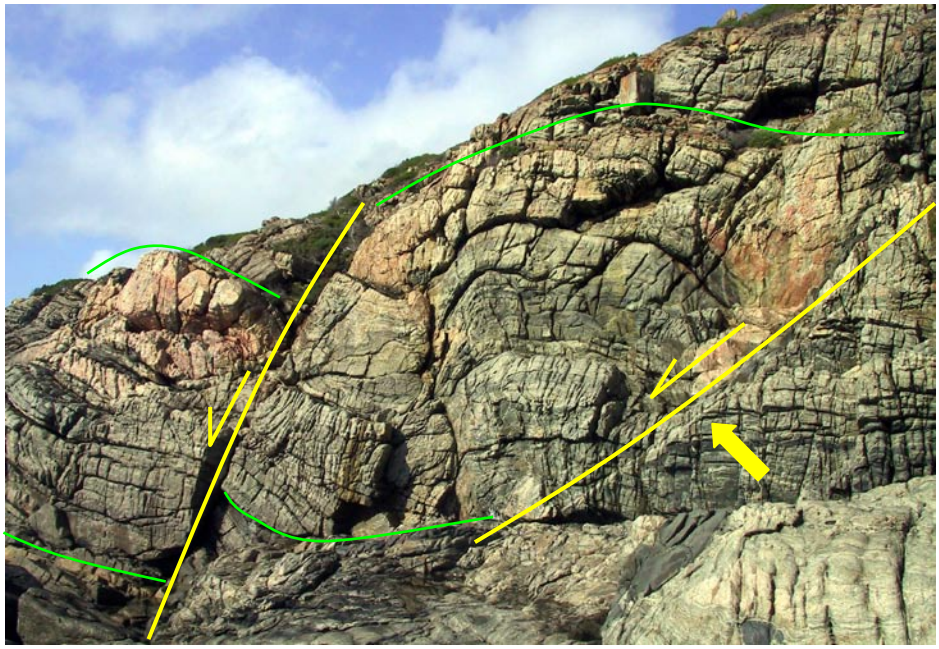

Figure 2.9. Decameter-size NW-trending asymmetric domino-style torn boudins of the migmatitic foliation and compositional banding. The boudins appear offset by normal shear zones, one of which (listric) is intruded by a felsic (white) pegmatitic melt (arrow). Felsic (pink) pegmatitic melt is present in the boudin neck areas. Fisheries Bay Headland.

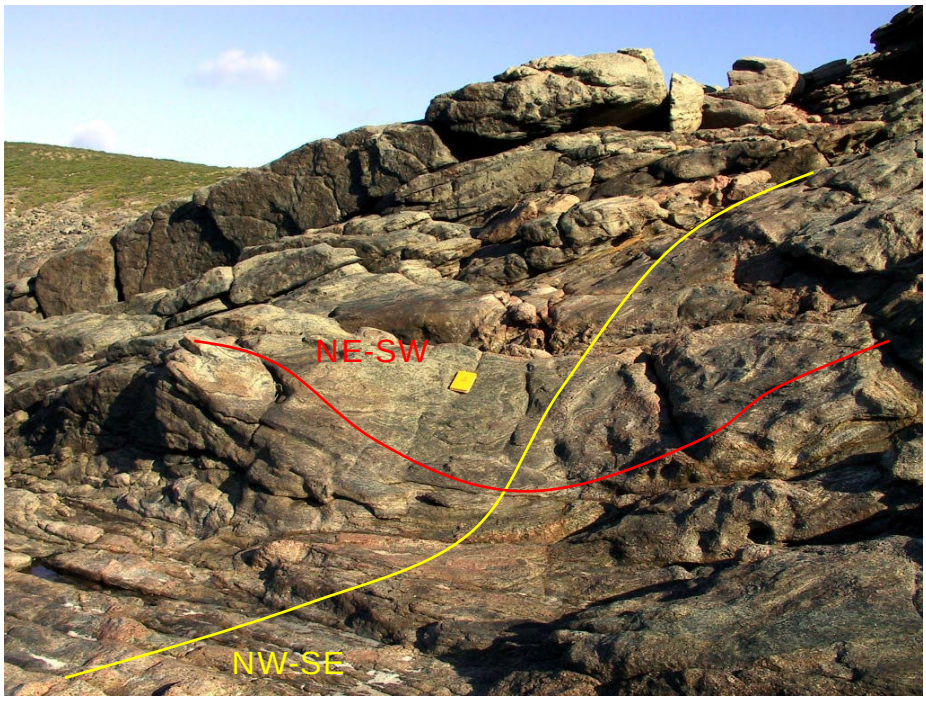

Figure 2.10. Hummocky topography resulting from the interference of NW and NE-trending boudin sets on the surface at Point Gordon Headland. Field book for scale is 19 cm long.

Figure 2.11. Meter-sized, slightly asymmetric, moderately tight, steeply SW-plunging fold of the migmatitic foliation at Banky Beach East Headland, formed during the latest folding phase in the Bremer Bay area. Field book for scale is 19 cm long.

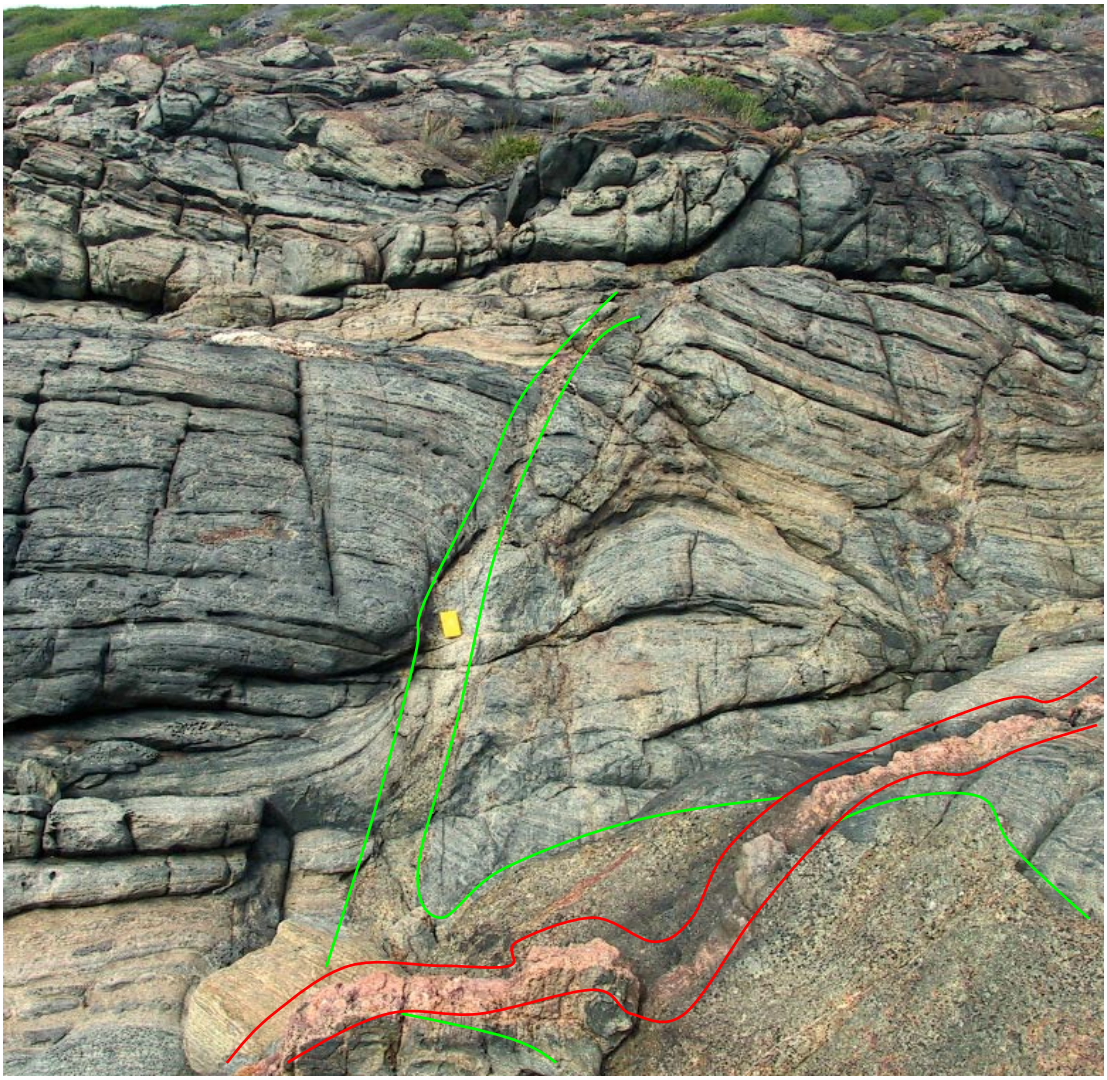

Figure 2.12a. Cross-cutting relationships between late melts of different chemistry at Fisheries Bay Headland. A N-NW trending intermediate (green in color) late melt band (outlined green) cuts through migmatitic fabric and intrudes through the neck area between two decameter-sized boudins. The boudins are offset by a normal shear zone; the intermediate melt intrudes along part of this zone but cross cuts the boudin near the top indicating it intruded at a later time. A NW-trending felsic (reddish pink to pale pink in color) late pegmatitic melt (outlined red) cuts across the N-NW trending intermediate melt band. Note nested boudins at the top of the hill. Field book for scale is 19 cm long.

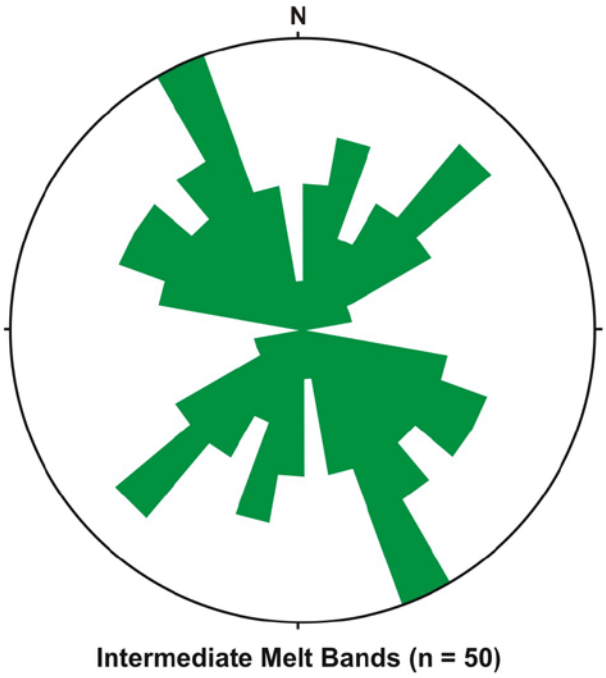

Figure 2.12b. Rose diagram showing dominant N-NW and NE trends for intermediate composition (green in color) late melt bands intruded in the Bremer Bay area.

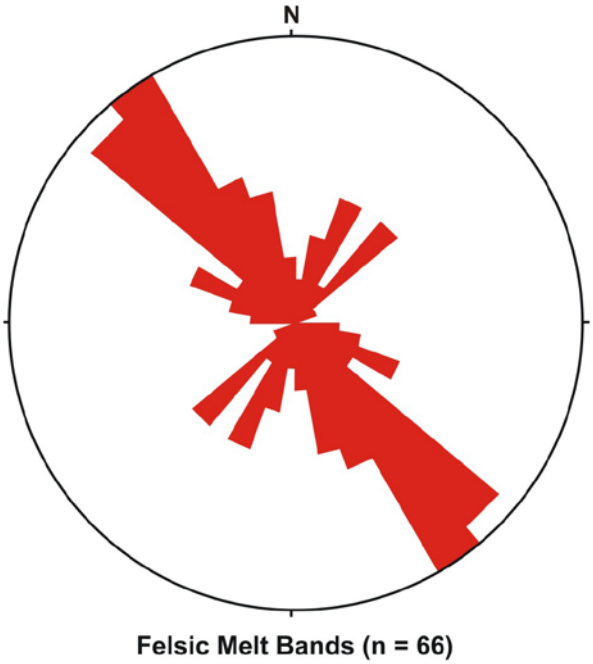

Figure 2.12c. Rose diagram showing dominant NW and weak NE trends for felsic (reddish pink to pale pink in color) late melt bands intruded in the Bremer Bay area.

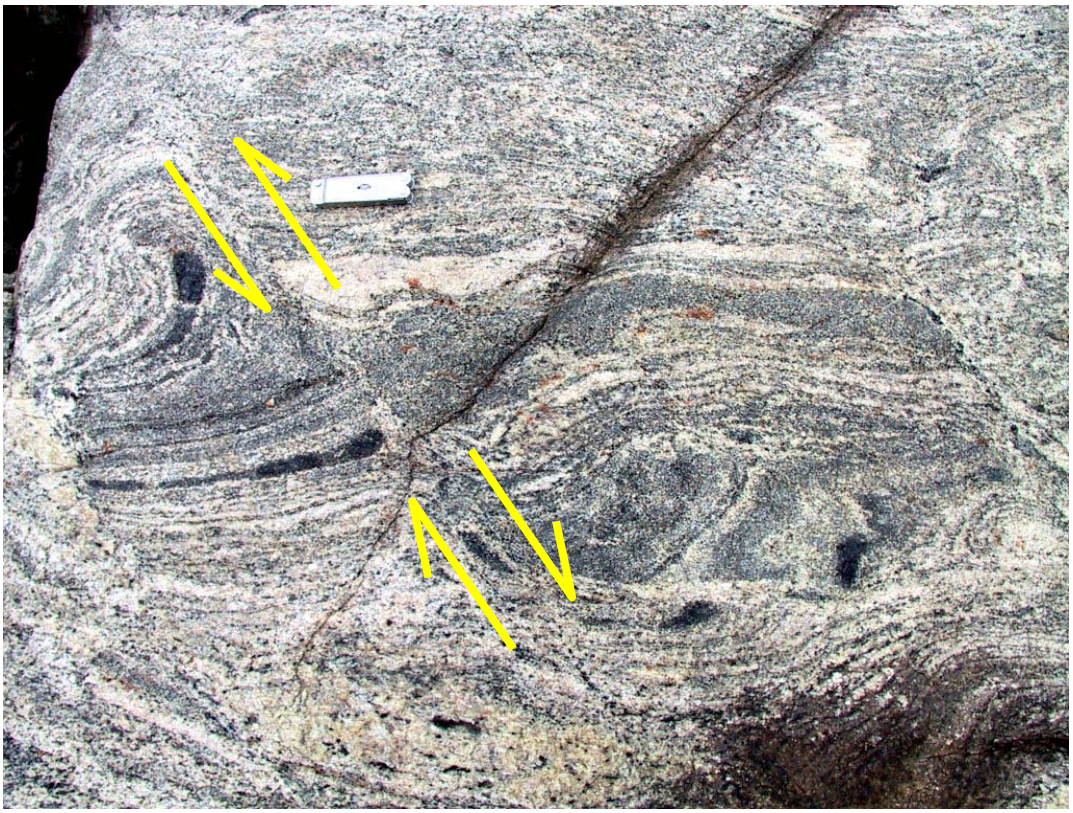

Figure 2.13. Small shear band with leucosome (former melt) present in the shear plane in Fisheries Bay Headland. Shear sense changes along strike of the shear plane from right-lateral to left-lateral. It offsets the migmatitic foliation, compositional layering and small, centimeter-sized boudins of mafic layers parallel to the main migmatitic fabric. Pocket knife for scale is 7 cm long.

Figure 2.14. Coarse-grained granodiorite intruding the neck of a decameter-size NW-SE trending boudin set with crystallization age and best estimate of synchronous high-grade metamorphism of 1178 ± 3 Ma. Fisheries Bay Headland. Sledge hammer for scale is 45 cm long.

Figure 2.15. Pegmatitic granodiorite intruded into the neck of an intermediate, meter-size NE-SW trending boudin set with a crystallization age of 1187 ± 5 Ma and high-grade metamorphic age of 1172 ± 16 Ma. Point Henry Headland. Sledge hammer for scale is 45 cm long.

Figure 2.16. Unmetamorphosed coarse-grained leucogranite intruded in the neck of a meter-sized NW-SE trending boudin set with an igneous crystallization age of 1148 ± 9 Ma. Short Beach North Headland. Sledge hammer for scale is 25 cm long.

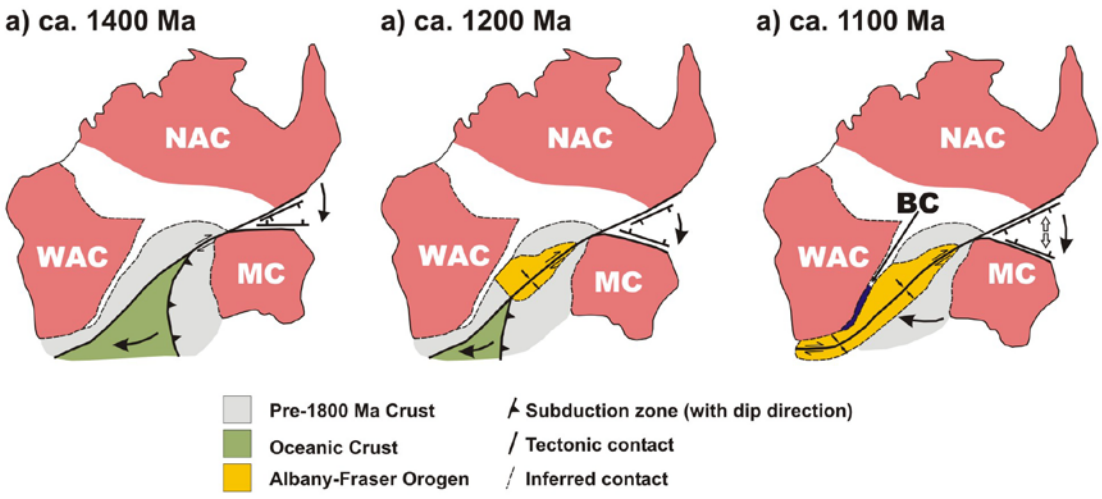

Figure 2.17. Tectonic model for closure of an asymmetric ocean basin between the West Australian Craton (WAC) and the Mawson Craton (MC, and its South Australian counterpart) prior to and during the Albany-Fraser Orogeny (modified after Bodorkos and Clark, 2004b). The location of the Biranup Complex (BC) of the Albany-Fraser Orogen is noted. (a) Clockwise asymmetric motion of an E-dipping subduction zone towards the West Australian Craton, with corresponding rifting on the margin between the Mawson Craton and the North Australian Craton (NAC). (b) Continued closure of the asymmetric ocean basin between the West Australian and Mawson Cratons resulted in a diachronous Albany-Fraser Orogen during Stage I of the orogeny. Complete closure of the ocean basin took place on the eastern side of the orogen, where it resulted in NW-oriented collision and/or dextral transpression. Subduction was ongoing on the western side of the orogen, and acted as the driving force for continued NW-oriented contraction. (c) Complete closure of the ocean basin between the West Australian and Mawson Cratons was achieved towards the end of Stage II of the orogeny, and resulted in renewed NW-oriented collision and/or dextral transpression throughout the length of the orogen.

Summary of SHRIMP U-Pb Zircon Geochronology, Fisheries Bay Headland	
Protolith Lithology (sample GSWA 184311)	opx-cpx-biotite quartz monzonite orthogneiss
Protolith Crystallization Age	1680 ±7 Ma
Protolith high-grade metamorphic age	No age obtained
Bidirectional boudinage phase intruded by neck melt	Dm-size, NW- trending boudins
Boudin Neck Orientation	NE-SW
Boudin Neck Melt Lithology (sample GSWA 184310)	leucocratic granodiorite (metamorphosed)
Boudin Neck Melt crystallization age	1178 ± 3 Ma
Boudin Neck Melt high-grade metamorphic age	1178 ± 3 Ma

Table 1. Summary of SHRIMP U-Pb Zircon Geochronology from Fisheries Bay Headland, Bremer Bay. Complete ion microprobe analytical results, and cathodoluminescence (CL) images and descriptions of the zircons from each of the two samples dated are given in Bodorkos and Wingate (2008g, h).

Summary of SHRIMP U-Pb Zircon Geochronology, Point Henry Headland	
Protolith Lithology (GSWA 184119)	leucocratic quartz monzonite orthogneiss
Protolith Crystallization Age	1670 ±12 Ma
Protolith high-grade metamorphic age	1178 ± 4 Ma
Bidirectional boudinage phase intruded by neck melt	meter-sized NE- trending boudins
Boudin Neck Orientation	NW-SE
Boudin Neck Melt Lithology (sample GSWA 184307)	pegmatitic granodiorite (metamorphosed)
Boudin Neck Melt crystallization age	1187 ± 5 Ma
Boudin Neck Melt high-grade metamorphic age	1172 ± 16 Ma

Table 2. Summary of SHRIMP U-Pb Zircon Geochronology from Point Henry Headland, Bremer Bay. Complete ion microprobe analytical results, and cathodoluminescence (CL) images and descriptions of the zircons from each of the two samples dated are given in Bodorkos and Wingate (2008e, f).

Summary of SHRIMP U-Pb Zircon Geochronology, Short Beach Headland	
Protolith Lithology (GSWA 184312)	medium-grained leucocratic granodiorite
Protolith Crystallization Age	1689 ± 11 Ma
Protolith high-grade metamorphic age	1154 ± 25 Ma
Bidirectional boudinage phase intruded by neck melt	meter-sized NW- trending boudins
Boudin Neck Orientation	NE-SW
Boudin Neck Melt Lithology (sample GSWA 184326)	pegmatitic granodiorite (unmetamorphosed)
Boudin Neck Melt crystallization age	1148 ± 9 Ma
Boudin Neck Melt high-grade metamorphic age	N.A.

Table 3. Summary of SHRIMP U-Pb Zircon Geochronology from Short Beach Headland, Bremer Bay. Complete ion microprobe analytical results, and cathodoluminescence (CL) images and descriptions of the zircons from each of the two samples dated are given in Bodorkos and Wingate (2008i, j).

Chapter 3. Bidirectional extension in granulite-facies orthogneisses of the Biranup Complex, Bremer Bay, Western Australia: implications for progressive lithospheric delamination during the Albany-Fraser Orogeny.

3.1 Abstract

Mid-crustal granulite-facies migmatitic orthogneisses of the Grenville-aged Albany-Fraser Orogen, in the locality of Bremer Bay, southwestern Australia, record three phases of widespread, pervasive bidirectional extension ca. 1180 Ma, during Stage II (1215-1140 Ma) of the Albany-Fraser Orogeny, a period of NW-directed orogenic contraction. Three phases of coeval bidirectional extension formed three generations of NW- and NE- trending boudins of progressively increasing size, from centimeter to decameter in length. Bidirectional boudins alternate with shortening and/or shear related folding phases, which resulted in the formation of decimeter- to kilometer-sized folds. The first two phases of bidirectional extension resulted from breakoff of a subducting slab in the western part of the orogen. Breakoff of a subducting slab and possible lithospheric delamination caused ascent of asthenospheric material into mid-crustal levels, allowing for extensive partial melting and granulite-facies, high-temperature and medium-pressure metamorphic conditions, isostatic uplift and extension. Traction imposed by upwelling asthenospheric material coupled with isostatic uplift would result in a bidirectional extension response in the overlying crust, with: (a) extension parallel to the main convergence direction (NW-SE); and (b) coeval extension in the orthogonal direction (NE-SW) due to flow of rising asthenospheric material around the edges of the detaching slab. NW-directed orogenic contraction is re-established after catastrophic slab breakoff, resulting in the formation of kilometer-scale folds. Decameter-scale boudins formed after regional-scale folding during a third phase of coeval bidirectional extension could have resulted from orogenic collapse following complete closure of the intracratonic ocean basin between the West Australian and the Mawson cratons.

3.2 Introduction

Since the 1980's, significant research has greatly increased our understanding of mid- to upper crustal extension, most notably with respect to metamorphic core complexes and detachment fault systems and to rifting leading to passive margins and sedimentary basins (e.g. Davis and Coney, 1979; Davis et al., 1986; Lister and Baldwin, 1993; Hopper and Buck, 1996; Ruppel, 1995; MacCready et al., 1997; Müntener et al. 2000). The processes involved in mid- to lower crustal extension have been investigated through field studies (e.g. Lister and Davis, 1989; Wernicke, 1990; Westaway, 1998), and using geodynamic and analogue modeling (e.g. Brun and Tron, 1993; Boutilier and Keen, 1994; Ryan and Soper, 2001; Harris and Koyi, 2003; Huismans et al., 2005) and seismic imaging of areas affected by extension (e.g. Eaton et al., 1995; Kruger and Johnson, 1994; Korja and Heikkinen, 1995).

Most models, seismic imaging, and field studies of crustal extension have only considered the 2D kinematics of strain. Those that have investigated the 3D strain, either in the field or theoretically, have concluded that any divergence from plane strain is constrictional (e.g. Fletcher and Bartley, 1994; Chauvet and Séranne, 1994; Terry and Robinson, 2003; Kurz, 2005; Osmundsen et al., 2006). In contrast, a recent study by Perry (2005) of the Tanque Verde Ridge, a corrugation on the Catalina core complex in south-central Arizona, has documented bidirectional extension that produced large (up to 100 meters in length) boudins in two directions that formed during the transition from ductile to brittle conditions during unroofing. This result suggests that at least some corrugations on metamorphic core complexes could be the result of bidirectional extension that initiated in mid- to lower crust. Such bidirectional extension is compatible with many models for or that invoke mid- to lower crustal extension (e.g., Fossen, 1992; Burg and Ford, 1997; Schott and Schmeling, 1998; Koyi et al., 1999).

This chapter presents evidence for bidirectional extension (extension in orthogonal directions) associated with granulite-facies metamorphism and extensive partial melting concurrent with orogenic contraction in Mesoproterozoic granulite-facies orthogneisses of the Albany-Fraser Orogen in the locality of Bremer Bay, in Western

Australia (Figure 1.1, Chapter 1). Rocks in the Bremer Bay area display field evidence for three phases of widespread, bidirectional extension that took place during overall orogenic-wide contraction ca. 1180 Ma. These three phases of bidirectional extension recorded in mid- to lower-crustal orthogneisses in the Bremer Bay area are related to progressive breakoff of a relict subducting slab and possible associated lithospheric delamination during ongoing orogenic contraction.

3.3 Geologic Setting

The Albany-Fraser Orogen is a collisional Grenville-aged belt located along the southern margin of the Archean (3 – 2.6 Ga) Yilgarn Craton in southwestern Australia (Figure 1.1, Chapter 1). The orogen is currently interpreted to be the result of collision between the West Australian Craton and the Mawson Craton of eastern Antarctica ca. 1.3 Ga (Clark et al., 2000; Dawson et al., 2002; Fitzsimons, 2003). Two main Mesoproterozoic tectonothermal events have been identified in the Albany-Fraser Orogen based upon structural, petrographic and geochronological (SHRIMP zircon, monazite and rutile) work: Stage I, from 1345-1260 Ma, and Stage II, from 1215-1140 Ma (Clark et al., 2000). Stage I is associated with NW-directed orogenic contraction during cratonic collision, while Stage II has been interpreted as the result of intracratonic reactivation (Clark et al., 2000; Bodorkos and Clark, 2004b). Radiometric evidence for Stage II exists on both western and eastern parts of the Albany-Fraser Orogen, whereas Stage I appears restricted to the eastern part of the belt. Chapter 2 of this dissertation proposes that the Albany-Fraser is a diachronous orogen, in which Stage I of the orogeny records the collision between the West Australian and Mawson cratons on the eastern end of the orogen, while subduction is ongoing on the western end of the orogen. This tectonic setting explains the occurrence of Stage I contractional deformation on the eastern part of the belt, and the absence of such deformation on the western part. Stage II records the collision between the West Australian and Mawson cratons on the western part of the orogen during the final closure of an asymmetric ocean basin between these two cratons. Therefore Stage II deformation would be the first phase of NW-directed contraction

recorded on the western part of the belt, and would be recorded as renewed NW-directed convergence on the eastern part of the belt.

The Albany-Fraser Orogen has been divided into four different lithotectonic units (Figure 1.1, Chapter 1) (Myers, 1990; Myers 1995): (1) Northern Foreland, which comprises 3-2.6 Ga old gneisses from the southern margin of the Yilgarn Craton structurally and thermally reworked during the Albany-Fraser Orogeny, as well as two Paleoproterozoic metasedimentary units that were thrust northwards over the Archean gneisses; (2) Biranup Complex, which includes ca. 1.6 Ga amphibolite- to granulite-facies orthogneisses thrust over the southern margin of the Yilgarn Craton; (3) Nornalup Complex, apparently thrust onto the southern margin of the Biranup Complex, which includes a ca. 1.5-1.2 Ga assembly of varied lithologies, including granites, ortho- and paragneisses; and (4) Fraser Complex, which consists of a thrust package of granulites of mainly gabbroic composition derived from at least three different mantle sources and with geochemical anomalies consistent with an oceanic arc origin (Condie and Myers, 1999).

This field study was conducted in the locality of Bremer Bay on the western part of the orogen (Figure 1.1 in Chapter 1, and Figure 2.1 in Chapter 2), where the rocks are granulite-facies, felsic to intermediate, migmatitic orthogneisses of the Biranup Complex, which have been partially to completely retrograded to amphibolite-facies assemblages. As discussed in Chapter 2 of this dissertation, deformation of rocks of the Biranup Complex in the Bremer Bay area took place ca. 1180 Ma during Stage II of the Albany-Fraser Orogeny.

3.4 Metamorphic Conditions

Deformation in Bremer Bay took place at granulite-facies conditions, and partial melts were generated and emplaced during all stages of deformation and continued to migrate through the country rock after ductile deformation ceased. Granulite facies mineral assemblages include orthopyroxene, clinopyroxene, plagioclase, and locally garnet, and comprise the leucosome and residuum–rich layers within the country rock as

well as the pegmatitic material within boudin necks, axial planes of folds, and shear bands. Later retrogression to amphibolite-facies conditions is recorded by partial to complete replacement of orthopyroxene and clinopyroxene by hornblende. This retrogression apparently occurred after all or nearly all of the deformation described below. Melts associated with late structures contain evidence of earlier granulite-facies mineralogies, with the exception of the very last crosscutting felsic pegmatites. Black et al. (1992) conducted geothermometry on a late pegmatite axial planar to what they describe as a late-stage fold generation from Fisheries Bay Headland (Figure 2.1 in Chapter 2) and on a pegmatite in a late stage shear band at Short Beach. They obtained a temperature of 900°C using the two-pyroxene thermometer of Lindsley (1983) for mineral rims and temperatures as high as 1000°C for Al-enriched clinopyroxene cores. Using the calcic amphibole-plagioclase geothermometer of Blundy and Holland (1990), they obtained a temperature of 800°C ± 75°C, most likely recording the later retrogression. Only the very last stage of folding has styles indicative of lower temperatures and no associated melts.

3.5 Bidirectional Extension

Granulite-facies orthogneisses of the Biranup Complex in the Bremer Bay area display field evidence for three phases of bidirectional extension during overall orogenic contraction related to Stage II of the Albany-Fraser Orogeny. Bidirectional extension resulted in the formation of coeval NW- and NE-oriented boudins of compositional layering and/or migmatitic foliation with qualitatively the same magnitude of extension in both orientations. Boudin size increased with time reaching decameter scales.

3.5.1 First bidirectional extension phase

The earliest extensional structures observed in orthogneisses in the Bremer Bay area are small, centimeter to decimeter, square to rectangular boudins of mafic-rich layers parallel to the dominant migmatitic fabric (Figure 2.4 in Chapter 2). The layers range in thickness from 2-3 centimeters up to 10 centimeters and may represent original mafic

layers, sills or residuum from partial melting. These boudins are common throughout the entire field area, and nearly all centimeter- to decimeter-scale mafic layers show evidence of this early extension. The boudins are dominantly symmetric torn blocky boudins, either equidimensional or elongate (from 2:1 up to 10:1 length to width ratio), but always displaying no to very slight curvature in the inter-boudin faces. These boudins are observed in two orthogonal directions in the field, indicating both NW-SE and NE-SW extension (Figure 2.4a in Chapter 2). No differences in dimensions and style or cross cutting relationships are observed. As can be seen in Figure 2.4b in Chapter 2, commonly leucosomes (former melt) fill the neck areas of these small boudins, and the foliation in the adjacent layers is not deflected into the neck region regardless of the amount of extension. Locally leucosomes are observed along the boudinaged layer as well. The contact between the boudins and leucosomes is commonly sharp (Figure 2.4b in Chapter 2). Leucosomes are felsic, containing mostly plagioclase, quartz, and locally potassium feldspar.

Centimeter-wide and few-centimeter-long shear bands, with or without shear-plane leucosomes, offset early square boudins of foliation-parallel mafic layers (Figure 3.1). If present, leucosomes are commonly felsic (white in color) and show diffuse boundaries with the host orthogneiss. In many locations these leucosomes display textural continuity with leucosomes defining the migmatitic foliation (Figure 3.1).

The existence of these boudins in two orthogonal directions, with no observable crosscutting relationships or change in style or size, indicates that they formed coevally as a result of NW- and NE-directed extension. The symmetrical nature of most boudins indicates extension parallel to the layers, with the less common asymmetrical offsets most likely the result of later reorientation and reworking during folding or later larger-scale boudinage (Figure 3.1). Their blocky shape suggests a high competency contrast between the boudinaged mafic layers and the surrounding lithology during extension. The presence of abundant leucosomes associated with the boudinaged layers indicates that bidirectional extension took place at temperatures high enough for the rocks to undergo partial melting, with melt migrating towards and pooling into boudin necks. In addition,

the lack of flow of the migmatitic foliation into boudin necks implies that extension parallel to layers, rather than perpendicular shortening, was the primary cause of the bidirectional boudinage.

3.5.2 Second bidirectional extension phase

A second generation of extensional structures forms intermediate-scale (few decimeters up to a few meters in length) boudins of the migmatitic foliation and compositional layering. These structures are demonstrably later because folds of first generation boudins are boudinaged by this generation of extensional structures (see Chapter 2 of this dissertation). The first-generation boudins are also affected by these intermediate-scale boudins (Figures 2.4b, 3.2). These boudins are also observed throughout the entire field area and form in two orthogonal orientations, NW-SE and NE-SW. They display several different morphologies:

(1) Symmetric drawn boudins, where the foliation tapers into and is generally continuous across the boudin neck (Figure 3.2), show moderate flow of the adjacent rock migmatitic foliation into boudin necks. These boudins vary in size from a few decimeters up to a meter in length and are the most common boudin morphology observed throughout the field area.

(2) Symmetric meter-sized torn boudins that have convex faces on the inter-boudin plane (Figure 3.3) show limited to no deflection of the adjacent rock migmatitic foliation into the boudin neck. These boudins appear only locally in the field area.

(3) Asymmetric shear-band boudins, with flanking shear bands on the inter-boudin planes (Figure 3.4) display top-down to the NE and top-down to the SW asymmetries. Boudins vary in size from a few decimeters up to a few meters in size and appear throughout the entire field area.

(4) “Pinch and swell” structures, where actual boudin blocks are not well defined (Figure 3.5), display limited deflection of the adjacent rock migmatitic foliation into

boudin necks. These structures are also variable in size, from a few decimeters up to a few meters and are common throughout the field area.

These four different morphologies of intermediate boudins are not associated with any specific lithology in the field area, or with a specific geographic location. The same lithological unit can display intermediate bidirectional boudins of different morphologies within the same headland or on different headlands in the field area. Generally boudins affect a more competent layer or package of layers, but in many localities, foliation boudinage is prevalent, forming decimeter-scale boudin blocks of the migmatitic foliation with no apparent competency contrast (Figure 3.6).

Intermediate bidirectional boudins of all sizes are present throughout the entire field area, but are more easily observed in those headlands along the Bremer Bay peninsula where the foliation and compositional banding strike NE-SW and dip steeply to the SE (Figure 2.7a in Chapter 2). These headlands display continuous exposures of transverse sections of intermediate NE-trending boudin trains with steeply SE-plunging neck axes. In these areas, intermediate NW-trending boudin trains with shallowly SW-plunging neck axes are clearly seen when foliation planes and compositional layering boundaries are exposed by differential weathering.

Boudin necks can be filled by flow of the adjacent rock migmatitic foliation into the necks, by leucosomes, or, in many cases, by a combination of both (Figure 3.7). Leucosomes in boudin necks are felsic (plagioclase, potassium feldspar and some quartz) to intermediate (intermediate plagioclase, hornblende, pyroxene and some quartz), medium- to coarse grained, and display either diffuse or discrete (more common) boundaries with the surrounding orthogneisses. Diffuse leucosomes in boudin necks appear to be derived from leucosomes in the compositional banding that defines the migmatitic fabric, where melt along the foliation pools into boudin necks during extension, or from in situ partial melting (Figure 3.8). Discrete leucosomes display several different morphologies. Some are irregular bodies that intrude dominantly into the neck area of boudins (Figure 3.7), whereas others are straight-edged veins that cut the foliation (Figure 3.9). In some cases, discrete leucosomes parallel the boudinaged layer

(and migmatitic foliation) and fill boudin necks of the same boudinaged layer (Figure 3.10).

NE-trending intermediate boudins of the migmatitic foliation and compositional layering exposed in headlands with steeply SE-dipping migmatitic foliation (Figure 2.7a in Chapter 2) are commonly offset by conjugate sets of high-angle decimeter- to meter-scale shear bands with dip-slip motion, some without leucosomes present along the shear planes, and some with associated felsic (more dominant) and locally intermediate leucosomes, which display top-down to the NE or top-down to the SW sense of shear (Figure 3.11). These shear bands can appear as locally well defined, narrow, centimeter-wide bands that disrupt the migmatitic foliation, or can be defined by deflection of the migmatitic fabric and compositional layering into a wide zone of shear without a localized shear plane. Where present, leucosomes are apparently felsic (white to pale pink in color) to intermediate (pale green in color), with diffuse to sharp boundaries with the host orthogneiss. Leucosomes with diffuse boundaries display textural continuity with leucosomes defining the migmatitic foliation, and their apparent chemistry is thus controlled by the chemistry of the leucosomes defining the migmatitic foliation. Diffuse leucosomes in textural continuity with leucosomes in the migmatitic foliation are commonly leucocratic (apparently felsic), as leucosomes defining the migmatitic fabric throughout the field area are dominantly leucocratic. Melanocratic (intermediate, pale green in color) diffuse leucosomes in textural continuity with foliation leucosomes appear in one localized area in Fisheries Bay Headland (Figure 2.7a in Chapter 2; Plate 11) where the host quartz-monzonite orthogneiss locally develops apparently intermediate (pale green in color) leucosomes defining the migmatitic fabric.

The size of intermediate bidirectional boudins is rather variable, from a few decimeters up to a few meters in scale, and locally in the field area it is possible to see the interaction of consecutive generations of these boudins, such as decimeter-scale intermediate boudins contained within meter-scale intermediate boudins (Figure 3.12), and pegmatitic pull-apart bands intruded into intermediate boudin neck areas that are boudinaged by later intermediate boudins (Figure 3.13). This sequence of different

boudin block geometries, sizes and components is evidence of progressive bidirectional extension, in which sequential generations of intermediate bidirectional boudins formed during progressive orthogonal stretching of the orthogneisses.

The formation of different generations of intermediate bidirectional boudins in two orthogonal directions suggests that they formed coevally as a result of NW- and NE-directed extension (Stereogram in Plate 1). Most intermediate boudins are symmetrical, which points to layer-parallel extension. Asymmetric shear-band boudins may have resulted from later reworking due to shear or folding, may represent local zones of shear, or may be locations where layering was oblique to the extension direction. The lensoidal or drawn morphology of most intermediate boudins, and the common occurrence of "pinch and swell" boudins, suggests that there was a low competency contrast within the compositional layering of the orthogneisses during deformation. The largest of the intermediate-scale boudins also tend to be the result of foliation boudinage. Rare symmetric torn boudins point to localized high competency contrast within orthogneisses during deformation, as they boudinage foliation-parallel mafic layers contained within the host orthogneisses. The presence of leucosomes associated with boudinaged layers suggests that bidirectional extension occurred at temperatures high enough to allow for partial melting of the orthogneisses, with melt migrating along migmatitic foliation planes and pooling or intruding into boudin neck areas, or forming in situ. The most common intermediate boudins that display moderate flow of the migmatitic foliation into boudin neck areas suggest a higher degree of layer-parallel shortening than for the first extensional phase of bidirectional extension. This moderate flow, common presence of leucosomes in the boudin necks, and presence of boudins with no flow into the neck regions, however, indicates that layer-parallel extension is still the dominant mechanism responsible for boudinage. The existence of conjugate sets of high-angle, top down-to-the-NE and top down-to-the-SW decimeter-scale shear bands that offset NE-trending intermediate boudins of the migmatitic fabric also indicates layer-parallel extension.

3.5.3 Third bidirectional extension phase

A third generation of extensional structures forms large, decameter-sized boudins of the migmatitic foliation and compositional layering, which appear in orthogonal NW-SE and NE-SW orientations. Unlike the previous two generations that appear throughout the field area regardless of foliation attitude, these boudins are visible only in areas with NW-trending, shallow SW-dipping migmatitic foliation and not on the steeply dipping overturned limbs of regional folds (see section 3.6.2 for description of regional-scale folds) (Figure 2.7a in Chapter 2). This localization of boudinage on shallow dipping limbs indicates these boudins formed after the regional folding whereas the other two generations are folded and thus reoriented by the regional folds.

These boudins exhibit different morphologies. Most are nested boudins that result from foliation boudinage, but locally more competent layers form boudins.

(1) Symmetric drawn boudins, in which the foliation within boudins tapers into and is generally continuous across the boudin neck (Figure 3.14), show significant flow of the adjacent rock foliation into boudin neck areas.

(2) Symmetric, lensoidal to convex-faced torn boudins, in which individual boudins display faces that are drawn into the boudin neck area, generally show moderate to limited flow of the adjacent rock foliation into boudin necks (Figure 3.15). The foliation within the boudinaged layers is generally truncated by the boudin faces but may also be drawn into the neck regions. Where significant extension has occurred, the neck area is predominantly filled by flowage of the adjacent rock foliation.

(3) Asymmetric, domino-style, torn boudins, usually blocky (straight inter-boudin faces) or barrel-shaped (slightly convex inter-boudin faces), show no flow of the adjacent rock foliation into boudin neck areas and are seen only in Fisheries Bay Headland (Figures 3.16 and 3.17). Foliation within the boudins is usually truncated, especially where offsets are at a high angle, but in some cases shows deflection into the shear plane.

Only two headlands in the Bremer Bay area, Point Gordon and Fisheries Bay (Figure 2.1 in Chapter 2), display near vertical cliff cross-section exposures of decameter-sized boudins. In these two headlands, decameter-sized boudins appear nested, with boudins resting on the neck areas of underlying boudin trains (Figures 3.14 and 3.17). Nested boudins exposed in Point Gordon Headland are drawn boudins, whereas nested boudins exposed in Fisheries Bay Headland display any of several different morphologies within one set of nested boudins: symmetric drawn, symmetric lensoidal torn, symmetric convex-face torn, asymmetric blocky and asymmetric barrel-shaped. In Fisheries Bay Headland, asymmetric boudins appear offset by high-angle and listric normal shear zones (Figure 3.17). The size of large boudins also changes within nests, with larger boudins commonly located topographically lower and smaller boudins (sometimes three or four meters in size) topographically higher within a nest.

In outcrops where adequate vertical cross-section exposures of nested boudins are lacking, decameter-size boudins can be most easily identified in areas of shallow dipping foliation by their topographic expression. As a result of the interference of NW and NE-trending boudin sets on the surface, topography has a “hummocky” appearance, with domes and troughs corresponding to the top of boudins and boudin neck areas respectively (Figure 2.10 in Chapter 2). Trains of domes and troughs can be followed in NW and NE directions, and no given set is seen clearly disrupting the other. The amplitude of many late boudins results in an “apparent, openly folded” cross section across the shallow limbs of the regional folds (see cross-sections of Point Henry, Banky Beach East, Point Gordon and Fisheries Bay Headland in Plates 5, 7, 8 and 11 respectively). The geometry of the individual boudins, whether they are drawn or torn, lensoidal or blocky, can have an appreciable topographic expression. Boudins on Point Henry and Point Gordon headlands have more round or tapered edges (Plates 5 and 8), probably reflecting an overall lensoidal shape, whereas boudins in Banky Beach East Headland and Fisheries Bay headlands have sharp, almost “kink-like” edges, suggesting overall blocky boudin shapes.

As seen in boudins from the two previous extension phases, former melts are located in the neck areas of these two sets of boudins. Leucosomes in boudin necks are felsic (granitic and granodioritic) to intermediate (monzogranitic to monzonitic) and medium- to coarse-grained. Boudin neck leucosomes display different morphologies:

(1) irregular bodies that display either diffuse or discrete, sharp boundaries with the surrounding orthogneisses (Figure 3.18);

(2) regular bodies or veins with relatively straight edges and sharp boundaries, though locally some of these grade into diffuse boundaries (Figure 3.18);

(3) diatexite migmatites, in which melt is pervasively distributed throughout the orthogneiss disrupting the migmatitic foliation.

No boudin neck leucosomes were seen cross-cutting in the field or cutting across an orthogonal set of decameter-sized boudins. Most leucosomes and pegmatitic bodies observed where two orthogonal boudins meet to form “basin” or “dome” shaped boudin neck regions displayed irregular shapes. Rarely on flat surfaces, intermediate composition pegmatites in two orthogonal directions form an irregular rectilinear pattern with neither direction offsetting the other (Figure 3.19). These pegmatites could be related to either intermediate or decameter-scale orthogonal boudins, but given their spacing are more likely intermediate. Pegmatitic leucosomes were observed intruding along listric and high-angle shear zones that offset asymmetric torn boudins in Fisheries Bay Headland.

Large, several decimeters-wide and several meters-long shear bands locally offset and/or bound some of the large, decameter-sized boudins (Figures 3.16 and 3.17). These shear bands are normal, commonly high-angle, locally conjugate, and rarely listric, and generally appear brittle, truncating the foliation within the boudinaged layers. Except in rare cases, any deflection into the shear bands is minor. These shear bands typically display pegmatitic leucosomes with sharp boundaries apparently intruded along the shear planes. Pegmatitic leucosomes are of felsic (white) or intermediate (green in color) compositions, and up to several decimeters wide. Locally some of these pegmatitic leucosomes might postdate shearing, as they intrude beyond the lateral extent of shear bands and cut into overlying nested boudins.

Topographic interference patterns of the trains of boudins in NE-SW and NW-SE orientations, and similarity in size suggest that they formed coevally in those two orthogonal orientations. The lack of cross cutting relationships between leucosomes intruding into boudin necks in different orientations and absence of boudin neck leucosomes that disrupt complementary orthogonal boudin trains also indicate that decameter-size boudins result from coeval NE- and NW- directed bidirectional extension. The predominance of symmetrical boudins indicates that layer-parallel extension is the dominant mechanism during boudinage. The large, notably asymmetric boudins with both listric and high angle normal offsets, however, locally accommodated the extension. Symmetrical drawn and lensoidal torn boudins suggest ductile stretch of the boudinaged layer, whereas blocky boudins in which the boudin faces are high-angle surfaces suggest that the boudinaged layer could have been dissected by “brittle” planes of failure. Deflection of the migmatitic foliation of the adjacent rock into boudin neck areas indicates some degree of layer-perpendicular shortening, but the nested structure of most boudins supports extension of this highly anisotropic material as a the primary driving force. The presence of leucosomes in boudin neck areas shows that bidirectional extension took place at temperatures high enough to allow for partial melting of the orthogneisses and migration and emplacement of melts into boudin necks, or melting in situ. Leucosomes intruding along normal high-angle and listric shear bands could have intruded along the shear-band planes during boudinage, although some of them are clearly late melts that postdate boudinage, as they disrupt the migmatitic foliation through different sets of boudins in a nest.

3.6 Extension-concurrent Shortening

Bidirectional extension in granulite-facies orthogneisses of the Biranup Complex in the Bremer Bay area is coeval with NW-directed contraction, interpreted to be driven by ongoing subduction on the western part of the belt during Stage II of the Albany-Fraser Orogeny. NW-directed contraction results in the formation of a very pervasive foliation and three phases of folding that alternate with phases of bidirectional boudinage

in rocks in the Bremer Bay area. Shear-related structures also appear in the Bremer Bay area and could be associated with layer-parallel extension during deformation.

3.6.1 Foliation and early isoclinal folding phase

Throughout the field area, a pervasive migmatitic (gneissic) foliation is defined by both a compositional segregation and parallel alignment of tabular and platy minerals (mainly amphibole and biotite) (Figure 2.2 in Chapter 2). The compositional banding appears as alternating centimeter scale leucosome bands, enriched in felsic or leucocratic minerals, such as plagioclase, potassium feldspar and some quartz, and residuum bands, where mafic minerals, principally pyroxene, hornblende, biotite and opaque minerals, are concentrated. Individual leucosome and residuum bands defining the migmatitic foliation display diffuse boundaries, and are not very laterally continuous. Alignment of leucosome and residuum bands gives the migmatitic foliation its pervasive character.

The migmatitic foliation is locally axial planar to isoclinal folds of centimeter-wide, laterally continuous, discrete leucosomes that differ from the diffuse, discontinuous leucosomes that define the migmatitic foliation (Figure 2.3). These isoclinal folds are less than a meter in amplitude and relatively rare, and most common on the western side of the Bremer Bay peninsula.

3.6.2 Second folding phase

The migmatitic foliation and the small, square boudins of mafic layers formed during the first bidirectional extension phase recorded in the Bremer Bay area are folded by small (few centimeters up to a meter in amplitude) open to isoclinal folds (Figure 2.5 in Chapter 2 and Figure 3.1). The folds are upright to recumbent with a shallow to moderate SW plunge (from 3° to nearly 40°). When overturned, these folds verge dominantly to the NW (Figure 2.5b). The folded layers typically flow towards the hinge areas and attenuate in the limbs. Although the folds are observed throughout the entire field area, they commonly appear localized in zones parallel to sub-parallel to the overall foliation, displaying varying degrees of inclination of their axial planes, from upright to

overturned and locally recumbent. These zones are up to two meters wide and up to ten meters long. In one locality, a shear zone rich in leucosomes contains jumbled pieces of these folds and boudins, indicating complete disruption of the layering because of the abundance of melt in the shear zone (Figure 3.20).

Leucosomes (former melts) are commonly associated with these folds. Leucosomes are felsic (potassium feldspar, quartz and plagioclase) to intermediate (intermediate plagioclase, potassium feldspar, some quartz) in composition, fine- to medium-grained, and commonly intrude along the axial planes. Small, parallel, axial planar leucosomes appear in the hinge areas of the folds, disrupting the folded migmatitic layering (Figure 3.21a). In some folds hinge-area leucosomes form a divergent fan that also disrupts the folded migmatitic layering, suggesting folding continued after emplacement of the leucosomes (Figure 3.21b). Locally the disrupted layering across hinge-area axial planar or radiating leucosomes shows evidence of lateral offset along the former melt planes, which suggests that the leucosomes accommodate some amount of non-coaxial shear. In addition, disrupted layering and boudinaged mafic layers in the hinge areas of these folds are commonly completely surrounded by leucosomes: blocks of disrupted gneissic layering and early small boudins of mafic layers behave as “rafts” floating in former melt, so that they lose their original orientations and appear as disarranged or “jumbled” blocks surrounded by leucosome (Figure 3.21b).

Centimeter-scale blocky boudins of mafic layers folded during the second folding phase locally become asymmetric on one limb of folds and remain symmetrical on the other, or are asymmetrical on both, suggesting that they were rotated during folding (Figure 3.1). These asymmetric boudins can be locally bound by centimeter-scale shear bands with fine-grained felsic to intermediate leucosomes present along the shear bands. Small blocky boudins of mafic layers can also be attenuated along the limbs of these folds: attenuation could be related to shearing by limb-parallel shear bands, with or without leucosomes present along the shear band planes, or could be the result of flow of the folded layers during deformation when no shear bands are present along the fold limbs.

3.6.3 Third folding phase

Regional, km-scale, asymmetric, overturned folds with long shallow limbs affect the Bremer Bay area. Migmatitic foliation either strikes dominantly NE and dips moderately to steeply SE (Native Dog, Blossoms Beach, Little Boat Harbour, Banky Beach, Short Beach, Short Beach North and John's Cove headlands; Figure 2.7a in Chapter 2) corresponding to steeply dipping, overturned limbs of these folds, or strike NW and dip shallowly SW (Point Gordon and Fisheries Bay headlands; Figure 2.7a in Chapter 2), representing the upright, shallow dipping limbs. Continuous exposure along Banky Beach East Headland exposes both limbs and the hinge region of one of the regional antiforms (Figure 2.7b). The three headlands where foliation changes attitude from NE-strike and steep SE-dip to NW-strike and shallow SW-dip correspond to the anticlinal hinge areas of these folds: Point Henry and Banky Beach East are two outcrops of the hinge area of the southernmost antiformal fold, whereas Back Beach is the hinge area of the northernmost antiformal fold (Figure 2.7a in Chapter 2; Plates 5, 7, and 12). In Short Beach North Headland the migmatitic foliation changes attitude from NE-strike and steep SE-dip to NW-strike and shallow SW-dip, corresponding to the only outcrop in the field area of the hinge region of the synformal fold located between the two antiforms (Figure 2.7a in Chapter 2; Plate 10). The stereonet in Figure 2.8 in Chapter 2 shows that the regional fold axes average trend is 219° and the average plunge is 19° to the SW.

Previously described structures including (a) small boudins of foliation-parallel mafic layers, (b) small folds of these boudins and the migmatitic foliation, and (c) intermediate boudins of the migmatitic fabric and compositional layering closely follow the attitude of the foliation over the entire field area. Thus these same structures dip steeply to the SE in areas where the foliation trends NE and dips steeply to the SE, and dip shallowly to the SW in areas where the foliation trends NW and dips shallowly to the SW. Large, decameter-scale boudins described previously appear only on the upright, shallow SW-dipping limbs of these large, kilometer-scale overturned folds, which indicates that they postdate this third folding phase (Plates 5, 7, 8, 11 and 12).

3.6.4 Late folding

Metric-sized, symmetric to slightly asymmetric, SW-plunging, upright to overturned open folds of the migmatitic foliation and compositional banding exist in the Bremer Bay area. When overturned they verge dominantly to the NW (Figure 2.11 in Chapter 2 and Figure 3.22). These folds appear very sparsely throughout the field area, and can be seen on shallow, S- to SW- dipping limbs of large, regional-scale overturned folds. Their style of deformation is different from folds formed during the second folding phase in the field area: folded layers do not flow towards the hinge regions or attenuate on the limbs, and there are no associated axial planar or hinge-area leucosomes. Differences in deformation style suggest that these folds could have formed at lower temperatures than earlier folds seen in the area, and thus could postdate higher temperature deformation, including the third phase of bidirectional boudinage.

3.6.5 Shearing

Throughout the field area, shear bands with both left-lateral and right-lateral senses of motion are observed to cut and/or be associated with previously described structures, including the migmatitic foliation, small, intermediate and decameter-size boudins, and folds. In some cases the shear bands can be tied to specific phases of deformation, and have been described earlier, but in other cases either no or limited information on the timing of formation is available. The shear bands range from a few centimeters up to a few meters in length and from one centimeter to over two decimeters in width. Generally shears contain leucosomes (former melt) along the shear plane. When present, leucosomes in shear planes show different apparent chemistries, with some of intermediate composition, rich in Ca-bearing plagioclase, amphibole and some pyroxene (dominantly green in color), some of more felsic composition, rich in potassium feldspar (dominantly red to pale pink in color), and some of probably intermediate granitic composition (white in color). Leucosomes present in shear bands of centimeter-wide and centimeter and few-decimeter-long shears commonly display diffuse, gradual contacts with the surrounding orthogneiss. Leucosomes in decimeter-wide and up to several

meters long shears display sharp boundaries with the surrounding orthogneisses. No association between sense of motion and/or size and presence of leucosome on the shear plane or between sense of motion and leucosome chemistry was observed. Also leucosome chemistry did not appear to have any relationship to the specific lithology of the host orthogneiss in which they form: felsic (white and pale pink in color) and intermediate (green in color) leucosomes can be seen in shear bands developed within a few meters of each other, within the same lithology. Different headlands where orthogneisses of the same lithology crop out can display shear-band leucosomes of different chemistries. In only one locality in the field area, the southern-most part of Fisheries Bay Headland (Figure 2.1 in Chapter 2; Plate 11), the orthogneiss lithology seems to have control over the chemistry of leucosomes present on centimeter- to decimeter-wide, few decimeters to meters-long shear bands of the migmatitic foliation and compositional banding. Here the host orthogneiss is magnetite-bearing charnockite (see Chapter 2), the only occurrence of this lithology found in the field area, and all shear bands present display apparently felsic (white in color) leucosomes intruded along the shear planes.

Some shear bands (centimeter- to few centimeters-wide and up to few decimeters-long) offset intermediate folds of the migmatitic foliation (formed during the second folding phase in Bremer Bay), compositional layering or early square boudins, but their relationship to later structures is unknown (Figure 3.23). Small, sub-decimeter long shear bands commonly offset boudins in the limbs or hinge regions of these folds, whereas larger, few-decimeters long shears usually attenuate the limbs of the folds. These shears commonly contain leucosomes along the shear planes. Leucosome compositions are felsic (white to pale pink) to intermediate (green in color), and their boundaries with the host orthogneisses are diffuse to sharp. Leucosomes with diffuse boundaries are present in smaller, sub-decimeter-long shear bands, whereas larger shear bands commonly display leucosomes with sharp boundaries.

Short Beach Headland (Figure 2.1 in Chapter 2; Plate 9) displays a 40-meter-wide zone with sets of N-S trending left-lateral (more dominant) and E-W trending right-lateral

centimeter-wide and decimeter-long shear bands with associated felsic leucosomes in the shear planes appear (Figure 3.24). The shear bands affect the compositional layering, migmatitic foliation, and asymmetrical intermediate-scale boudins (e.g. Figure 3.3). These shear bands were described by Harris et al. (2002) and Harris (2003) as examples for the process of back-rotation between shear bands causing folding of the foliation and compositional banding. N-S left-lateral and E-W right-lateral shears of Harris et al. (2002) and Harris (2003) were observed in this study to have a dip-slip component when shear-band planes are exposed, and correspond to high-angle shears with top down-to-the-NE and top down-to-the-SW respectively. Although conjugate shear bands associated with back-rotation described by Harris et al. (2002) and Harris (2003) can be seen locally in other headlands in the field area, the concentration of these structures along a relatively narrow zone in Short Beach Headland (Plate 9) suggests that they could be associated with a localized, dominantly coaxial, shear zone in this headland.

The true sense of displacement in many shear bands and timing of formation are unclear throughout the field area due to limited or inexistent exposure of the shear plane. Many shear bands crop out on horizontal pavement surfaces, and only their apparent strike-slip sense of shear can be observed. Whenever shear planes are exposed, most shear bands appear to have a component of dip-slip motion, as well as strike-slip motion. Shear-band field measurements were therefore limited by the nature of the outcrops. Also it was common for smaller shear bands (sub-decimeter to few-decimeter long) to display two different strike-slip senses of motion along the same shear plane, indicating they are related to overall extension (Figure 2.13). Apparently right-lateral shear bands of all scales throughout the field area occur in nearly all orientations and are associated with all leucosome types. Right-lateral shears associated with felsic (white) and intermediate (green) leucosomes are dominantly E-trending; right lateral shears associated with felsic (pink) leucosomes show N- to NE- E- and NW- trends. (Figure 3.25a). Apparently left-lateral shear bands of all scales throughout the field area are NE- and N-trending and associated with all leucosome types. Left-lateral shears associated with intermediate (green) and felsic (pink) leucosomes are dominantly NE- to N- trending; left-lateral

shears associated with felsic (white) leucosomes are dominantly N-S trending (Figure 3.25b).

3.7 Partial melting during deformation

3.7.1 Partial melting during bidirectional extension and shortening

Ductile deformation in the granulite-facies orthogneisses in the Bremer Bay area took place at conditions that resulted in widespread partial melting during most of their deformation history. Field structures suggest that most melts crystallized effectively "in situ" (at or very near the location where they were generated) or traveled short distances along different pathways. The earliest structures seen in the field are small, tight to isoclinal folds of cm-wide quartz-feldspar leucosome bands, to which the dominant migmatitic foliation is axial planar (Figure 2.3 in Chapter 2). The migmatitic foliation is mostly defined by a compositional segregation of felsic-rich (leucosome) and mafic-rich (restitic) bands (Figure 2.2 in Chapter 2), due to "in-situ" generation, very short-distance migration (millimeters to a few centimeters) and subsequent crystallization of felsic phases of the country rocks (mostly quartz and plagioclase).

Granitic to intermediate melts crystallized in the necks of bidirectional boudins of all three generations. Nearly all early small, square boudin trains of foliation-parallel mafic bands have their necks completely filled with melt, and in most cases the individual boudins are completely surrounded by felsic melt, with leucosomes bounding the top and bottom surfaces and the corresponding necks on either side (Figure 2.4b in Chapter 2). Granitic melts are relatively common in the neck areas of second generation intermediate, meter-sized boudins of the migmatitic foliation and compositional layering. Their morphologies vary from irregular bodies with very diffuse boundaries with the country rock, to irregular bodies with more discrete boundaries with the surrounding migmatitic orthogneiss, to regular, discrete bodies that form "pull-apart" veins (Figures 3.7, 3.8, 3.9, 3.10). Granitic melts emplaced in the neck areas of decameter-size boudins of the gneissic fabric are dominantly discrete bodies that clearly disrupt the migmatitic

foliation (Figure 2.9 in Chapter 2 and Figure 3.17), although rarely they display diffuse boundaries within the boudin neck (Figure 3.18). Diffuse melt bodies (Figures 3.8 and 3.18) present in boudin necks are interpreted to have formed by melt produced at or very near those sites, and thus having migrated very short distances, possibly along foliation planes, a common melt pathway in migmatites. Discrete granitic bodies in boudin necks (Figures 3.7, 3.9, 3.17) are probably the result of emplacement and crystallization of melts that could have potentially travelled longer distances through the country rock. In both cases, boudin necks are areas of low differential stress as the rock was pulled apart. Melt generated at the time of extension will tend to migrate towards such low stress areas.

Migmatitic orthogneisses throughout the field area commonly display diatexitic textures, where partial melt is pervasively distributed throughout the rock. In these cases partially melted and unmelted portions of the rock are not segregated into a migmatitic fabric, and the rock becomes essentially "isotropic neosome" (Figure 3.26). The width, length, overall shape, and attitude of areas displaying diatexitic texture are highly variable. Sub-meter to several meter-wide laterally continuous areas roughly parallel to the compositional layering are present throughout the field area. Irregular, sub-meter to several meter-wide and several meters long areas of diatexitic texture also exist in the field area. They appear as "patches" within the host orthogneisses where the migmatitic foliation is inexistent. Some small, sub-meter sized irregular areas of migmatitic orthogneiss displaying diatexitic texture are locally associated with fold-hinge regions of meter-sized folds of the migmatitic fabric and compositional layering in the field area. Other apparent "patches" of diatexitic texture of variable size (few-centimeters to several decimeters wide and few-centimeters up to few meters long) locally disrupt the migmatitic foliation, compositional banding and other structures, such as boudinaged mafic layers and intermediate folds.

Diatexitic bands or layers also cut across previously formed structures. Small, centimeter to decimeter-wide and sub-decimeter long diatexite bands, at high angles with the dominant migmatitic fabric, disrupt the compositional banding, foliation, and small

folds of the compositional layering (Figure 3.27). Sub-meter to several-meters-wide bands of diatexitic texture at high angles with the dominant migmatitic fabric are also seen disrupting the foliation and compositional banding. In some cases the compositional layering appears completely disarranged within some of the larger diatexitic bands, where isolated blocks of mafic layers, folds, and centimeter to decimeter-scale boudin blocks of mafic layers behave as "rafts" floating in the surrounding granodioritic to monzogranitic leucosome (Figure 3.28).

It is possible that many of these diatexitic bands, particularly those observed clearly disrupting the migmatitic fabric and compositional banding, could have acted as melt channel-ways that could have been active throughout all stages of deformation. In Fisheries Bay Headland (Figure 2.1 in Chapter 2) one outcrop exposes the sub-rounded transverse section of a meter-wide melt channel-way where leucocratic melt has completely disrupted the compositional layering and boudinaged mafic layers. This structure, together with adjacent relatively undisturbed compositional layering in the orthogneisses appears to have been sheared, most probably while melt was flowing, and later boudinaged (Figure 3.20).

3.7.2 Late melts

Discrete, undeformed, few centimeter- to few decimeter-wide, late pegmatite bands cut through all other structures in the field area. These bands are dominantly of two distinct chemistries: (1) intermediate composition, mostly composed of Ca-rich plagioclase, amphibole, and some pyroxene (green); and (2) felsic composition, dominantly potassium feldspar and quartz (red to pink). Intermediate (green) bands show two dominant orientations, NNW to NW and NNE to NE, with the former being slightly more dominant (Figure 2.12b in Chapter 2). Intermediate to mafic pegmatite veins cut through foliation, all folds, and all generations of bidirectional boudins. Felsic bands trend dominantly NW, although a small set of them show NE-trending orientations (Figure 2.12b in Chapter 2). Felsic pegmatite veins cut through all other structures in the field, including intermediate to mafic pegmatite bands (Figure 2.12a).

3.8 Discussion

Rocks of the Biranup Complex in the Bremer Bay area show evidence for extension in two orthogonal directions (bidirectional extension) at mid- to lower-crustal levels. This type of 3D strain field during extension is in marked contrast to the commonly considered plane strain or constrictional deformation (e.g. Fletcher and Bartley, 1994) associated with widespread extension. Moreover, the bidirectional extensional structures overprint and are overprinted by shortening and/or shear-related structures. Additionally, pressure estimates for the structurally underlying Mt. Barren Group and for rocks of the Coramup Gneiss (Biranup Complex) on the eastern part of the Albany-Fraser Orogen, near Esperance (Bodorkos and Clark, 2004a) suggest that rocks in the Bremer Bay area were most likely at mid-crustal levels during Stage II deformation. Yet these rocks show evidence of granulite-facies metamorphism and partial melting throughout the deformational history, suggesting unusually high heat flow. Any tectonic model for this area must explain this unusual combination of structures, 3-D strain field, and deformation conditions.

Previous work (Beeson at al., 1998; Clark et al., 2000; Bodorkos and Clark, 2004 a&b; Giles et al., 2004) has shown that the Albany-Fraser belt represents a convergent orogen that records NW-directed contraction along its entire length. Chapter 2 presents a model for a diachronous Albany-Fraser Orogeny, in which initial collision between the West Australian and Mawson cratons occurs on the eastern part of the belt during Stage I, and final closure of the asymmetric ocean basin on the western end occurs during Stage II (Figure 2.14). This model is in contrast to previous models that had complete closure occurring during State I. Instead, the subduction zone migrates westward as the ocean basin closes in a zipper-like manner, and continuing subduction along the western plate boundary is the driving force for continued contraction after collision.

Field evidence from orthogneisses of the Biranup Complex in the locality of Bremer Bay shows that widespread extension occurred at ca. 1180 Ma during Stage II of the Albany-Fraser Orogeny, as indicated by the presence of multiple stages of extension that increases in magnitude with time and U/Pb dating of zircons from melts formed in

boudin necks. As noted above, pressure estimates for adjacent rocks indicates extension most probably took place at mid-crustal levels, yet it is coupled with granulite-facies metamorphism, abundant partial melting that occurred throughout deformation, and the presence of numerous melt channels up to several meters in width. Given the tectonic setting in an overall contractional orogen, these features observed in the Bremer Bay area are best explained by removal of the mantle lithosphere and, most likely, part of the deep crust and by subsequent upwelling of asthenospheric material adjacent to rocks that were at mid-crustal levels. Either delamination of an overthickened crust or slab break off are two mechanisms that could explain such removal. Either mechanism would result in a rapid temperature increase allowing partial melting of mid-crustal material and high-temperature, medium-pressure metamorphic conditions as seen in the Bremer Bay area.

The bidirectional extension of these rocks was the result of coaxial deformation with shortening perpendicular to the migmatitic foliation and apparently nearly equal extension in the other two directions (i.e. flattening strain). Evidence for this strain field includes the generally symmetrical boudinage with no consistency to local senses of asymmetry, the nested nature of the intermediate (less than a meter to a few meters in scale) and large (decameter-scale) boudins that indicate the entire package has been stretched in two directions, and the lack of any large zones of non-coaxial shear in the field area. Thus, the extension observed in these rocks does not result from a large-scale mid-crustal, non-coaxial shear zone or from mid-crustal channel flow in the core of the Albany-Fraser Orogen. Instead the rocks indicate widespread coaxial extension in orthogonal directions and flattening.

Phases of extension in the Bremer Bay area are interspersed with phases of shortening and/or shear-related folding. Second generation folds of centimeter- to decimeter-scale mafic layer boudins formed during the first phase of bidirectional extension are commonly associated with meter-scale zones of non-coaxial shear in the field. Thus, it is possible that these folds could have formed in an extensional regime as a result of back-rotation between shear zones, as described by Harris (2003). However, such folds show both NW- and SE- vergence, again consistent with overall coaxial

deformation. For the regional third generation folds, it is unlikely that they formed in an extensional environment As stated above, no large-scale noncoaxial shear zones that could have resulted in formation of the folds are observed in the area, plus these folds are comparable with the regional folds observed in the Biranup Complex further west (Beeson et al., 1988), and appear to be related to the overall NW-directed convergence observed elsewhere in the orogen (Beeson et al., 1988; Myers et al., 1996; Clark et al., 2000; Duebendorfer, 2000; Bodorkos and Clark, 2004a&b). Therefore all structures prior to the regional third generation folds could be ascribed to overall extension, as can the last phase of bidirectional boudinage and late pegmatites and melts, but there appears to be a major phase of regional NW-directed contraction in between.

The extensive partial melting during bidirectional extension and contraction, combined with high-temperature (800ºC-1000 ºC; Black et al. 1992) granulite-facies metamorphism indicates that these rocks were rheologically weak and flowed throughout most of the ductile deformation phases recorded in the field area. Additionally, the magnitude of extension increases with time, but melt becomes less pervasive and somewhat more localized in boudin necks, melt channels and finally in late cross cutting pegmatites, suggesting an overall cooling with time.

Several possible explanations for widespread extension in mid- to lower crustal levels in the core of a collisional orogen include:

(1) Collapse of a gravitationally unstable, overthickened crust, which could result in flattening in mid- to lower-crustal levels where rocks are rheologically weaker (Coney and Harms, 1984; Dewey, 1988; Vanderhaeghe and Teyssier, 2001). Several authors (England and Houseman 1989; Molnar et al. 1993) suggest that the transition from early crustal thickening to late orogenic collapse during orogenesis could be the result of: (a) increase in potential energy of an overthickened wedge due to removal of the lithospheric mantle and subsequent asthenospheric upwelling; and (b) decrease of the tectonic forces that drive orogenic convergence. Some authors (Vanderhaeghe and Teyssier, 2001) also suggest that orogenic collapse could be the result of changes in crustal rheology during

orogenesis resulting from an increase in temperature due to radiogenic heat production and thermal relaxation in an overthickened crust.

(2) Slab break off results in isostatic uplift, cessation of convergence, and upwelling of the asthenosphere, all of which can trigger extension (Sacks and Secor, 1990; Platt and England, 1994; Davies and Von Blackenburg, 1995). Lithospheric delamination and removal of an overthickened crustal root also result in isostatic uplift and upwelling of the asthenosphere. The latter causes softening and flow of the newly exposed crust, and coupling with the upwelling asthenosphere may cause extension and spreading (i.e. tractional stresses).

(3) Channel flow in the mid- to lower-crust, with possible extrusion of high-grade metamorphic rocks between coeval non-coaxial normal- and thrust-sense shear zones (Beaumont at al., 2001).

The bidirectional nature of the extension and the lack of major noncoaxial shear zones put some constraints on which of these models are plausible and additional considerations are required to explain the 3D strain observed. The lack of mayor noncoaxial shear zones excludes channel flow and any other models that invoke dominantly noncoaxial shear. Given the likelihood of slab break off initiating the partial melting and granulite facies metamorphism, it is most likely that the early stages of extension (and probably the early folding) are related to this catastrophic event. The regional folding most probably is the result of continued subduction along strike. The lack of major noncoaxial shear zones and regional extent of these structures strongly suggests folding resulted from overall convergence. Such renewed convergence is common in other orogens where slab breakoff is postulated (Sacks and Secor, 1990; Collins, 1994; Davies and Von Blackenburg, 1995). The final stages of extension may reflect flattening at depth as a result of collapse of the orogenic wedge once the driving force for convergence is gone after final closure of the ocean basin and collision along the entire belt. The bidirectional extension requires a 3D view of these tectonic processes as proposed in the model below.

Tectonic Model for the Albany-Fraser Orogen

As collision on the western part of the orogen culminated during Stage II and the active subduction zone moved further west along the orogenic front, the subducting slab in the subduction zone on the western part of the orogen detached (Figure 3.29). This slab breakoff and associated lithospheric delamination caused convergence to cease, isostatic uplift and extension, plus allowed upwelling of the asthenosphere to higher crustal levels under the newly formed orogen (Figure 3.29). Upwelling of the asthenosphere would result in extensive partial melting and granulite-facies metamorphism of the overlying crust which would significantly softened the rocks causing widespread flow. Traction imposed by the upwelling asthenospheric mantle on the overlying continental crust, coupled with uplift, could result in extension perpendicular to the orogenic front as usually observed (NW-SE; Figure 3.29c). However, when the effects of removing part of the slab are considered in three dimensions, it becomes apparent that asthenosphere could also flow around the edges of the detaching slab. This upwelling could cause a second coeval extension parallel to the orogenic front (NE-SW; Figure 3.29d) caused by traction imposed on the overlying crust by flow of the asthenospheric mantle. This extension would be enhanced by isostatic uplift both parallel and perpendicular to the orogen.

Breakoff of a subducting slab would have been a catastrophic event, and the bidirectional extension response triggered in the overlying crust would dissipate with time. The continued active subduction along the western extent of the plate boundary would cause the overall convergence to be reestablished, causing continued NW-directed contraction to again become the dominant deformation regime. NW-directed contraction could have resulted in the formation of the large, kilometer-scale overturned folds seen in the field area. Regional, kilometer-scale overturned folds are later boudinaged by decameter-scale bidirectional boudins, for which field observations suggest that the magnitude of coeval extension in both NE- and NW-directions is comparable.

The third phase of bidirectional extension most likely resulted from orogenic collapse after complete closure of the intracratonic ocean basin between the Mawson and West Australian cratons (e.g. Scott and Schmeling, 1998). During orogenic collapse the

rheologically weakened mid- to lower crust in the core of the orogen could have acted as a coaxial detachment zone for a collapsing overburden, and thus have undergone flattening that resulted in the third phase of coeval bidirectional extension. Melt flow was still active during the third bidirectional extension phase, although it was more focused suggesting the rocks were somewhat cooler, and the larger melt channel-ways most likely formed at this time.

Previous authors have suggested possible tectonic models that could explain the extension observed in the Bremer Bay area, but none explain the continued convergence during extension or recognized the bidirectional extension. Pisarevsky and Harris (2001) interpreted decameter-sized NW-SE oriented boudins in the Bremer Bay area as a result of 1200-1140 Ma extension due to one of three causes: orogenic collapse, lithospheric delamination, or rebound of a thickened crustal root. Pisarevsky and Harris (2001) did not account for, and in many cases recognize, smaller, earlier boudins or the bidirectional nature of the boudins that exist in the Bremer Bay area, or the alternation of extensional and shortening and/or shear related structures in the field area. They envision boudinage in Bremer Bay as resulting from an episode of orogenic NW-directed extension during the Albany-Fraser Orogeny that was preceded by NW-directed convergence resulting from cratonic collision, and was followed by renewed intracratonic NW-directed convergence. This field study demonstrates that three phases of NE- and NW-directed bidirectional extension in the Bremer Bay area alternate with shortening and/or shear related deformation. This field study also shows that deformation in Bremer Bay occurred ca. 1180 Ma during Stage II of the Albany-Fraser Orogeny, a period of NW-directed contraction driven by active subduction in the western-most end of the orogen. Bidirectional extension is related to breakoff of a relict subducting slab in the western part of the orogen, which resulted in isostatic uplift and the rise of asthenospheric material, producing a bidirectional extension response and extensive partial melting at mid-crustal levels.

Bidirectional extensional structures such as those observed in the Bremer Bay area of the Albany-Fraser Orogen should be expected elsewhere when the driving force

for extension is: (1) upwelling of the asthenosphere in a localized region where traction imposed by the asthenospheric material on the overlying crust is the driving force; or (2) collapse of an overthickened lithospheric wedge on a ductile mid-to lower crust that acts as a coaxial detachment for the collapsing wedge, and thus undergoes flattening that could result in bidirectional extension. In addition to slab breakoff, other types of delamination or slab rollback are potential mechanisms where traction of the upwelling asthenosphere on the overlying crust could trigger bidirectional extension.

3.9 Conclusions

Granulite-facies migmatitic orthogneisses from the Biranup Complex of the Albany-Fraser Orogen in the locality of Bremer Bay, Western Australia, show field evidence for at least three phases of widespread extension in orthogonal directions (bidirectional extension) at ca. 1180 Ma, which alternate with shortening and/or shear related structures. Bidirectional extension phases are interpreted as the result of breakoff of a subducting slab in the western part of the belt during Stage II of the Albany-Fraser Orogeny.

Bidirectional extension resulted in boudins that formed coevally in two directions, NE-SW and NW-SE. The shape and size of the boudins are different for each bidirectional extension phase. Deformation took place under granulite-facies conditions.

- The first bidirectional extension phase formed centimeter-scale, torn, blocky boudins of thin mafic layers parallel to the main compositional banding. These boudins and the migmatitic foliation are folded by small, upright to overturned folds that locally appear to have formed in diffuse shear zones.
- The second bidirectional extension phase formed meter-sized boudins of the migmatitic fabric, compositional layering, and all previous structures. This phase of extension is followed by regional scale folding, which results in the formation of kilometer-scale, overturned, strongly asymmetric, NW-verging folds of all previous structures.

- The third bidirectional extension phase generated decameter-sized boudins of the migmatitic foliation and compositional layering. These boudins are visible only on the shallow-dipping, upright limbs of kilometer-scale, NW-verging folds. This last extension event was potentially followed by renewed folding, which formed meter-sized, upright to slightly overturned folds of the migmatitic foliation, which are very sparse throughout the field area.

Melt was generated and melt pathways were active during all stages of ductile deformation, and some melt was still being transported and emplaced after ductile deformation terminated.

- Pervasive migmatitic foliation defined by alternating leucosomes and residuum layers requires partial melting of the country rock.
- Melt was generated and mobilized into boudin necks during all three bidirectional extension phases.
- Melt was present during all but possibly the very last stages of folding and during the formation of widespread shear bands.
- Melt pathways were still active after ductile deformation terminates, as evidenced by the presence of late intermediate (green) and felsic (pink) pegmatitic bands that cross-cut all ductile structures in the field.

Breakoff of a subducting slab and associated lithospheric delamination in the western part of the Albany-Fraser Orogen would: (1) cause isostatic uplift, extension and rise asthenospheric material into higher crustal levels, thus resulting in a rapid temperature increase that would allow for partial melting of crustal material and high-temperature, medium-pressure metamorphic conditions; and (2) result in a bidirectional extensional response in the overlying crust due to traction imposed by the upwelling asthenospheric mantle, with (a) extension parallel to the main convergence direction (NW-SE) and (b) coeval extension in the orthogonal direction (NE-SW) due to flow of material around the edges of the detaching slab.

Breakoff of the subducting slab would have been a catastrophic event, and continued active subduction in the western-most part of the orogen would allow for overall NW-directed cratonic convergence to be re-established after extension. NW-directed convergence could have led to the formation of the regional, kilometer-scale, NW-verging folds seen in the Bremer Bay area.

Large, decameter-scale boudins formed after regional-scale folding during a third phase of coeval bidirectional extension in the Bremer Bay area most likely resulted from orogenic collapse following the complete closure of the intracratonic basin between the West Australian and Mawson cratons.

Figure 3.1. Centimeter-wide and decimeter-long dextral shear bands that offset centimeter-scale blocky boudins of foliation-parallel mafic layers. Shear bands are associated with felsic (white leucosomes that show diffuse boundaries with the host orthogneisses. Note associated folding of migmatitic layering. Banky Beach East Headland. Compass for scale is 10 cm long.

Figure 3.2. Meter-scale NE-trending symmetric drawn boudins of the migmatitic fabric and compositional banding formed during the second bidirectional extension phase in Bremer Bay. Banky Beach East Headland. Compass for scale is 20 cm long.

Figure 3.3. Meter-scale, NW-trending symmetric torn boudins of the main compositional banding and migmatitic foliation. Felsic leucosome localized in the boudin necks and along the boudinaged layer. Note thinner mafic layer within the boudin that was previously extended during the first phased of boudinage. Fisheries Bay Headland. Field book for scale is 19 cm long.

Figure 3.4. Meter-scale NE-trending asymmetric shear band boudins of the migmatitic foliation and compositional banding formed during the second bidirectional extension phase in Bremer Bay. Short Beach Headland. Shear band offsetting the boudins displays top-down to the SW sense of asymmetry. Pocket knife for scale is 7 cm long.

Figure 3.5. Meter-scale, NE-trending “pinch and swell” boudins of the migmatitic fabric and compositional banding formed during the second bidirectional extension phase in Bremer Bay. Native Dog Beach Headland. Field book for scale is 12 cm wide.

Figure 3.6. Decimeter-scale asymmetric NE-trending foliation boudinage, which forms individual boudin blocks of the migmatitic foliation with no apparent competency contrast. Fisheries Bay Headland. Pencil for scale is 12 cm long.

Figure 3.7a. Intermediate NE-trending symmetric torn boudin of a mafic layer where the boudin neck has been filled by a combination flow of the adjacent rock migmatitic foliation and felsic (pink) leucosome. Fisheries Bay Headland. Compass for scale is 20 cm long.

Figure 3.7b. Intermediate NW-trending symmetric torn boudins of the compositional banding and migmatitic foliation where the boudin neck has been filled by a combination flow of the adjacent rock migmatitic foliation and felsic (white) leucosome. Banky Beach Headland. Compass for scale is 20 cm long.

Figure 3.8 Diffuse felsic leucosome in the neck of NW-trending lensoidal boudins of the migmatitic fabric and a mafic layer. The diffuse felsic leucosome could be derived from the leucosomes that defined the migmatitic foliation or from in situ partial melting. Fisheries Bay Headland. Compass for scale is 20 cm long.

Figure 3.9a. Meter-sized NE-trending boudin of the migmatitic foliation and compositional layering in which discrete, relatively straight edged felsic leucosome veins intrude the boudin necks. Banky Beach Headland.

Figure 3.9b. Meter-sized NE-trending boudin of the migmatitic foliation and compositional layering in which a discrete, irregular leucosome veins intrudes the boudin neck. Banky Beach East Headland.

Figure 3.10 Sub-meter size NE-trending boudins of the migmatitic foliation and compositional banding where discrete felsic (pink) leucosomes parallel the boudinaged layer and fill in necks of the same boudinaged layer. Banky Beach East Headland. Compass for scale is 20 cm long.

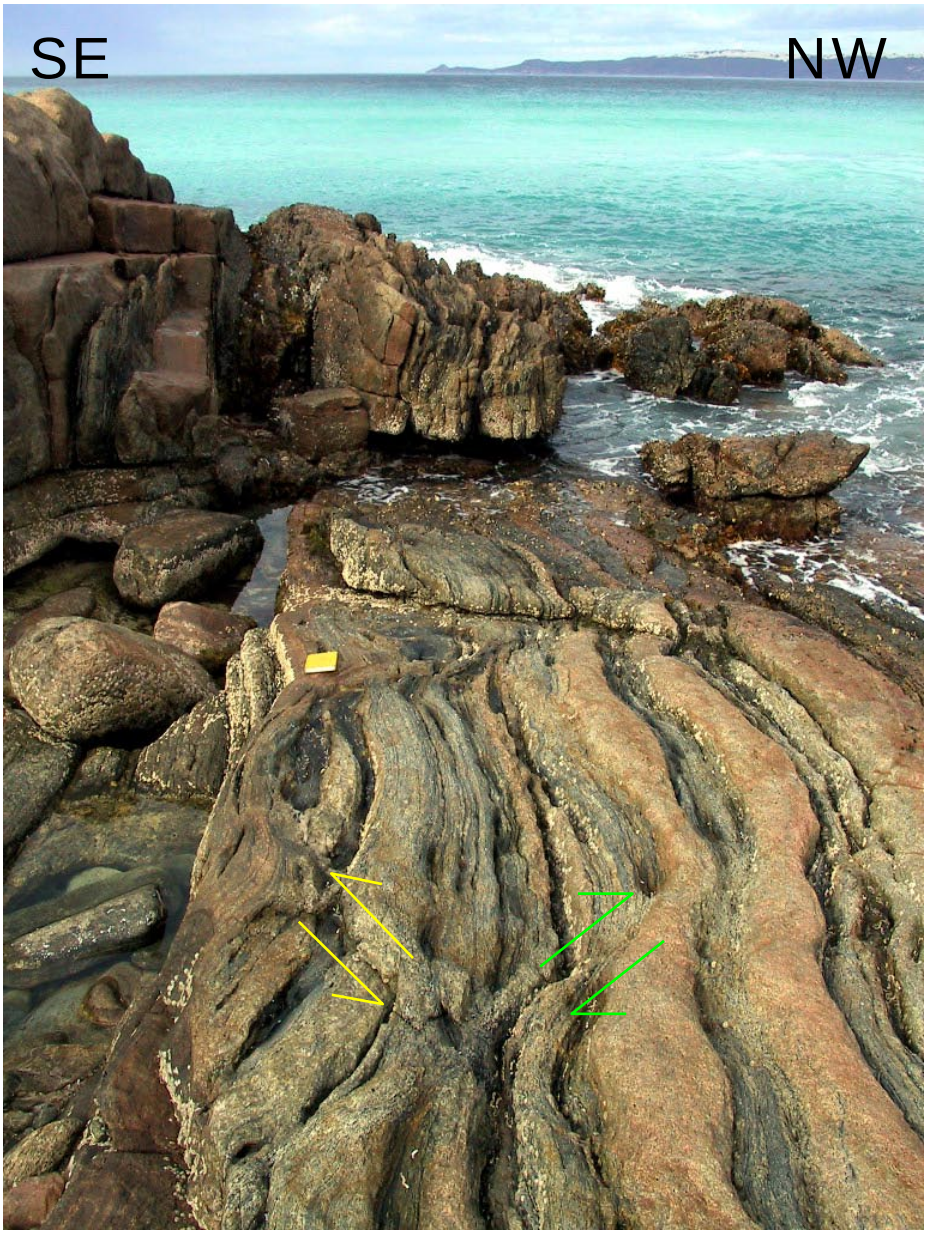

Figure 3.11. Conjugate top down-to-the-NE (green motion arrows) and top down-to-the-SW (yellow motion arrows) subvertical shear bands offsetting metric NE-trending boudins of steeply SE-dipping migmatitic foliation and compositional banding. Native Dog Beach Headland. Field book for scale is 19 cm long.

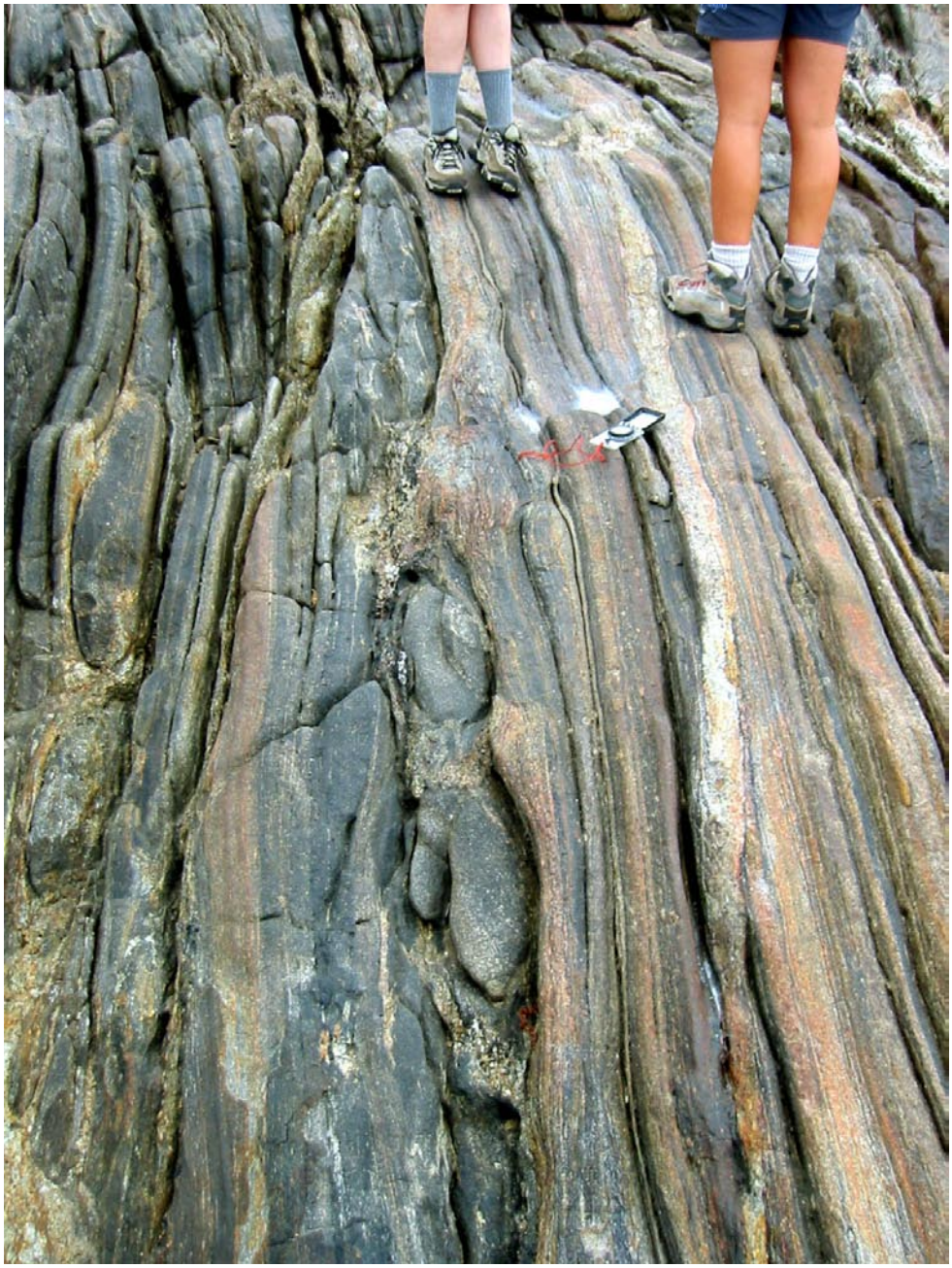

Figure 3.12. Decimeter-scale NE-trending symmetric lensoidal torn boudins contained within meter-scale NE-trending lensoidal drawn boudins. Boudinage of the migmatitic fabric and compositional banding. Banky Beach East Headland.

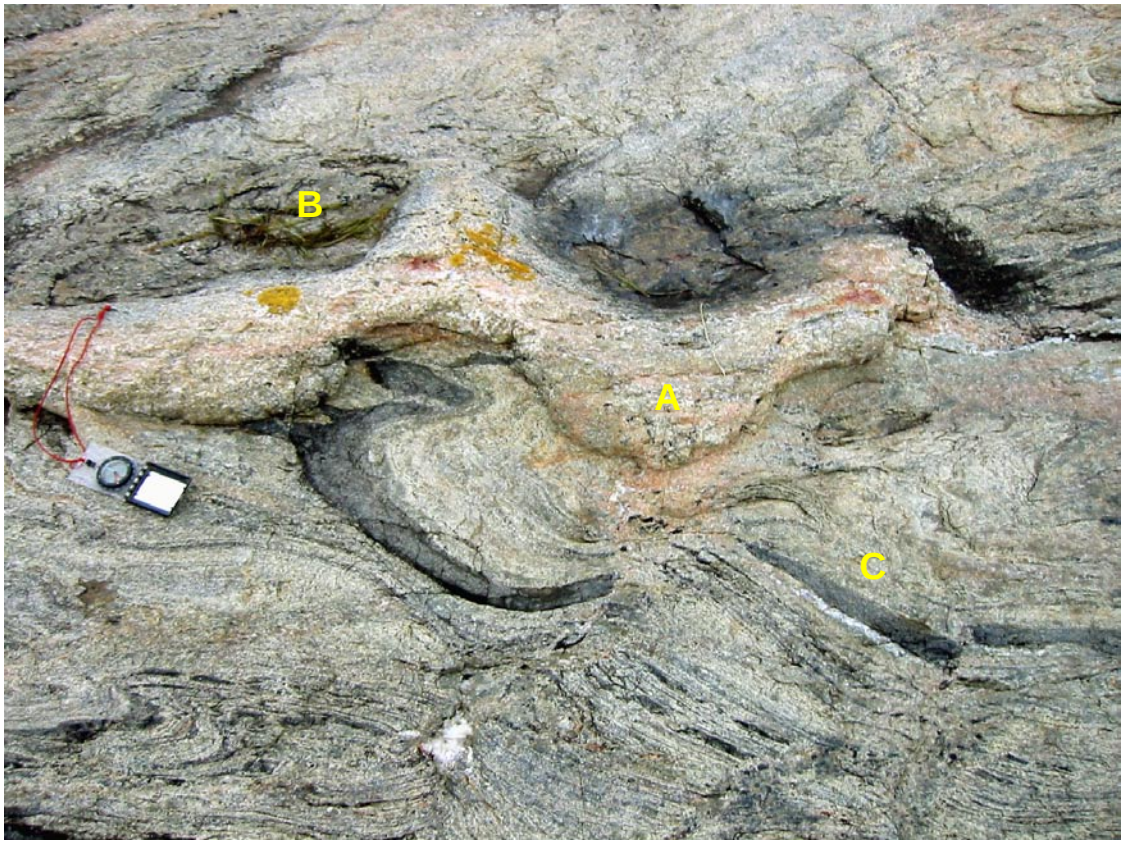

Figure 3.13. Multiple stages of boudinage as a result of progressive bidirectional extension recorded in the Bremer Bay area. Blocky boudins of thin mafic layers are folded. Felsic leucosome band (a; center of photograph) represents the neck of a larger boudin that formed after folding. Later boudinage in an orthogonal direction extended thicker mafic layers (b), and previously formed felsic leucosome flowed into neck region. Foliation boudinage (lower portion of photograph) may have formed at the same time, though neck region is filled with nearly pure quartz. Note nearly pure quartz layer along the margin of one larger blocky boudin (c), suggesting extension in this orthogonal direction during foliation boudinage.

Figure 3.14. Large, decameter-sized NW-trending symmetric drawn nested boudins of the migmatitic fabric and compositional layering. Field of view is 60 m wide. Point Gordon Headland.

Figure 3.15. Large, decameter-sized NW-trending symmetric lensoidal torn nested boudins of the migmatitic foliation and compositional layering. Field of view is 15 meters wide. Fisheries Bay Headland.

Figure 3.16. Decameter-size NW-trending asymmetric blocky and barrel shaped boudins of the migmatitic foliation and compositional layering. Boudins are offset by high-angle conjugate sets of normal shear bands, some of which display intermediate (green in color; highlighted by green motion arrows) pegmatitic leucosomes with sharp boundaries apparently intruded along the shear planes. Field book for scale is 19 cm long. Fisheries Bay Headland.

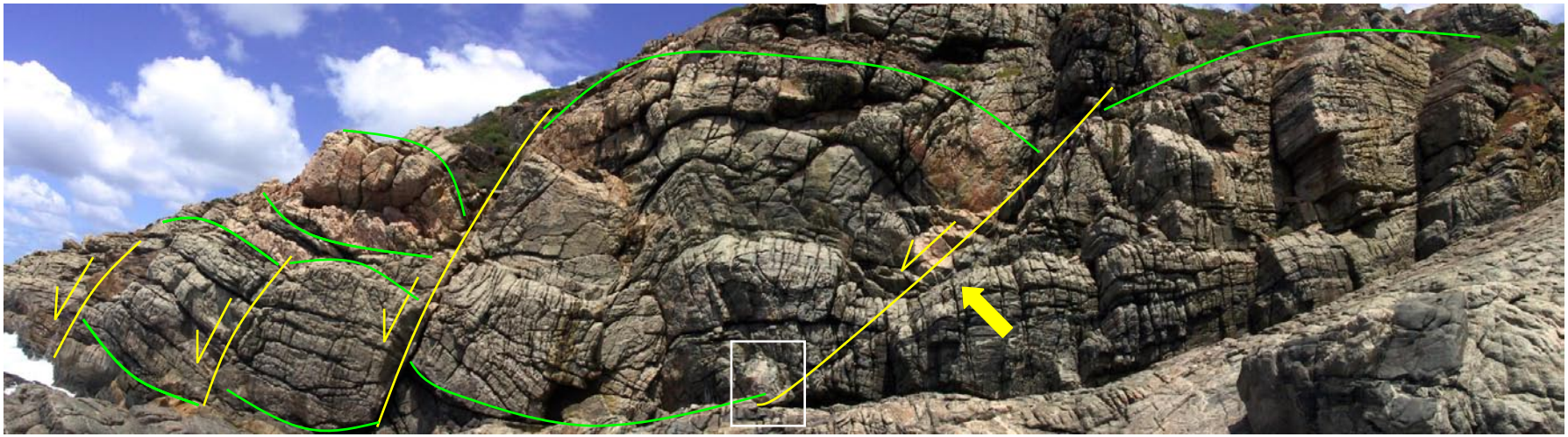

Figure 3.17. Decameter-size NW-trending asymmetric domino-style torn nested boudins of the migmatitic foliation and compositional banding. The boudins appear offset by normal shear zones, one of which (listric) is intruded by a felsic (white) pegmatitic melt (arrow). Felsic (pink) pegmatitic melt is present in the boudin neck areas. Field of view is 70 meters wide. Fisheries Bay Headland. Area highlighted in the lower part of the normal listric zone (white box) corresponds to Figure 3.18.

Figure 3.18. The migmatitic foliation and compositional banding boudinaged by decameter-size NW-trending asymmetric boudins in Figure 3.16 are clearly truncated by the normal listric zone that offsets the boudins. Leucosomes of different morphologies are intruded into this boudin neck: (A) irregular felsic (white) leucosome with discrete to diffuse boundaries with the surrounding orthogneiss; (B) felsic (white to pink) pegmatitic vein with straight edges and sharp boundaries with the surrounding orthogneiss. Fisheries Bay Headland.

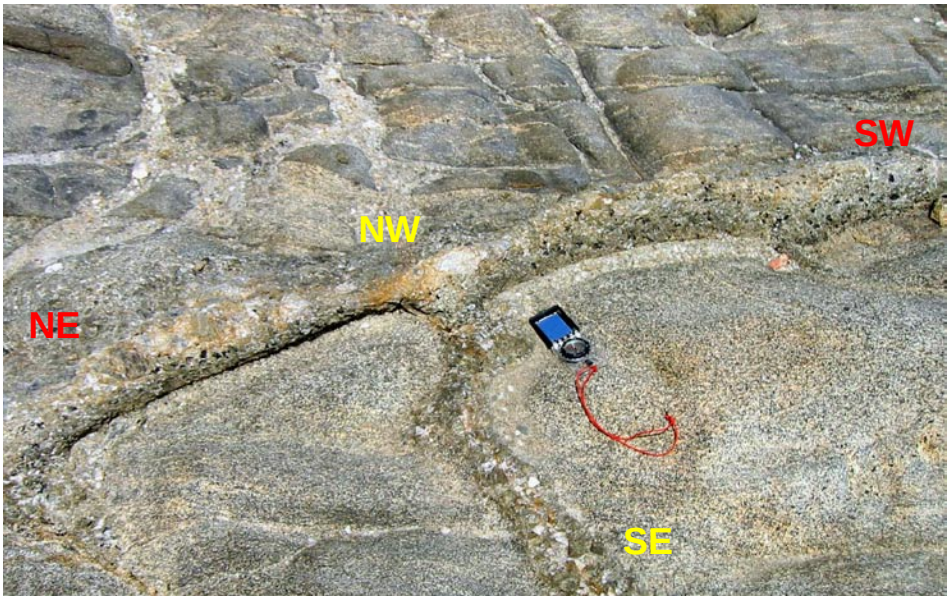

Figure 3.19. Pegmatitic veins of intermediate composition in two orthogonal directions, NE-SW and NW-SE, forming an irregular rectilinear pattern in which neither direction offsets the other, which suggests that these veins could have intruded simultaneously as a result of bidirectional extension. Native Dog Beach Headland. Compass for scale is 20 cm long.

Figure 3.20a. Shear zone rich in felsic leucosome that contains disarranged pieces of folds of the compositional banding and centimeter-scale boudins of mafic layers. Disruption of layering was probably related to the presence of melt. Shearing probably occurred during melt flow, and the structure was later boudinaged. Fisheries Bay Headland. Yellow box corresponds to Figure 3.20b.

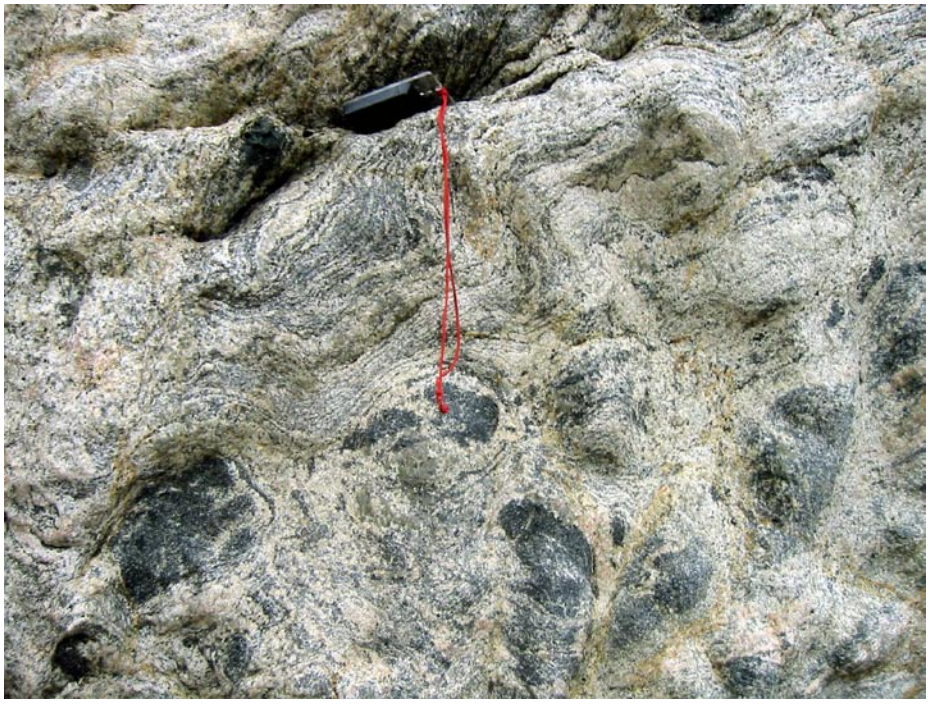

Figure 3.20b. Close-up of the texture displayed by jumbled compositional banding and boudinaged mafic layers in the boudinaged shear zone described in Figure 3.19. Individual boudin blocks and layering blocks are completely surrounded by felsic leucosome. Fisheries Bay Headland. Compass for scale is 10 cm long.

Figure 3.21a. Decimeter-scale axial planar felsic leucosomes in the hinge area of a meter-scale fold of a boudinaged mafic layer and compositional layering. Back Beach Headland. Field book for scale is 19 cm long.

Figure 3.21b. Decimeter-scale felsic leucosomes in the hinge area of a meter-scale fold of a boudinaged mafic layer. The leucosomes form a divergent fan, suggesting that folding continued after leucosome emplacement. Some small boudin blocks are completely surrounded by melt and behave as "rafters" surrounded by leucosome. Point Gordon Headland.

Figure 3.22. Late open, NW-verging, SW-plunging meter-scale folds of the migmatitic fabric and compositional layering in Point Henry Headland. These folds probably formed during a late folding phase recorded in the Bremer Bay area. Field book for scale is 19 cm long.

Figure 3.23. Shear band with associated felsic leucosome that offsets an intermediate meter-sized fold of the migmatitic foliation. Fisheries Bay Headland. Compass for scale is 20 cm long.

Figure 3.24. Folds of the gneissic fabric and compositional banding formed between N-S trending left-lateral shear pairs due to back-rotation of the shear bands, as described by Harris et al. (2002) and Harris (2003) in Short Beach Headland. Pocket knife for scale is 7 cm long.

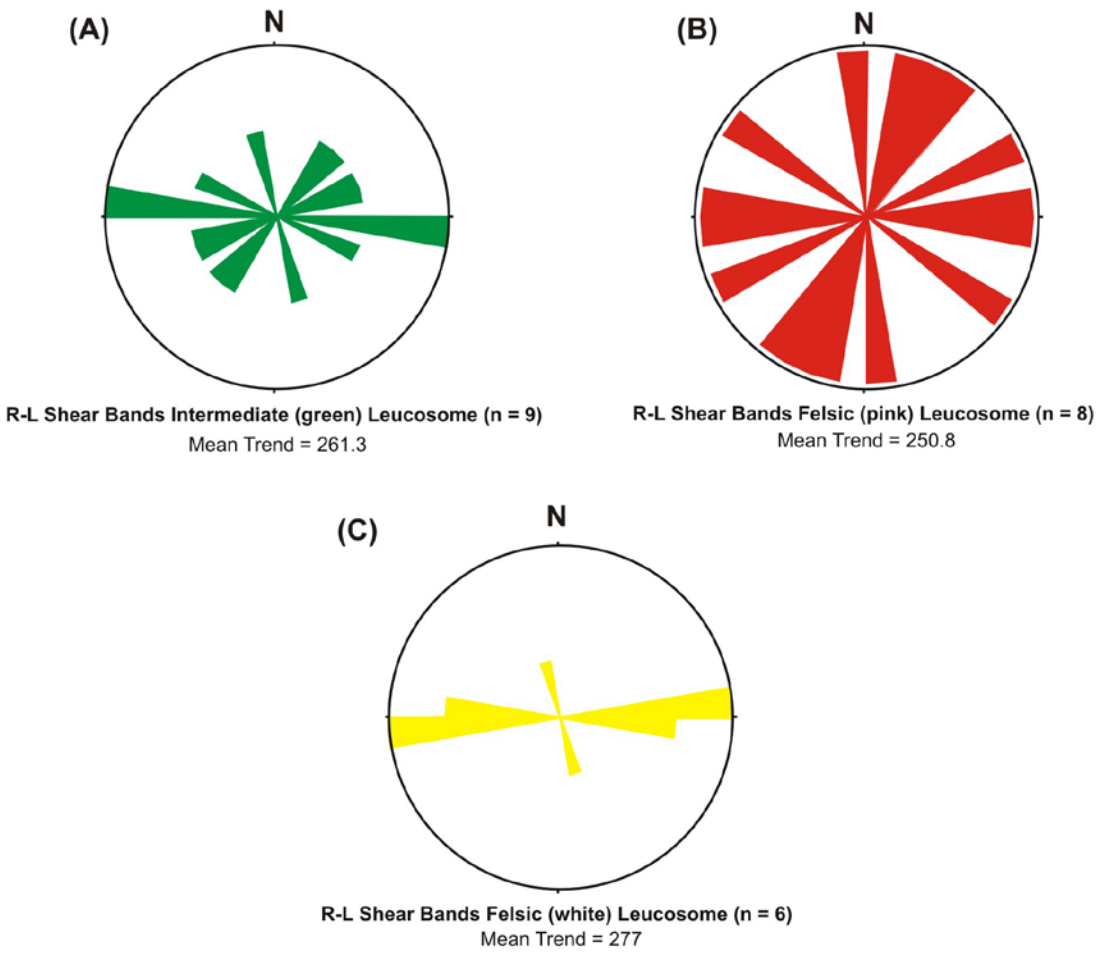

Figure 3.25a. Rose diagrams with orientations for right-lateral shear bands of all scales measured in the Bremer Bay area. Chemistry of shear-plane leucosomes is also noted: (A) Intermediate (green in color); (B) Felsic (pink in color); (C) Felsic (white in color).

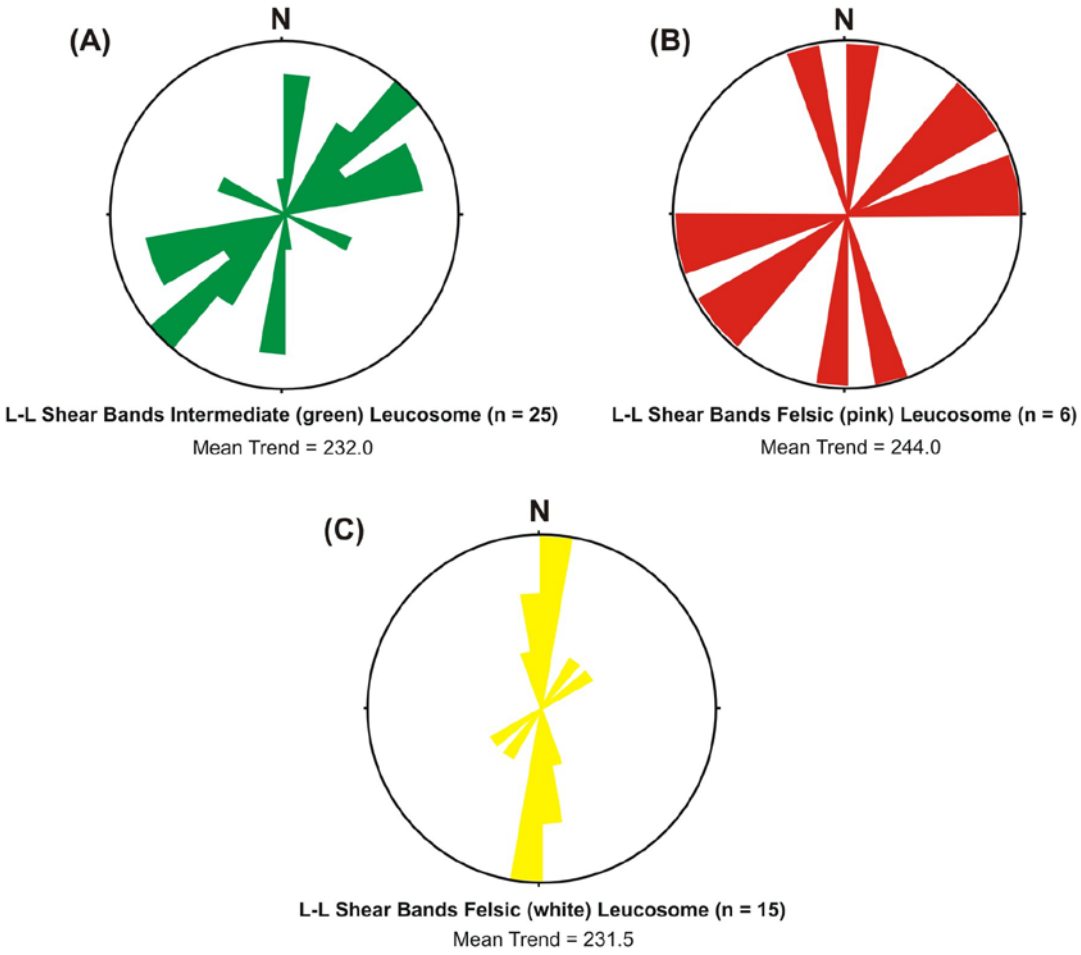

Figure 3.25b. Rose diagrams with orientations for left-lateral shear bands of all scales measured in the Bremer Bay area. Chemistry of shear-plane leucosomes is also noted: (A) Intermediate (green in color); (B) Felsic (pink in color); (C) Felsic (white in color).

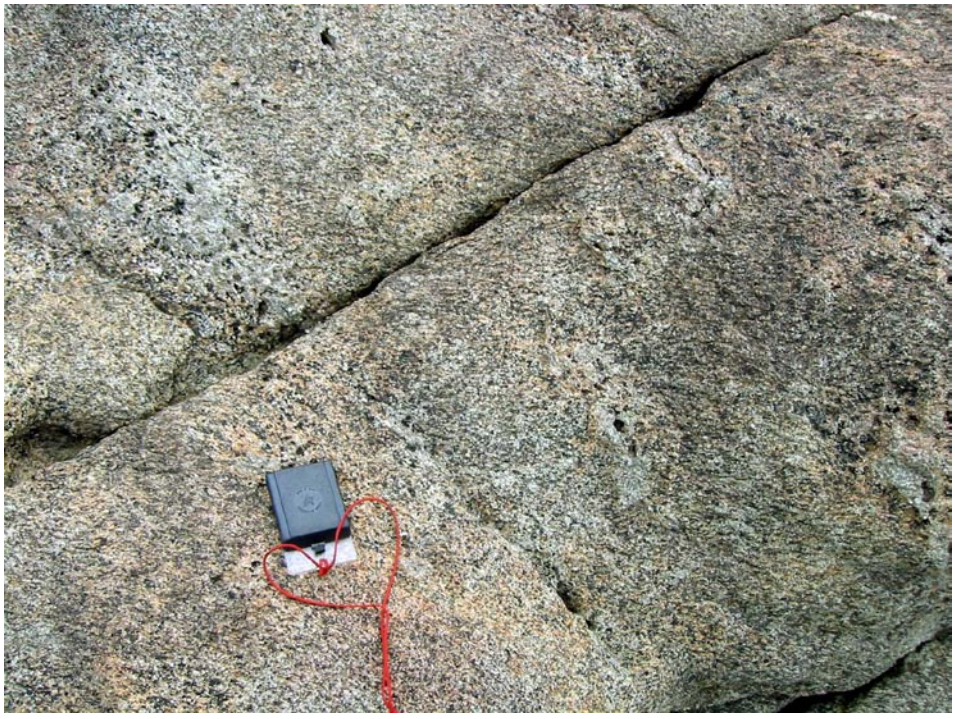

Figure 3.26. Diatexitic texture in quartz monzonitic orthogneisses in Back Beach Headland. Pencil for scale is 12 cm long.

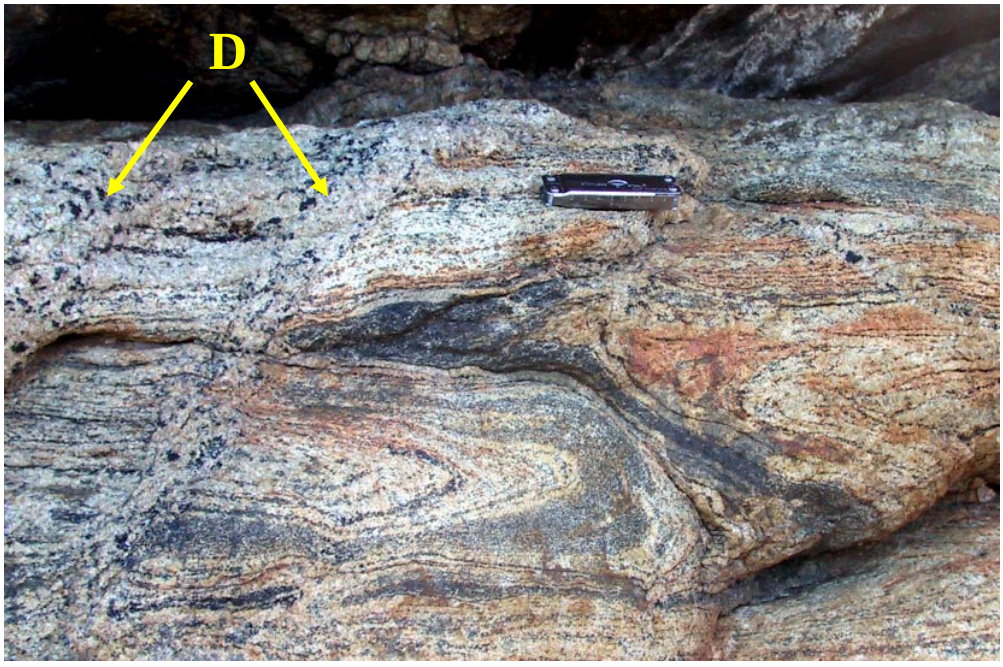

Figure 3.27. Diatexite bands (D) disrupting the migmatitic foliation, compositional layering and early folds of compositional layering. Fisheries Bay Headland. Pocket knife for scale is 7 cm long.

Figure 3.28. Jumbled mafic boudin blocks and folds of compositional layering surrounded by monzonitic leucosome. Short Beach North Headland. Compass for scale is 20 cm long.

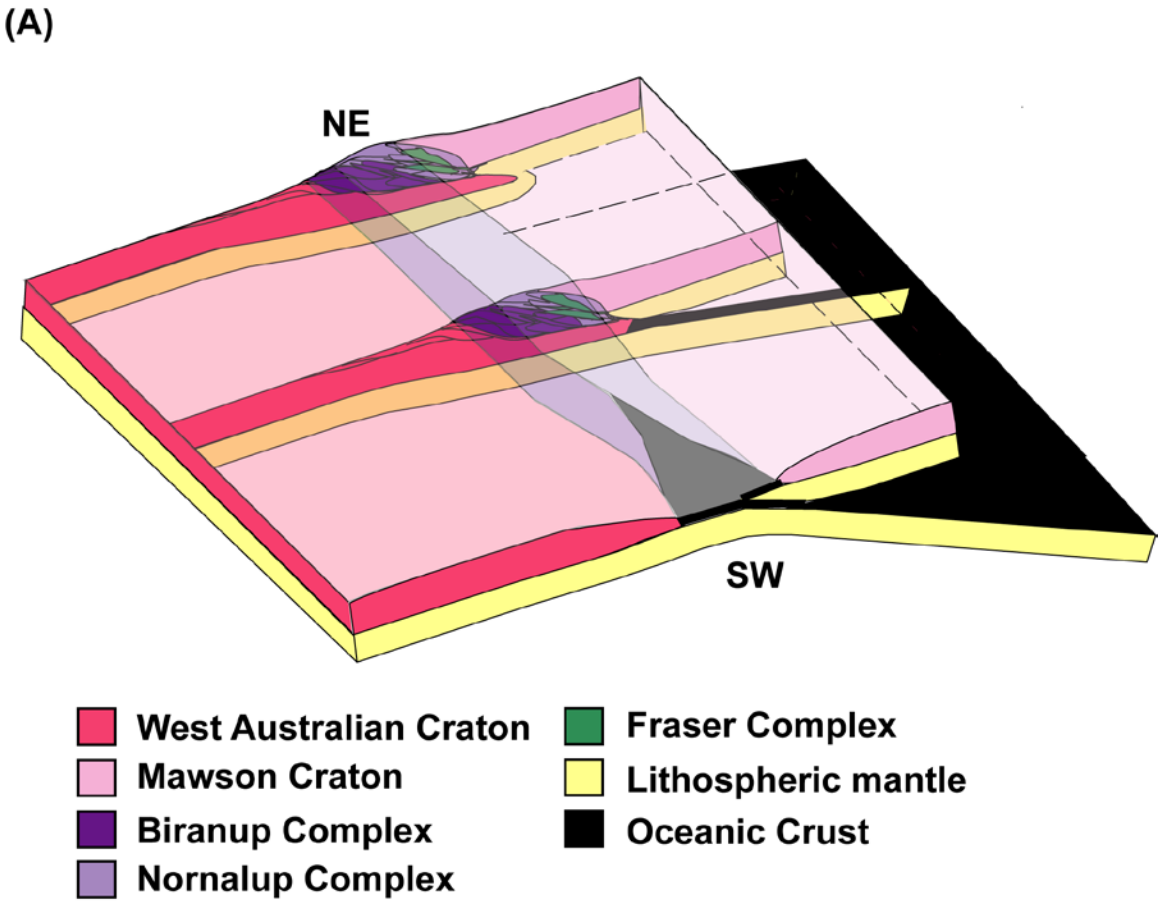

Figure 3.29a. Collision on the eastern side of the Albany Fraser orogen culminated during Stage I of the Albany-Fraser Orogeny as shown on the NE end of the block diagram. Active subduction further westward along the orogenic front results in overall NW-directed contraction and closure of the western part of the ocean basin during Stage II of the orogeny.

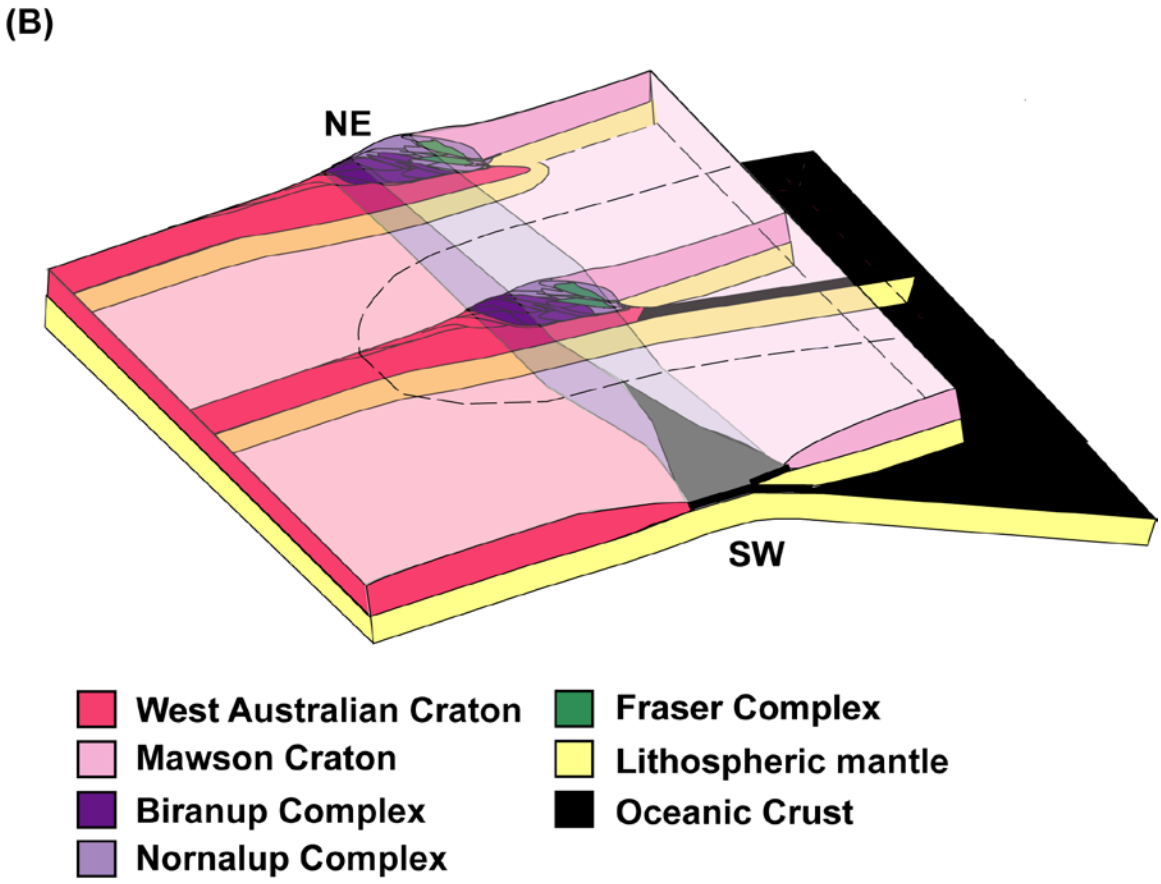

Figure 3.29b. Subducting lithosphere in a "jammed" subduction zone on the western side of the Albany-Fraser Orogen delaminates during Stage II of the Albany-Fraser Orogeny. Dashed line shows location of part of slab that delaminates in Figure 3.29c.

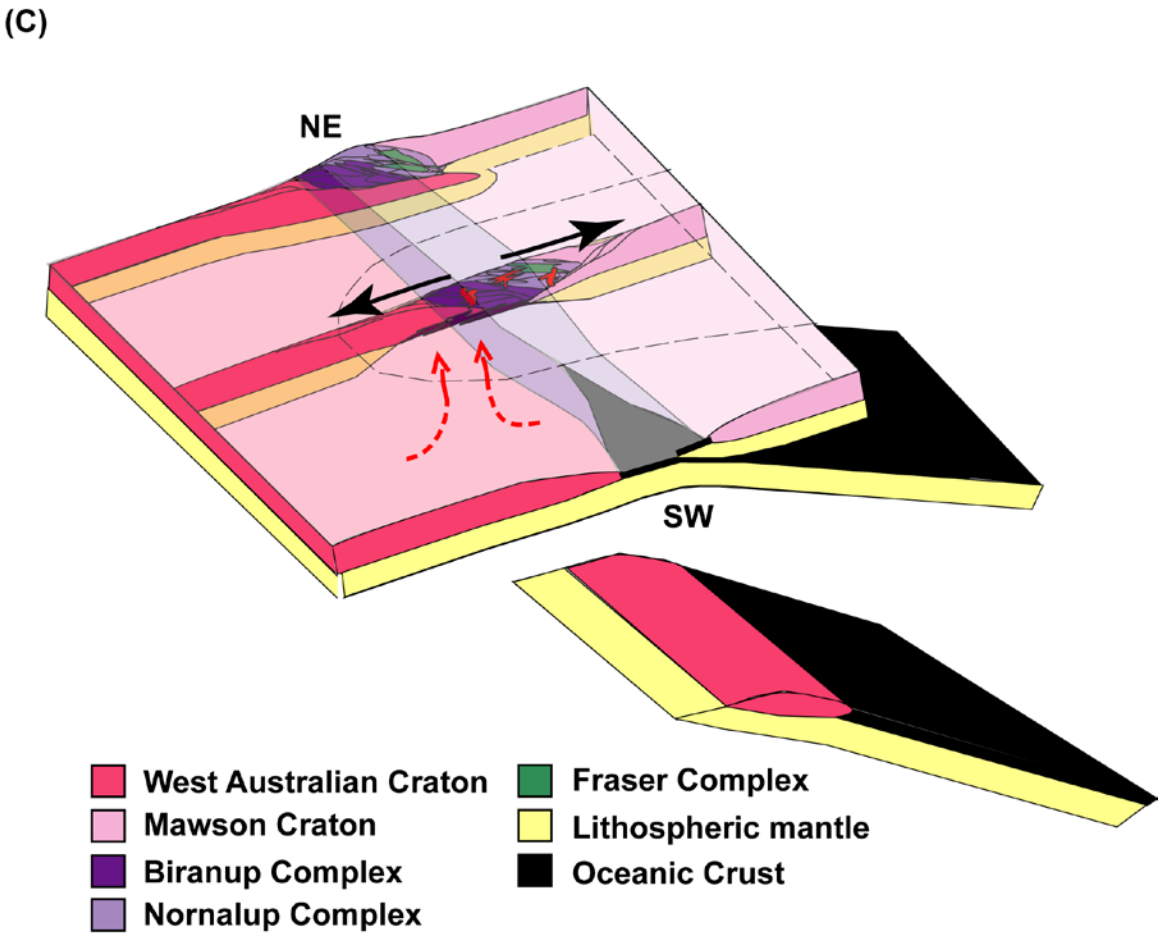

Figure 3.29c. Breakoff of the subducting slab on the western side of the Albany-Fraser Orogen. Rise of asthenospheric material into mid-crustal levels in the core of the orogen resulted in granulite-facies metamorphism and extensive melting of crustal rocks. Upwelling asthenosphere exerts traction on the over-riding plate and results in NW-SE extension perpendicular to the orogenic front. Continued subduction further west caused continued NW-directed convergence.

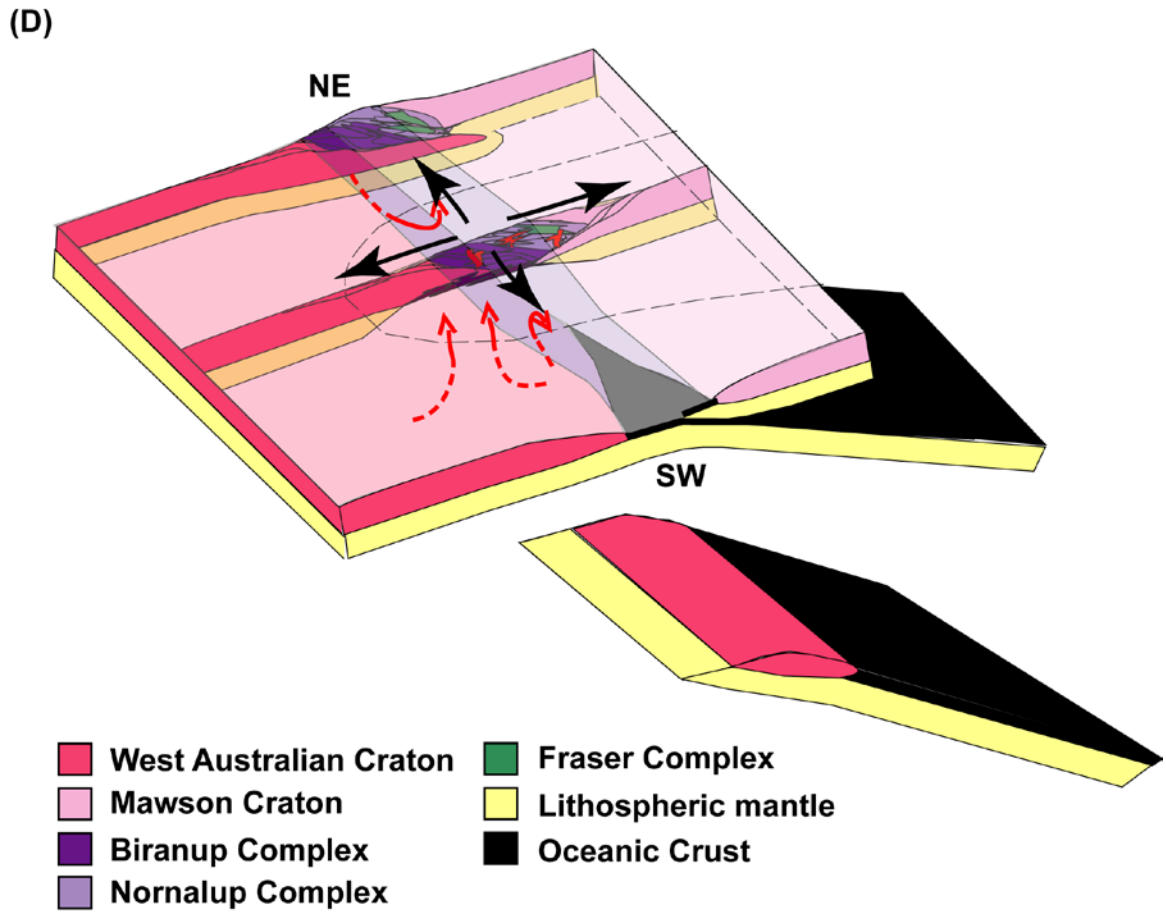

Figure 3.29d. Upwelling asthenosphere flows around the edges of the detaching slab and produces traction in the over-riding crust that results in extension in a NE-SW direction, perpendicular to the orogenic front.

Chapter 4. Structural Mapping

4.1 Introduction

During this dissertation, I carried out structural mapping at a scale of 1:500 and 1:250 of twelve different headlands along the Bremer Bay peninsula. This chapter discusses the structure observed on each of these headlands in detail and is accompanied by thirteen different plates, which consist of:

(1) Plate 1, which contains: (a) overall geologic map of the twelve headlands mapped along the Bremer Bay peninsula, scale 1:6666; (b) stereogram and rose diagram plots of structural data for each one of the twelve mapped headlands; and (c) overall stereogram and rose diagram plots of combined structural data for the entire field area.

(2) Plates 2 through 13, each of which contain: (a) geologic map of each individual headland at scale of 1:1000; (b) geologic cross-section of each individual headland at scale 1:1000; (c) stereogram and rose diagram plots of structural data for each individual headland.

This chapter also provides a detailed description of the lithology, structural petrology, and structures of migmatitic orthogneisses of the Biranup Complex (Dalyup Gneiss) in the Bremer Bay area. This chapter includes:

(1) Description of the eight different lithology types identified in the field area.

(2) Structural petrology of the orthogneisses, comprising descriptions of the pervasive migmatitic foliation, partial melt features, mineral lineation, deformation mechanisms, grain fabrics and other deformation structures observed in 178 petrographic thin sections obtained from oriented rock samples collected in the field area.

(3) Detailed field description of the structure, lithology and deformation features of each of the twelve individual headlands.

Methods are described in Appendix 1.

4.2 Lithologies

Rocks in the Bremer Bay area are granulite-facies, felsic to intermediate migmatitic orthogneisses, which have commonly been partially to completely retrograded to amphibolite-facies assemblages. The gneisses display a strong compositional banding (migmatitic fabric), defined by alternating leucosome-rich and residuum rich-layers, commonly 1-5 cm wide. I differentiated a total of eight different lithologies in the Bremer Bay area based on mineral assemblages, crystal size and leucosome structures. What follows is a more complete description of these eight different lithologies than the one provided in Chapter 2 of this dissertation. Description of the different lithologies seen in the Bremer Bay area is based on petrographic descriptions from 178 oriented thin sections obtained from 85 oriented rock samples. It takes into account descriptive features observed in the field and recorded in the geologic headland maps for the area that were omitted in Chapter 3, as they had no bearing on the crux of the geological problem addressed by that chapter.

- **Lithology 1. Orthopyroxene-clinopyroxene-biotite ± hornblende quartz monzonite orthogneiss**: this is the most common lithology in the Bremer Bay area, and it appears on most of the headlands mapped in the peninsula (see Plates 2 through 13). The orthogneiss is medium-grained and displays a light to moderate green hue that becomes darker with increasing percentage of mafic minerals, which make up to from 7% to 30% of the overall rock volume. (Hereinafter all mineral percentages refer to whole rock composition unless otherwise specified). This rock type displays two slightly different mineral assemblages and one textural variation on some headlands along the Bremer Bay peninsula, which I have defined as three different subtypes of the main lithology:
    1. Lithology 1A: the mafic assemblage is orthopyroxene (up to 2%), clinopyroxene (up to 1%), biotite (up to 3%), and magnetite (less than 1%); the rock is light gray to green and commonly medium-grained, although locally coarse-grained.

2. Lithology 1B: the mafic minerals include hornblende (10-20%), orthopyroxene (up to 3%), clinopyroxene (up to 1%), biotite (up to 5%), and magnetite (less than 1%). Hornblende replaces orthopyroxene + clinopyroxene. The rock is dark green and typically medium-grained, with local coarse-grained to porphyritic layers.

On headlands on the eastern side of the Bremer Bay Peninsula, particularly along Banky Beach East, Point Gordon, Fisheries Bay and Back Beach headlands (Figure 4.1; Plates 7, 8, 11, 12) lithologies 1A and 1B appear segregated into centimeter-wide, foliation parallel, felsic-enriched and mafic-enriched compositional bands.

- **Lithology 2. Hornblende-biotite quartz monzonite orthogneiss**: this lithology appears mainly in two localities in the Bremer Bay area, Blossoms Beach and Little Boat Harbour headlands (Figure 4.1, Plates 3 and 4). This unit is medium- to coarse-grained, locally porphyritic, dark grey to dark green, with a mafic mineral content of 10-15%: biotite (up to 5%), and hornblende (up to 15%). This unit is very similar in thin section to Lithology 1 described above, and the different mineral assemblage could indicate that this is a retrograde, amphibolite-facies equivalent of the former. On the geologic maps for Blossoms Beach and Little Boat Harbour headlands, I described two different varieties of this lithology based on crystal size, as their mineralogy in thin section is essentially identical.
    - Lithology 2A: medium-grained variety.
    - Lithology 2B: coarse-grained, locally porphyritic.
- **Lithology 3. Hornblende-orthopyroxene-clinopyroxene monzodiorite orthogneiss**: this lithology is a medium- to coarse-grained, dark green to almost black in color, with a mafic mineral content of 40-65%: hornblende (up to 40%), clinopyroxene (from 10 to 15%), orthopyroxene (quite variable, from 1% to 10%), and biotite (less than 1%). This unit is common across the entire field area and appears in two distinct ways: (1) discrete layers from a few centimeters up to one meter in thickness; and (2) as "jumbled" parts of formerly discrete layers,

locally showing evidence of prior deformation and floating in a leucocratic matrix of monzogranitic orthogneiss. These layers usually display very variable thickness and commonly are not laterally continuous.

- **Lithology 4. Garnet-biotite quartz monzonite orthogneiss**: this lithology is a medium-grained, fairly leucocratic unit that occurs in four of the twelve headlands in the Bremer Bay peninsula: Point Henry, Banky Beach, Short Beach and Fisheries Bay headlands (Figure 4.1, Plates 5, 6, 9, 11). This unit appears either as discrete, several meters to decameters wide layers, or thin, few meter wide, irregular slivers within a different host lithology. Mafic mineral contents range from 5% to 30%, including garnet (5-15%), biotite (5-10%), hornblende (rare, less than 2%) and opaque minerals (mostly magnetite) up to 5%. On the geologic maps for the headlands in which this lithology appears, I described two different varieties of this lithology on the basis of presence or absence of hornblende in the mineral assemblage, which even if present in a very low amount with respect to the other mineral phases, gives the rocks of this lithology a slightly different hue that was noticeable in the field.
    - Lithology 4A: no hornblende is present in the mineral assemblage, and the rocks usually display an off-white or pale pink hue.
    - Lithology 4B: hornblende is present in the mineral assemblage, and thus the rocks display a slightly green tone.
- **Lithology 5. Orthopyroxene-garnet quartz monzonite orthogneiss**: this lithology appears as a discrete layer less than 10 meters thick only in one locality, Banky Beach East Headland (Plate 7). The unit is medium-grained, dark in color, and contains 20-25% mafic minerals, including orthopyroxene (about 10%), garnet (up to 5%), biotite (about 5%), and magnetite (less than 2%). This unit represents the only mineral assemblage in the field area of study that preserves a peak P-T metamorphic assemblage, as garnet and orthopyroxene were deemed to have grown in thermodynamic equilibrium (Harley and Green, 1982; Aranovich and Berman, 1997).

- **Lithology 6. Leucocratic granodiorite orthogneiss with pink felsic veins**: this lithology is a medium- to coarse-grained white granitic unit with pink veins and is common throughout the field area. The unit bears no mafic minerals, but for rare biotite (less than 2%) in some samples. Commonly thin (up to a few centimeters wide), straight to anastomosing, medium- to coarse-grained pink veins, mostly made of potassium feldspar and quartz, are subparallel to the foliation.
- **Lithology 7. Magnetite-granodiorite orthogneiss**: this lithology appears exclusively on Banky Beach Headland (Plate 6) as relatively laterally continuous 5 to 40 meters wide layers. It is grey in color, fairly coarse-grained, and granitic in composition: quartz, plagioclase and potassium feldspar, biotite (up to 3%), magnetite (up to 5%), and accessory hornblende and chlorite.
- **Lithology 8. Charnockite orthogneiss**: this lithology is a leucocratic unit, which is only present on the southern end of Fisheries Bay Headland (Plate 11). The unit contains quartz, plagioclase, some potassium feldspar, variable amounts of orthopyroxene, and accessory biotite. This lithology is segregated into dm-wide white layers, with less than 3% orthopyroxene, and cm-wide dark gray layers, with up to 20% orthopyroxene.

4.3 Structural Petrology

The pervasive migmatitic foliation seen in the orthogneisses in the Bremer Bay area is defined by an alternation of centimeter-wide leucosome and residuum bands. Leucosome bands contain felsic mineral phases including plagioclase, potassium feldspar and quartz. Leucosome bands locally contain accessory biotite and opaque minerals. Residuum bands contain mafic mineral phases including orthopyroxene, clinopyroxene, hornblende, biotite, garnet (when present) and opaque minerals, mostly magnetite. Ortho- and clinopyroxene are characteristic of peak granulite-facies assemblages and appear moderately to extensively replaced by hornblende, which grew under retrograde amphibolite-facies metamorphic conditions. Even when not partially replaced by amphibole, orthopyroxene and clinopyroxene commonly appear altered in thin section,

with anomalous colors in plane polarized light and frayed edges. Residuum bands also contain felsic phases, interpreted as un-mobilized felsic minerals, including plagioclase, potassium feldspar and quartz. The percentage of felsic mineral phases varies from 20% to 50%. The transition between leucosome and residuum domains defining the migmatitic fabric is sharp, and I did not observe any evidence of mineral reactions, such as mineral replacements, coronas, or textural changes at the boundaries between leucosome and residuum bands in thin section. Also, no structures clearly suggest migration of partial melt from residuum layers into leucosome layers.

Orthogneisses in the Bremer Bay area preserve multiple evidences for partial melting in thin section. Most melt features are present in leucosome bands, where crystals crystallized from partially melted material. Evidence for partial melting includes:

(1) Felsic mineral phases (plagioclase, potassium feldspar and some quartz) in leucosome bands and locally in residuum bands show lobate, cuspate and scalloped crystal boundaries, where mineral phases are embayed into each other (Figure 4.2). The presence of this type of boundary is a result of the reaction between crystals and a melt phase. Crystals with lobate boundaries reacted with the surrounding melt, whereas crystals with cuspate boundaries represent the dominant melt phase that crystallized last, effectively infilling the available space in between the existing grains. Crystals with cuspate boundaries are commonly referred to as former melt pools. Lobate boundaries are common in plagioclase and quartz, whereas potassium feldspar more commonly displays cuspate boundaries.

(2) Presence of former melt veinlets, which are small, narrow, vein-like felsic crystals, commonly potassium feldspar, that grow along crystal boundaries between other felsic mineral phases, or along structural planes of weakness in crystal lattices, such as tiltwalls or subgrain boundaries (Figures 4.2 and 4.3). Former melt veinlets are very common features in leucosome bands and rare in residuum bands. Similarly to former melt pools, melt veinlets represent the last crystals to solidify out of the melt fraction, and they formed from thin strands of melt “trapped” between other crystals or along crystalline planes in the mineral framework.

(3) Mafic phases with rounded or lobate crystal faces, displayed by mafic crystals present within leucosome bands and locally some mafic phases in residuum bands (Figure 4.4). Mafic minerals with rounded or lobate crystal faces probably result from either reaction with a surrounding melt phase or from melting reactions where mafic phases acted as reactants during partial melting.

(4) Myrmekite growths, vermicular intergrowths of quartz and plagioclase, commonly in contact with potassium feldspar (Figure 4.2). Myrmekite growths are traditionally described as igneous textures, and as such are very common in granitic rocks. Nevertheless, as the orthogneisses in the Bremer Bay area underwent several phases of deformation at granulite-facies conditions at temperatures ca. 800°C to 1000°C (Black et al. 1992), it is improbable that protolith igneous textures would have been preserved after deformation. Therefore myrmekite growths in these rocks most probably formed during crystallization of the partial melt fraction segregated during partial melting.

The weak mineral grain lineation on migmatitic foliation planes formed in residuum layers and appears locally in the field area. In the field, it is defined by an alignment of acicular to sub-acicular minerals such as pyroxene and amphibole. In thin section, the mineral grain lineation is not easily seen, particularly within residuum layers with low percentages of relict felsic phases, where it becomes difficult to identify aligned sub-acicular mafic minerals. Observation of the mineral grain lineation in thin section is also hindered by the coarse grain size displayed by these rocks.

Petrographic thin sections of orthogneisses from the Bremer Bay area did not show any evidence of lattice preferred orientation (LPO) fabrics. Quartz and feldspar display some evidence for dynamic deformation and recovery mechanisms. Dynamic deformation mechanisms in quartz include sweeping undulose extinction and presence of deformation lamellae. Evidence for dynamic deformation in feldspar is restricted to sweeping undulose extinction. Recovery mechanisms in quartz include patchy undulose extinction and the formation of extinction domains, tiltwalls and incipient subgrains. The most common recovery mechanism exhibited by feldspar is patchy undulose extinction.

The type of the orthogneiss lithology had no influence on dynamic deformation mechanisms and evidence for recovery exhibited by quartz and feldspar.

Sampled fold hinges of decimeter-scale folds of the migmatitic fabric and compositional layering showed no evidence of secondary axial-planar foliations or layer-parallel or layer-perpendicular shear. In the field, many of these folds displayed flow in the hinge regions, as did some of the sampled folds. Hinge areas of these folds displayed no evidence of LPO fabric or shape preferred orientation (SPO). Quartz and feldspar present in the hinge areas of these folds display the same dynamic deformation and recovery mechanisms recorded in other samples from the field area.

Sampled neck areas of small centimeter-scale boudins of fabric-parallel mafic layers showed no evidence of LPO or SPO parallel or perpendicular to the boudin neck axes. Quartz and feldspar present in the leucosomes that in-filled the sampled boudin necks exhibited similar dynamic deformation and recovery mechanisms seen in other samples from the field area. The contact between the boudin blocks and the layer-parallel and neck leucosomes is sharp, and there is no evidence in thin section in favor of or against partial melt migration out of the mafic layers and into the layer-parallel and neck leucosomes during boudinage.

The partial melt textures observed within the orthogneisses, coupled with the lack of dynamic recrystallization, LPO and SPO, plus the minor deformation and recovery features, indicates that the field-scale ductile structures, such as flow into fold hinges and boudin necks, most likely was accommodated by partial melts rather than by intracrystalline plastic strain.

4.4 Geologic maps and cross sections of individual headlands

Each of the twelve headlands mapped along the Bremer Bay peninsula display different aspects of the complex structure. Rocks in the Bremer Bay area are folded by kilometer-scale asymmetric, NW-verging, SW-plunging overturned folds with long shallowly-dipping upright limbs and steep SE-dipping overturned limbs (Figure 2.7a in Chapter 2). These kilometer-scale folds across the Bremer Bay peninsula can be

identified by the map pattern of the migmatitic foliation: (1) headlands displaying NE-striking and moderately to steeply SE-dipping foliation that correspond to overturned limbs of these folds; (2) headlands displaying NW-striking and shallowly SE- to S-dipping foliation that correspond to upright, shallow-dipping limbs of these folds (Figure 2.7a). Continuous exposure along Point Henry and Banky Beach East headlands shows both limbs and the hinge area of the southern-most antiform in the area, whereas Back Beach Headland shows both limbs and the hinge area of the northern-most antiform in the field area. Outcrops along Short Beach North Headland preserve both limbs and the hinge area of the synform that formed in between the two regional antiforms (Figure 2.7a). Plate 1 shows stereogram and rose diagram plots with structural data collected for the entire field area:

(1) A stereogram of poles of the migmatitic foliation shows that the foliation is folded by regional fold axes that trend 219° and plunge 19° to the SW.

(2) A stereogram of fold axes and poles to axial planes of decimeter- to meter-scale folds of the migmatitic foliation and compositional banding indicates that these folds trend 228°, plunge 24° to the SW and verge dominantly to the NW. A rose diagram shows a mean trend of 232° for axial traces of these same folds.

(3) Rose diagrams of leucosome bands of intermediate melt chemistry (plagioclase, hornblende, pyroxene and some quartz; green in color) shows that these trend NE and NW, with the latter being more dominant.

(4) A rose diagram of leucosome bands of felsic melt chemistry (potassium feldspar, quartz, some plagioclase and some biotite; pink in color) shows that these trend dominantly NW, with a small subset displaying NE trends.

(5) A stereogram of boudin neck axes and extension directions for bidirectional boudins indicate NE- and NW-trending extension directions that correspond to NW- and NE-trending boudin axes, respectively. Most of these data were collected from meter-sized boudins of the migmatitic fabric and compositional banding interpreted to have formed during the second bidirectional extension phase in the Bremer Bay area. A few measurements correspond to centimeter-scale boudins of mafic layers

parallel to the gneissic fabric interpreted to have formed during the first bidirectional extension phase in the Bremer Bay area. Centimeter-scale boudins were very rarely exposed in faces that allowed reliable measurement of boudin neck axes.

(6) Rose diagrams of shear bands show a variety of orientations. Right-lateral shear bands of all scales throughout the field area occur in nearly all orientations and are associated with all leucosome types. Right-lateral shears associated with felsic (white) and intermediate (green) leucosomes are dominantly E-trending; right lateral shears associated with felsic (pink) leucosomes show N- to NE-, E- and NW- trends. Left-lateral shear bands of all scales throughout the field area are NE- and N-trending and associated with all leucosome types. Left-lateral shears associated with felsic (pink) and intermediate (green) leucosomes are dominantly NE- to N- trending; left-lateral shears associated with felsic (white) leucosomes are dominantly N-S trending.

Each area mapped is described in detail below.

4.4.1 Native Dog Beach Headland

Native Dog Beach Headland is the first headland on the western side of the Bremer Bay peninsula (Figure 4.1; Plates 1 and 2). This headland comprises the two coastal rock exposures on either side of Native Dog Beach, from which the headland takes its name. The migmatitic foliation on Native Dog Beach Headland displays a consistent NE-SW strike and steep SE-dip (Plates 1 and 2), and it corresponds with the steeply SE-dipping overturned limb of one of the regional-scale folds that exist in the Bremer Bay area (Figure 2.7a in Chapter 2). A mineral grain lineation that developed on migmatitic foliation planes trends SW and plunges shallowly to the SW.

Native Dog Beach Headland is dominated by an interleaving of orthopyroxene-clinopyroxene-biotite quartz monzonite orthogneiss (lithologies 1A) and hornblende-orthopyroxene-clinopyroxene-biotite quartz monzonite orthogneiss (lithology 1B), with layers of hornblende-orthopyroxene-clinopyroxene monzodiorite orthogneiss (lithology 3), leucocratic granodiorite orthogneiss with pink felsic veins (lithology 6), and the

occurrence of a mafic dike (Plate 2). The layers of the different lithologies that alternate along Native Dog Beach Headland display very variable thickness and lateral continuity.

On the western side of the headland the orthopyroxene-clinopyroxene-biotite quartz monzonite orthogneiss (lithologies 1A) frequently displays a diatexitic texture, where formed melt is pervasively distributed throughout the rock such that partially melted and unmelted portions of the rock are not segregated and the rock becomes essentially "isotropic neosome" (Figure 4.5; Plate 2). Also on the western side of the headland, hornblende-orthopyroxene-clinopyroxene-biotite quartz monzonite orthogneiss (lithology 1B) displays very coarse (up to 4 centimeters long) plagioclase megacrystals aligned with the dominant migmatitic orientation, which are unique to this location (Figure 4.6). The significance of these plagioclase megacrystals is unclear; they could be the result of fast-paced crystal growth associated with fluid flow during deformation, as the feldspar megacrystals do not overprint the migmatitic foliation, but instead appear to have grown synchronously with the development of this foliation. Alternatively they could represent older crystals that have been partially resorbed and reoriented during partial melting and formation of the foliation.

Early small (less than a meter in amplitude) isoclinal folds that fold centimeter-wide leucosome-rich bands to which the migmatitic foliation is axial planar are present in Native Dog Beach Headland (Figure 2.3 in Chapter 2; Plate 2). These folds formed during the first folding phase recorded in the Bremer Bay area (described in Chapters 2 and 3 of this dissertation). Although they appear throughout the entire headland, they are particularly concentrated in an area on the western side of the headland, in a layer of hornblende-orthopyroxene-clinopyroxene-biotite quartz monzonite orthogneiss (lithology 1B) that displays plagioclase megacrystals. However, other occurrences of these early isoclinal folds along this headland are not associated with presence of plagioclase megacrystals. Formation of plagioclase megacrystals was most likely coeval with the development of the migmatitic foliation axial planar to these folds, and thus postdates the early folding phase from which they result.

The migmatitic foliation is also folded by tight to isoclinal upright folds of a few centimeters in amplitude (Figure 4.7). The fold axial traces trend NE-SW (rose diagram in Plates 1 and 2). These folds formed during the second folding phase recorded in the Bremer Bay area, described in Chapters 2 and 3 of this dissertation.

The migmatitic foliation and first and second generation folds in Native Dog Beach Headland are boudinaged into meter-sized NE- and NW-trending bidirectional boudins formed during the second bidirectional extension phase in the Bremer Bay area (Figure 3.5 in Chapter 3). Meter-scale boudins with NE-directed extension of the migmatitic fabric and compositional layering are the most readily visible in the headland, whereas the orthogonal boudins with NW-directed extension of the same layers are less well exposed because of the steep dips and lack of vertical exposures (Figure 3.5 in Chapter 3 and Figure 4.8). This limited exposure biases the field measurements of boudin neck axes and extension directions from Native Dog Beach Headland, which represent solely data from boudins with NE-directed extension (stereogram plot in Plates 1 and 2).

Centimeter- to decimeter-wide NE- and NW-trending pegmatitic veins filled dominantly with intermediate (green) leucosomes and locally with felsic (pink to pale red) leucosomes appear in this headland (Figure 3.19 in Chapter 3). I have interpreted these veins as resulting from NE- and NW- oriented bidirectional extension, as elsewhere in the field area similar bands are clearly associated with intermediate (second phase) bidirectional boudins of the migmatitic fabric. It is possible that some of these bands could have also formed during the third bidirectional extension event that formed decameter-sized boudins in the Bremer Bay area. Locally some pegmatitic veins display changes in melt chemistry, from intermediate (green) on the outside to felsic (pink) in the inside of the band.

Late intermediate (green; Plate 2) and felsic (pink-to-red and white; Plate 2) decimeter-wide and several meters long pegmatitic veins that cut through all ductile structures appear throughout the Native Dog Beach Headland. Intermediate (green) veins trend dominantly NW-SE, with a minor set trending NNE-SSW (Plates 1 and 2). Where these veins meet, neither cross cuts the other, the pegmatitic material in the veins merge

and become indistinguishable, suggesting they formed at the same time. Felsic (pink) veins clearly postdate intermediate veins, and their orientation is dominantly NNE and NNW (rose diagrams in Plates 1 and 2). Late felsic (white) veins trend NE-SW and generally do not interact with either of the other two sets of late veins (rose diagram in Plates 1 and 2). Late felsic and intermediate pegmatites elsewhere in the Bremer Bay area clearly cut across second and third-phase boudins and boudin-related structures, thus I have interpreted these several meters long felsic and intermediate pegmatitic veins seen in Native Dog Beach Headland as postdating felsic and intermediate "pull apart" bands described above. On one outcrop in Native Dog Headland a NE-trending, sub-decimeter wide and less than two meters long felsic (white) pegmatitic vein was laterally offset by a NW-trending, centimeter-side, sub-meter long intermediate (green) "pull-apart" leucosome band, which suggests the possibility of there being several generations of felsic (white) pegmatitic veins intruding in this headland.

4.4.2 Blossoms Beach Headland

Blossoms Beach Headland is a small headland located southwest of Native Dog Beach Headland, adjacent to the southern end of Blossoms Beach, from which it takes its name (Figure 4.1; Plates 1 and 3).The migmatitic foliation in Blossoms Beach Headland is dominantly NE-trending and moderately to steeply SE-dipping (Plates 1 and 3). A very slight change in attitude of the migmatitic foliation from Native Dog Beach to Blossoms Beach headlands is observable in the geologic maps in Plates 2 and 3. As shown in stereogram plots in Plate 1: the migmatitic foliation on Blossoms Beach Headland trends slightly more easterly and dips shallower than the migmatitic foliation on Native Dog Beach Headland. This change in attitude of the migmatitic fabric could reflect the accommodation of two unexposed regional-sale hinge areas (antiformal and synformal) between Native Dog and Blossoms Beach Headlands (Figure 2.7a in Chapter 2).

This headland is dominated by medium- and coarse-grained hornblende-biotite quartz monzonite orthogneiss (lithologies 2A and 2B respectively), with one occurrence

of leucocratic granodiorite orthogneiss with pink felsic veins (lithology 6) on the southern side of the headland (Plate 3).

Early, few centimeters to few decimeters in amplitude isoclinal folds that fold centimeter-wide leucosome-rich bands to which the migmatitic foliation is axial planar, appear within medium-grained hornblende-biotite quartz monzonite orthogneiss (lithology 2A) throughout Blossoms Beach Headland (Plate 3). These folds formed during the first folding phase recorded in the Bremer Bay area.

Intermediate, meter-sized NW- and NE-trending bidirectional boudins of the migmatitic fabric and compositional layering formed during the second bidirectional extension phase in the Bremer Bay area are not readily visible on Blossoms Beach Headland. The width and height of exposed outcrop is very limited as this headland barely rises above mean tide level, and it is extensively covered by rock debris. Moreover, coarse-grained, nearly porphyritic orthogneisses present on this headland do not display a well-developed compositional layering or migmatitic foliation. The lack of strong rheological contrast within compositional layering and pervasive planar features in these rocks probably hindered the formation of well defined bidirectional boudins during extension.

Late felsic (pink) pegmatitic veins, few decimeters up to a few meters wide, cut through previously discussed structures on Blossoms Beach Headland (Plate 3). These pegmatitic veins are dominantly NW-trending, with a small subset of NE-trending veins (Plate 1). Locally NW- and NE-trending felsic (pink) pegmatitic veins cross-cut in the field, but they do not affect each other and become indistinguishable, which would represent evidence that they could have intruded at the same time.

4.4.3 Little Boat Harbour Headland

Little Boat Harbour Headland is separated from the southern end of Blossoms Beach Headland by a narrow beach called Little Boat Harbour, from which it takes its name (Figure 4.1; Plates 1 and 4). The topography changes abruptly from the northwest, where the rock outcrop barely rises above sea level, to the southeast side of the headland,

where the coastal exposure is now atop 40 meter-high nearly vertical cliffs (Plate 4). The migmatitic foliation is dominantly NE-trending and moderately to steeply SE-dipping (Plates 1 and 4), which corresponds with the steeply SE-dipping overturned limb of one of the regional-scale folds present in the Bremer Bay area (Figure 2.7a in Chapter 2). A very weak SW-trending and shallowly SW-plunging mineral grain lineation, defined by the alignment of acicular mafic mineral grains, forms on some migmatitic foliation planes (Plates 1 and 4).

Little Boat Harbour Headland is dominated by medium- and coarse-grained hornblende-biotite quartz monzonite orthogneiss (lithologies 2A and 2B respectively) , with interspersed more or less laterally continuous, variably wide layers of leucocratic granodiorite orthogneiss with pink felsic veins (lithology 6) and one occurrence of hornblende-orthopyroxene-clinopyroxene-biotite quartz monzonite orthogneiss (lithology 1B). Throughout the headland, interlayering of melanocratic quartz-monzonite and leucocratic granodiorite are common, where irregular, lensoidal, not very laterally continuous, few-meters wide layers of one lithology are weaved into the other lithology (Plate 4; Figure 4.9). The boundaries between leucocratic and melanocratic interweaved domains along Little Boat Harbour Headland are of two different kinds: (1) discrete, with a sharp transition leucocratic to melanocratic material, and (2) gradual, where the transition from melanocratic to leucocratic material is achieved by an incremental enrichment in felsic granodiorite of the monzonitic orthogneiss (Figure 4.10). Gradual transitions between the two lithologies are more common throughout the headland, which could suggest a genetic relationship between the two rock types. Perhaps the more felsic, leucocratic granodiorite corresponds to the mobilized part, or leucosome, segregated from an original protolith (paleosome) of which only the more restitic melanocratic quartz-monzonite remains.

Early small (few centimeters to few decimeters in amplitude) isoclinal folds that fold centimeter-wide leucosome-rich bands to which the migmatitic foliation is axial planar and formed during the first folding phase recorded in the Bremer Bay area appear

in two areas where medium-grained hornblende-biotite quartz monzonite (lithology 2A) as host rock (Plate 4).

Few intermediate, meter-scale folds of the migmatitic foliation and compositional layering, formed during the second folding phase recorded in the Bremer Bay area, appear on this headland. An axial trace for one of these folds (Figure 4.11) showed a NE-SW trend.

Late felsic (pink), few decimeters up to few meters-wide, pegmatitic veins cut through previously described structures on Little Boat Harbour Headland (Plate 3). These pegmatitic veins are dominantly NW-trending, with a small subset of NE-trending veins (rose diagram in Plates 1 and 3). The two sets do not cross-cut each other in the field. A large, up to three meters wide, felsic pegmatite located on the northern side of the headland, transitions from a quartz + potassium feldspar assemblage on the outside of the vein to pure quartz on the inside of the vein (Figure 4.12). Although the contrast between the two different vein mineralogies is rather sharp, there is a certain amount of mingling of pure-quartz domains and quartz-potassium feldspar domains in the contact area between the two domains. This example of sudden change of melt chemistry within a small intrusive body on Little Boat Harbour Headland illustrates the overall complexity of former melt textures and chemistry seen throughout the orthogneisses in the Bremer Bay area. Other examples were observed elsewhere in the peninsula, and they will be discussed later in this chapter.

Intermediate, meter-sized NW- and NE-trending bidirectional boudins of the migmatitic fabric and compositional layering formed during the second bidirectional extension phase in the Bremer Bay area are not readily visible in Little Boat Harbour Headland. The lack of sufficient rheological contrast of compositional layering and of well defined migmatitic foliation within the orthogneisses on this headland probably hindered the formation of well defined bidirectional boudins during extension. Locally poorly defined “pinch and swell”-type structures can be observed in some areas on the headland where compositional layering is laterally continuous (Figure 4.9), but it is not possible to measure accurate boudin neck or extension directions in these structures.

4.4.4 Point Henry Headland

Point Henry Headland is located east of Little Boat Harbour Headland (Figure 4.1; Plates 1 and 5), separated from the latter by a stretch of 40 to 45 meter-high vertical cliffs with very limited surficial rock exposure on the top, of very difficult access, and very dangerous to traverse, on which I was not able to do any field work. The migmatitic foliation is folded about an axis that trends 220 and plunges 14º to the SW (Plates 1 and 5). Continuous outcrop along Point Henry Headland exposes one limb and hinge area, and partially exposes the other limb of a large, kilometer-scale, overturned, NW-verging, SW-plunging, asymmetric antiform of the migmatitic foliation, compositional layering, early folds and metric-sized bidirectional boudins (Figure 2.7a; Plate 5). As it can be seen in the geologic cross-section in Plate 5, most of the exposure along the headland corresponds to the upright, shallow SW-dipping limb of this kilometer-scale structure. The hinge area is located near the northern end of the headland. The geologic cross-section in Plate 5 depicts structures superimposed on the upright, shallow SW-dipping limb of the regional-scale antiform. Large, decameter-scale bidirectional boudins of the migmatitic foliation and late folds formed on shallow limbs of regional-scale folds during the third phase of bidirectional extension recorded in the Bremer Bay area, as discussed in Chapters 2 and 3 of this dissertation.

Point Henry Headland is chiefly composed of orthopyroxene-clinopyroxene-biotite quartz monzonite orthogneiss (lithology 1A), with some layers of hornblende-orthopyroxene-clinopyroxene monzodiorite orthogneiss (lithology 3), garnet-biotite-hornblende quartz monzonite orthogneiss (lithology 4B) and leucocratic granodiorite orthogneiss with pink felsic veins (lithology 6) (Plate 5).

Small, blocky, rectangular, centimeter-scale NW- and NE- trending bidirectional boudins of mafic layers parallel to the migmatitic foliation appear in Point Henry Headland (Figure 4.13). These boudins were formed during the first bidirectional extension phase recorded in the Bremer Bay area.

The foliation, early centimeter-scale blocky boudins of foliation-parallel mafic layers, and the compositional layering are folded by small, up to a meter in amplitude,

NW-verging and SW-plunging open to tight folds (Figure 4.13; Plate 1). These folds were formed during the second folding phase recorded in the orthogneisses in the Bremer Bay area.

Late, NW-verging, SW-plunging meter-scale open folds of the migmatitic fabric and compositional layering appear in Point Henry Headland (Figure 3.22 in Chapter 3). Their style of deformation is different from earlier folds seen in the field area: folded layers show very limited or non-existent flow towards the hinge regions, do not attenuate on the limbs, and have no associated axial planar or hinge-area leucosomes. Differences in deformation style suggest that these folds could have formed at lower temperatures than earlier folds seen in the area and could thus postdate higher temperature deformation, including the third phase of bidirectional boudinage. I have interpreted these folds as having formed during the third folding phase recorded in the Bremer Bay area, discussed in Chapters 2 and 3 of this dissertation. Outcrops of these folds are only seen in two headlands in the field area, Point Henry and Banky Beach East headlands.

4.4.5 Banky Beach Headland

Banky Beach Headland is located northeast of Point Henry Headland (Figure 4.1; Plates 1 and 6). The stretch of coast that separates the two headlands is of very difficult access, has little surface exposure, and it is subjected to strong wave action, so I was not able to carry out any field work on it. In Banky Beach Headland the migmatitic foliation strikes NE-SW and dips moderately to steeply to the SE (Plates 1 and 6), which corresponds to the overturned, steeply SE-dipping limb of one of the regional-scale overturned folds that exist in the Bremer Bay area (Figure 2.7a in Chapter 2).

Banky Beach Headland is dominated by orthopyroxene-clinopyroxene-biotite ± hornblende quartz monzonite orthogneiss (lithologies 1A and 1B) interlayered with magnetite-granodiorite orthogneiss (lithology 7), with a small occurrence of garnet-biotite quartz monzonite orthogneiss (lithology 4A).

Small, centimeter-scale, torn, blocky rectangular, early NE- and NW-trending boudins of mafic layers parallel to the migmatitic foliation, formed during the first

bidirectional extension phase in the Bremer Bay area, occur in this headland (Figure 4.14). NE-trending early blocky boudins of foliation-parallel mafic layers appear on sub-horizontal surfaces, as they parallel the strike of the migmatitic foliation. The NW-trending counterparts on the same biaxially boudinaged mafic layers appear on vertical surfaces, as these structures have been reoriented due to regional scale folding (Figure 4.14).

Small, few centimeters up to a meter in amplitude, NW-verging, SW-plunging, open to tight folds of the migmatitic foliation, compositional banding, and early centimeter-scale bidirectional boudins of foliation-parallel mafic layers occur in Banky Beach Headland (Figure 4.15; Plate 1). These folds are later boudinaged by numerous intermediate, meter-sized NW- and NE-trending bidirectional boudins that also boudinage the migmatitic foliation and compositional layering, which formed during the second bidirectional extension phase recorded in the Bremer Bay area (Figure 4.16).

Late, NW-verging, SW-plunging meter-scale open folds of the migmatitic fabric and compositional layering formed during the last folding phase in the Bremer Bay area exist in Banky Beach Headland (Figure 4.17).

Late, few decimeters up to a meter wide felsic (pink), N- to NW- to WNW-trending pegmatitic veins intrude the orthogneisses in Banky Beach Headland, cutting through all previously described structures (rose diagrams in Plates 1 and 6).

4.4.6 Banky Beach East Headland

Banky Beach East Headland is located immediately northeast of Banky Beach Headland, both headlands located on either side of a small beach called Banky Beach, after which they are named (Figure 4.1; Plates 1 and 7). The migmatitic foliation in Banky Beach East Headland is folded (Plates 1 and 7) as a result of regional-scale folding. A NE-trending and shallowly SW-plunging mineral grain lineation that forms on foliation planes is seen locally throughout the headland (Plates 1 and 7). Continuous exposure along the headland exposes both limbs and the hinge area of a kilometer-scale, NW-verging, SW-plunging, overturned, asymmetric antiformal fold, which is the same

antiformal structure exposed in Point Henry Headland (Figure 2.7a in Chapter 2). The structural complexity observable on the shallow upright limb of the regional antiform on the eastern-most part of the headland is related to large-scale, decameter-sized bidirectional boudins of the migmatitic foliation, compositional fabric and early folds, which formed during the third bidirectional extension phase recorded in the Bremer Bay area (Plate 7). The intersection of large bidirectional boudins at the surface in the western-most side of Banky Beach East Headland results in a "hummocky" topography with domes and basins, where the domes correspond to the top of large boudins, and the basins are the boudin neck areas (Figure 4.18).

The western part of Banky Beach East Headland consists dominantly of orthopyroxene-clinopyroxene-biotite quartz monzonite orthogneiss (lithology 1A), with intercalated layers of magnetite-granodiorite orthogneiss (lithology 7), orthopyroxene-garnet quartz monzonite orthogneiss (lithology 5) and coarse grained hornblende-biotite quartz monzonite orthogneiss (lithology 2B) (Plate 7). The central part of the headland is dominated by hornblende-orthopyroxene-clinopyroxene-biotite quartz monzonite orthogneiss (lithology 1B), with layers of hornblende-orthopyroxene-clinopyroxene monzodiorite orthogneiss (lithology 3). In the eastern part of the headland the quartz monzonite orthogneiss becomes segregated into centimeter-wide, foliation parallel, felsic-enriched and mafic-enriched compositional bands (lithology 1C) (Plate 7; Figure 4.19).

Centimeter- to decimeter-scale SW-plunging, NW-verging, open to tight folds of the migmatitic foliation, compositional layering, and foliation-parallel boudinaged centimeter-wide mafic layers exist in this headland, and they formed during the second folding phase identified in the Bremer Bay area (Figure 4.20; Plates 1 and 7). These folds are later boudinaged by intermediate, meter-sized bidirectional boudins of the migmatitic foliation and compositional layering, formed during the second bidirectional extension event recorded in the Bremer Bay area (Figure 4.20; Plates 1 and 7). On the western side of the headland, where migmatitic foliation and compositional layering trend NE and dip steeply to the SE (Plate 7), intermediate bidirectional boudins appear concurrently in their

two characteristic orientations: (a) NE-trending, presently sub-horizontal, following the strike of the migmatitic foliation; and (b) NW-trending , presently sub-vertical as a result of regional-scale folding (Figures 4.20 and 4.21). Intermediate boudins of the migmatitic foliation and compositional layering are sometimes offset by top-down to the NW or top-down to the SW shear zones (Figure 3.11). Some of these shear zones are discrete, centimeter-wide and decimeter-long bands with or without associated leucosomes in the shear plane. When present, leucosomes are felsic (white to pale pink) or intermediate (green) in composition. Some shear zones offsetting intermediate boudins are decimeter-wide zones of shear into which the boudinaged foliation and compositional banding are strongly deflected.

Late, NW-verging, SW-plunging, open metric folds of the migmatitic foliation and compositional banding appear in this headland (Figure 2.11 in Chapter 2). Similarly to late folds seen in Point Henry Headland, these folds show almost no flow of folded layers towards the hinge-regions of the folds, and no attenuation of folded layers in the limbs of the folds. There are also no axial-planar or hinge-area leucosomes. Unlike those at Point Henry, however, these folds are tighter. These folds formed during a late, potentially lower temperature folding phase that postdates the third bidirectional extension phase recorded in the Bremer Bay area.

Late, few decimeters up to a meter-wide felsic (pink) pegmatitic veins intrude the orthogneisses in Banky Beach East Headland (rose diagrams in Plates 1 and 7). They are dominantly NW-trending, with one trending E-W, and cut through all previously discussed structures.

4.4.7 Point Gordon Headland

Point Gordon Headland follows immediately east of Banky Beach East Headland (Figure 4.1; Plates 1 and 8). Point Gordon is the geographical name for the western-most point in the Bremer Bay Peninsula, from which the headland takes its name. Although Banky Beach East and Point Gordon headlands represent continuous rock exposure, the digital 1:1000 scale geologic map for both headlands cannot be accommodated to a

useful printed format, and therefore I arbitrarily divided the exposure in two different headlands. The migmatitic foliation along Point Gordon Headland appears folded about an axis that trends 218º and plunges 19º SW (Plate 1, 8). The migmatitic foliation along this headland displays varied NE, NW and E-W trends, with corresponding SE, SW and N or S dips that are consistently shallow (Plate 8). The change in strike direction of the migmatitic foliation along Point Gordon Headland is due to the interference of large, decameter-sized NE- and NW-trending boudins of the migmatitic fabric and compositional layering (Figure 2.10 in Chapter 2). This headland is the continuation of the upright, shallow SW-dipping limb of the overturned, NW-verging regional scale antiform whose overturned, steeply SE-dipping limb and hinge area are exposed in Banky Beach East Headland (Figure 2.7a in Chapter 2 and Plate 8). The structural complexity seen on the geologic cross-section of Point Gordon Headland in Plate 8 is the result of these decameter-scale bidirectional boudins formed during the third bidirectional extension phase seen in the Bremer Bay area. Cross-section exposures of large, decameter-size bidirectional boudins are not common on coastal exposures along the Bremer Bay peninsula, with Point Gordon Headland being only one of two exposures in the field area where a vertical cross-section of these boudins can be seen (Figure 3.14 in Chapter 3).

Point Gordon Headland is dominated by hornblende orthopyroxene-clinopyroxene-biotite quartz monzonite orthogneiss (lithology 1B) segregated into centimeter-wide, foliation parallel, felsic-enriched and mafic-enriched compositional bands, the same lithology that appears on the eastern-most part of Banky Beach East Headland (Plate 8). A layer of hornblende-orthopyroxene-clinopyroxene monzodiorite orthogneiss (lithology 3) appears in the western side of the headland (Plate 8).

Decimeter-scale SW-plunging, NW-verging, open to tight folds of the migmatitic foliation, compositional layering, and foliation-parallel boudinaged centimeter-wide mafic layers exist in this headland, and they formed during the second folding phase identified in the Bremer Bay area (Figure 2.5b in Chapter 2; Plate 1). A weak SW-plunging mineral grain lineation defined by the alignment of acicular mafic minerals

grows on some foliation planes along the headland (Plates 1 and 8). This mineral grain lineation appears parallel to the fold axes of one set of decimeter-scale, SW-plunging recumbent refolded folds of the compositional layering and migmatitic foliation on Point Gordon Headland (Figures 4.22 and 4.23), which suggests that the mineral grain foliation could have formed during the second folding phase in the Bremer Bay area. This is the only outcrop in the entire Bremer Bay area where such relationship between the mineral grain lineation and second generation folds has been seen.

Intermediate, meter-sized bidirectional boudins of the migmatitic foliation and compositional layering formed during the second bidirectional extension phase recorded in the Bremer Bay area appear on this headland (Figure 4.24). As the migmatitic foliation in this headland is dominantly shallow, surface exposures commonly follow foliation planes: only vertical exposures, somewhat limited along the headland, will allow for cross-section exposures of intermediate, meter-scale bidirectional boudins.

Late, decimeter- to meter-wide felsic (pink) pegmatitic veins intrude into the orthogneisses in Point Henry Headland, and cut through all previously described structures (Figure 4.25). They are dominantly NW-trending with a small subset of NE-trending veins (rose diagram in Plates 1 and 8). Pegmatitic veins of these two orientations were not observed cross-cutting in the field, but in two places on the western side of the headland, where the majority of these pegmatitic veins appear (Plate 8), a NW-trending vein is seen to abruptly turn into a NE-trending vein, with no distinguishable petrologic or textural differences between the melts in those two orientations.

A large, NW-trending felsic pegmatite (pink) intrudes into the Point Gordon orthogneisses on the western side of the headland (Plate 8). The width of this pegmatitic body decreases from over six meters on its southeastern end to less than one meter on its northwestern termination, where it disappears underneath the vegetation cover. This large pegmatite clearly cuts across other felsic pegmatitic veins intruded into the orthogneisses in this headland.

Locally in Point Gordon Headland there are areas where the dominantly shallow-dipping migmatitic foliation is disrupted by less than a meter wide subvertical bands of

diatexitic texture in the orthogneisses, such that the migmatitic fabric is completely disrupted or it appears as suddenly vertical (Figure 4.26). Similar structures are seen in other headlands in the field area, and I have interpreted them as melt conduits during deformation.

4.4.8 Short Beach Headland

Short Beach Headland follows northwest of Point Gordon Headland after a stretch of coastal outcrops of very difficult access, narrow exposures, and open to strong wave action on which I was unable to do any field work (Figure 4.1; Plates 1 and 9). Short Beach Headland is located on the southern end of Short Beach, one of the most picturesque and visited beaches in the Bremer Bay peninsula. The migmatitic foliation in Short Beach Headland trends NE-SW and dips moderately to the SE (Plates 1 and 9), which corresponds to the overturned, moderately to steeply SE-dipping limb of a regional-scale overturned antiform (Figure 2.7a in Chapter 2).

Short Beach Headland is mainly composed of interlayered orthopyroxene-clinopyroxene-biotite ± hornblende quartz monzonite orthogneiss (lithologies 1A and 1B), with layers of leucocratic granodiorite orthogneiss with pink felsic veins (lithology 6), very thin layers and veins of hornblende-orthopyroxene-clinopyroxene monzodiorite orthogneiss (lithology 3) and an area of garnet-biotite-hornblende quartz monzonite orthogneiss (lithology 4B) in the southern side of the headland (Plate 9).

Centimeter to decimeter-scale folds of the migmatitic fabric and compositional layering are observed in this headland (Figure 4.27). These folds are commonly inclined to recumbent, NW-verging, SW to SE-trending, and shallow to steeply SW- or steeply SE- plunging (Plate 9) and formed during the second folding phase in recorded in the rocks in the Bremer Bay area. The variability in trend and plunge of these folds is a unique feature of this particular headland (Plate 9 stereonet), and it is potentially related to later rotation of these folds by small shear bands.

The geologic map in Plate 9 highlights an area on the Short Beach Headland where small, up to 30 cm-long shear zones with pegmatitic material segregated along the

shear planes are associated with folds of the gneissic fabric and compositional banding (Figure 3.24 in Chapter 3). Harris et al. (2002) and Harris (2003) describe a process for this area by which back-rotation between pairs of shear zones generate folds. Although folds and shear-couple associations similar to those resulting from back-rotation are seen locally in other outcrops in the Bremer Bay area, the high concentration of these structures in a relatively narrow and well defined zone in Short Beach Headland (Plate 9) could result from localized accommodation of pure shear during deformation, a mechanism that Harris et al. (2002) and Harris (2003) suggest as most likely responsible for the process of back rotation in Short Beach Headland. It is also possible that the development of folds of the migmatitic fabric as a result of back-rotation between shear bands could post-date the second folding phase in the Bremer Bay area, and tight to isoclinal folds of the migmatitic foliation formed during this second folding phase could have been later rotated due to shearing and back-rotation between shear planes (Figure 4.28).

A well developed mineral grain lineation defined by aligned acicular mafic minerals grows on foliation planes in Short Beach Headland. The mineral lineation trends 224 and plunges 30º to the SW (Plate 9).

The migmatitic foliation, compositional layering and early decimeter-scale isoclinal folds are boudinaged by intermediate, metric bidirectional boudins formed during the second bidirectional phase in the Bremer Bay area (Figure 3.4 in Chapter 3).

Commonly meter-sized boudins in this headland are either asymmetric or offset by discrete shear bands (Figure 3.4 in Chapter 3), displaying top-down to the NE and top-down to the SW (more dominant) asymmetry. Asymmetry of NE-trending meter-sized boudins is also observed in other headlands, such as Native Dog Beach and Banky Beach headlands. All three of these headlands display steeply SE-dipping foliation, and compositional banding with adequate rheological contrast such that meter-size boudins of NE-extension direction, which are parallel to the trend of the foliation, are very well developed. Display of NW-trending meter-sized boudins in these three headlands depends on the amount of dip-slope outcrop, and it is generally limited. Therefore,

although I did not observe any field evidence for sense of shear or asymmetry associated with NW-trending meter-sized boudins, it cannot be ruled out completely, as this lack of evidence could be a result of limited exposure. The top-down-to- NE sense of asymmetry associated with NE-trending meter-sized boudins seen in Native Dog Beach, Banky Beach and Short Beach headlands is consistent with a regional component of dextral transpression, a mechanism commonly invoked in tectonic models for the western Albany-Fraser Orogen.

Also as a result of limited exposure of sub-vertical (NW-trending) meter-sized boudins in Short Beach Headland, boudin neck and extension directions in the stereogram plot for this headland in Plate 1 and 9 correspond only to NE-trending boudins, as boudins in this orientation were the only ones that could be reliably measured in the field.

4.4.9 Short Beach North Headland

Short Beach North Headland represents a small coastal exposure accessible from the northern end of Short Beach (Figure 4.1; Plates 1 and 10). Continuous outcrop along the headland exposes a transition in attitude of the migmatitic foliation and compositional banding from NE-trending and moderately SE-dipping at the southern end, to nearly E-trending and shallowly SE-to S-dipping in the northern end of the headland (Plates 1 and 10). This change in attitude represents the transition from the moderately SE-dipping overturned limb to the shallow S-dipping limb of an overturned regional-scale fold through a synformal hinge (Figure 2.7a in Chapter 2; Plates 1 and 10). The sudden change in attitude of the migmatitic foliation is very evident in the field, but there is no exposure of an unequivocal synformal hinge area. The section of headland that represents the transition between the two different migmatitic foliation attitude domains displays great structural complexity, with multitude of small folds of the foliation and compositional layering, and the presence of the irregular body of hornblende-orthopyroxene-clinopyroxene monzodiorite orthogneiss (lithology 3) that appears at a higher structural level in the northern part of the headland (Plate 10). This increased

structural complexity could easily be associated with the hinge area of a regional-scale structure.

Short Beach North Headland consists of hornblende-orthopyroxene-clinopyroxene biotite quartz monzonite orthogneiss (lithology 1B), with an occurrence of hornblende-orthopyroxene-clinopyroxene monzodiorite orthogneiss (lithology 3) in the northern side of the headland (Plate 10).

A weak SW-trending and shallowly SW-plunging mineral grain lineation is visible locally on foliation planes along this headland (Plate 10).

Small, centimeter-scale blocky bidirectional boudins of mafic layers parallel to the compositional layering, formed during the first bidirectional extension event in the Bremer Bay area, occur in Short Beach North Headland (Figure 4.29; Plate 1). These boudins are later folded by decimeter-scale, NW-verging, SW-plunging, open to isoclinal folds that also fold the migmatitic fabric and compositional banding (Figure 4.30), which resulted from the second bidirectional extension episode recorded in the Bremer Bay area.

Meter-scale bidirectional boudins of the compositional layering formed during the second bidirectional extension phase in the Bremer Bay area appear in Short Beach North Headland (Figure 4.31). Relatively shallow-dipping foliation (and compositional banding) and lack of sufficient amount of vertical exposure throughout most of the headland, limit the existence of outcrops that allow cross-sectional views of meter-sized boudins.

Two decimeter-scale, felsic (pink), NNW- to NNE-trending late pegmatitic veins intrude the orthogneisses in the southern-most part of Short Beach North Headland (Plates 1 and 10).

Decimeter-long, few centimeters-wide, intermediate (green) and felsic (pink) “pull apart” pegmatitic bands are common in the southern-most part of the headland. They occur in several different orientations and are probably related to localized accommodation of bidirectional extension. Their most distinguishing characteristic is that they display transitions in melt chemistry within individual bands, where the pegmatitic

material changes from intermediate composition (intermediate plagioclase and hornblende) at the outside of the vein to felsic composition (potassium feldspar and quartz) in the center part of the vein (Figures 4.32 and 4.33).

In Short Beach North Headland the migmatitic fabric and compositional banding are locally disrupted by sub-vertical bands of diatexitic texture. These bands are a few centimeters up to a meter in width, and from less than one decimeter up to two or three meters long (Figure 4.34). Some of the larger zones have completely disrupted the compositional banding and earlier structures, such as decimeter-size folds of the compositional banding and earlier boudins of mafic layers, so that parts of these structures appear as disarranged "rafters" surrounded by leucosome (Figure 4.35). The leucosomes in these zones are generally granodioritic to monzogranitic in composition, and fairly leucocratic. It is conceivable that these structures could reflect active melt conduits during high-temperature ductile deformation, where partial melt was being distributed throughout the orthogneisses.

4.4.10 Fisheries Bay Headland

Fisheries Bay Headland is an area of significant structural complexity, which preserves field evidence for all phases of deformation recorded in the Bremer Bay area, and for this reason I originally constructed a 1:250 scale geologic map of this headland. Nevertheless, reduction of the original 1:250 scale geologic map to a printable 1:1000 scale geologic map did not impact the accuracy of the geologic information conveyed by the re-scaled map, as only redundant structural data was removed in the process.

Fisheries Bay Headland is located north of Short Beach North Headland, following a section of 30 meter-high near vertical cliffs on which I was unable to carry out any field work (Figure 4.1; Plates 1 and 11). To the north the headland terminates against a small cove, Fisheries Bay, from which it takes its name. The migmatitic foliation in Fisheries Bay Headland is dominantly NW- to W- trending, and shallowly SW- to S- dipping (Plates 1 and 11). This headland represents the upright, shallow S- to SW-dipping limb of one of the regional-scale folds in the Bremer Bay area (Figure 2.7a;

Plate 11). A mineral grain lineation, which trends 230 and plunges 18º SW, appears on foliation planes throughout Fisheries Bay Headland (Plates 1 and 11). Large, decameter-sized bidirectional boudins of the migmatitic foliation and compositional layering exist in Fisheries Bay Headland (Figures 2.9 in Chapter 2; Figures 3.15, 3.16 and 3.17 in Chapter 3), and formed during the third bidirectional extension phase recorded in the Bremer Bay area. Decameter-sized boudins are dominantly drawn (lensoidal) throughout most of Fisheries Bay Headland (Figure 4.36; Figures 3.15 and 3.16 in Chapter 3), although in the southern end of the headland large boudins are torn (blocky) (Figure 3.17 in Chapter 3). These large boudins are also vertically stacked or nested, where overlying boudins rest on underlying neck areas (Figure 4.36). As nested decameter-sized boudins were also observed in large vertical cross-section exposures in Point Gordon Headland, it is conceivable that they could exist in all areas where large bidirectional boudins formed, which coincide with the shallow-dipping, upright limbs of regional-scale structures (Figure 2.7a in Chapter 2; Plate 1).

Fisheries Bay Headland displays three main lithologies: segregated orthopyroxene-clinopyroxene-biotite quartz monzonite orthogneiss (lithology 1A) in the northern side, hornblende-orthopyroxene-clinopyroxene-biotite quartz monzonite orthogneiss (lithology 1B) in the central part, and charnockite orthogneiss (lithology 8) in the southern side of the headland (Plate 11).

Small, centimeter-scale blocky bidirectional boudins of the migmatitic foliation and mafic layers parallel to the compositional banding formed during the first bidirectional extension event in the Bremer Bay area exist in Fisheries Bay Headland (Figure 2.4a in Chapter 2). Felsic leucosomes (former melt) are localized in the neck areas and commonly along the boudinaged layer as well (Figure 2.4a in Chapter 2).

The migmatitic foliation, compositional layering and early centimeter-scale boudins of mafic layers are later folded by centimeter up to a meter-sized, SW-plunging, SE- to NW-verging, open to tight folds formed during the second folding phase identified in the Bremer Bay area (Plates 1 and 11; Figures 4.37 and Figure 2.5a in Chapter 2). These folds are observed in up to three meter-wide zones parallel to the foliation and are

commonly associated with abundant leucosomes, suggesting the folds formed as a result of shearing.

Metric-sized bidirectional boudins of the migmatitic foliation, compositional layering and early folds of boudinaged mafic layers appear in Fisheries Bay Headland (Plates 1 and 11; Figure 2.6b in Chapter 2 and Figure 3.3 in Chapter 3). These boudins formed during the second bidirectional extension phase recorded in the rocks in the Bremer Bay area. Felsic leucosomes are commonly localized in the neck areas of these boudins and are locally seen along the boudinaged layers as well (Figure 3.3 in Chapter 3). NE- and NW-trending "pull-apart" bands filled with intermediate (green) or felsic (pink) pegmatitic material are common in the neck areas of meter-scale bidirectional boudins of the migmatitic fabric and compositional banding (Figure 3.13 in Chapter 3). The dominant shallow-dipping migmatitic foliation in Fisheries Bay Headland and lack of adequate cross-section exposures of boudins limited my ability to measure boudin neck orientations and extension directions for centimeter- and meter-scale bidirectional boudins, even though they are common throughout the entire headland.

Pegmatitic melts commonly intrude into the necks of decameter-scale boudins. The morphology and first order chemistry of these melts is fairly diverse: (1) felsic pegmatitic bodies with diffuse boundaries into the country rock (Figures 3.17 and 3.18 in Chapter 3); (2) discrete pegmatitic bodies of variable chemistry, locally intruded along shear zones that offset boudins (Figures, 4.38 and 4.39; Figure 2.9 in Chapter 2; Figures 3.17 and 3.18 in Chapter 3).

The interference between NE- and NW-trending large boudins results in a subtle "hummocky" topography (Figure 4.36), where large scale topographic undulations mirror the attitude of the boudinaged migmatitic foliation (Plate 11).

Late intermediate (green) and felsic (pink) pegmatitic veins cut through all ductile structures in Fisheries Bay Headland. Both types of pegmatitic veins are dominantly NE-trending though NW-trending sets are common (Plates 1 and 11), and felsic veins postdate intermediate pegmatitic veins (Figure 2.12a in Chapter 2).

Pegmatitic veins displaying intermediate (commonly on the outside of the vein) to felsic (commonly in the center of the vein) chemistry changes are also frequent in Fisheries Bay Headland (Figures 4.40 and 4.41), and affect pegmatitic melts in "pull-apart" bands and late pegmatitic veins that cut through all ductile structures.

4.4.11 Back Beach Headland

Back Beach Headland, located to the north of Fisheries Bay Headland, includes the coastal exposure between the northern end of Fisheries Bay and the southern end of Back Beach, after which it is named (Figure 2.7a in Chapter 2; Plates 1 and 12). Structural mapping of this headland was difficult, due to limited width of outcrop, particularly in the southern half of the headland. The migmatitic foliation changes from generally E-trending and shallowly S- dipping on the southern side of the headland, to NE-trending and moderately to steeply SE-dipping on the northern side of the headland (Plates 1 and 12). The change in attitude of the migmatitic foliation is due to large-scale folding, as Back Beach Headland contains the hinge area of the northern-most NW-verging regional antiform in the Bremer Bay area. The antiformal hinge is not recognizable in the field because of the lack of laterally extensive exposure in this headland, paired with increased structural complexity resulting from parasitic folding and increased melt presence, although it is evident from the change in attitude of the migmatitic foliation and compositional layering (Plate 12).

Back Beach Headland is dominated by segregated orthopyroxene-clinopyroxene-biotite quartz monzonite orthogneiss (lithology 1A), with layers of the hornblende-bearing variety of the same orthogneiss (lithology 1B), and one occurrence of leucocratic granodiorite orthogneiss with pink felsic veins (lithology 6) in the northern part of the headland (Plate 12).

Centimeter-scale blocky bidirectional boudins of mafic layers parallel to the compositional banding appear in Back Beach Headland (Figure 4.42). These boudins are later folded by upright to recumbent, SW-plunging decimeter-scale folds that also fold the migmatitic foliation and compositional banding (Figure 4.42; Plates 1 and 12).

The lack of well defined meter-sized boudins in Back Beach Headland is most probably due to the lack of strong rheological contrast and absence of a well defined migmatitic foliation within the orthogneisses.

Locally in Back Beach Headland possible high-temperature deformation melt conduits similar to those described in Point Gordon and Short Beach North headlands are present. In Back Beach Headland two of these conduits, which appear as approximately decimeter-wide zones of coarse-grained diatexitic texture in the orthogneisses, clearly cut through the hinge-region of a several meter-wide fold of the compositional layering and migmatitic foliation (Figure 4.43). Another possible meter-wide subvertical melt conduit was seen completely disrupting the shallowly S- to SW-dipping migmatitic fabric and compositional layering in the southern part of the headland, so that both features are now subvertical over a very narrow, sub-meter wide zone. This type of migmatitic fabric and compositional banding disruption is very similar to structures previously described in Point Gordon Headland.

Closed folds of the migmatitic foliation seen in the geologic cross section in the northern end of the headland (Plate 12) are probably related to the latest folding phase recorded in the Bremer Bay peninsula, although the outcrop does not allow for a cross-section view of these structures, and therefore I was not able to compare their deformation style to that of late folds seen in other headlands along the Bremer Bay peninsula.

A weak SW-trending and shallowly SW-plunging mineral grain lineation appears on migmatitic foliation planes along Back Beach Headland (Plate 12).

Late, several decimeter-wide intermediate (green) and felsic (pink) dominantly NW-trending pegmatitic veins intrude the orthogneisses in Back Beach Headland, cutting through earlier ductile structures (Plates 1 and 12).

4.4.12 John's Cove Headland

John's Cove Headland consists of a small section of coastal exposures located on the northern side of Back Beach, at the northeastern-most end of the Bremer Bay

peninsula (Figure 4.1; Plates 1 and 13). The migmatitic foliation strikes NE-SW and dips moderately to steeply to the SE (Plates 1 and 13), which corresponds to the overturned, moderately to steeply SE-dipping limb of a regional-scale overturned antiform (Figure 2.7a in Chapter 2). Closed folds of the migmatitic foliation seen in the geologic cross section (Plate 13) are probably related to the latest folding phase recorded in the Bremer Bay peninsula, similar to those seen in Back Beach Headland. However I was not able to see a cross-section view of these structures, and therefore I was not able to compare their deformation style to that of late folds seen in other headlands along the Bremer Bay peninsula.

John's Cove Headland consists of orthopyroxene-clinopyroxene-biotite quartz monzonite orthogneiss (lithology 1A), with a discrete layer of hornblende-orthopyroxene-clinopyroxene monzodiorite orthogneiss (lithology 3) in the northern end of the headland (Plate 13).

Centimeter-scale blocky bidirectional boudins of mafic layers parallel to the migmatitic foliation appear in John's Cove Headland (Figure 4.44).

The main lithology in this headland is relatively homogeneous and coarse-grained, with poorly developed migmatitic foliation and compositional banding. Homogeneity of the orthogneisses made very difficult to observe the presence of possible centimeter- to decimeter-scale folds of the foliation and compositional banding that are so common elsewhere along the Bremer Bay peninsula. The lack of sufficient competency contrast within the orthogneisses results in very poorly developed metric bidirectional boudins in John's Cove Headland.

Several late, sub-meter wide, NW- to N-trending, intermediate (green) pegmatitic veins intrude the orthogneisses in John's Cove Headland (Plates 1 and 13).

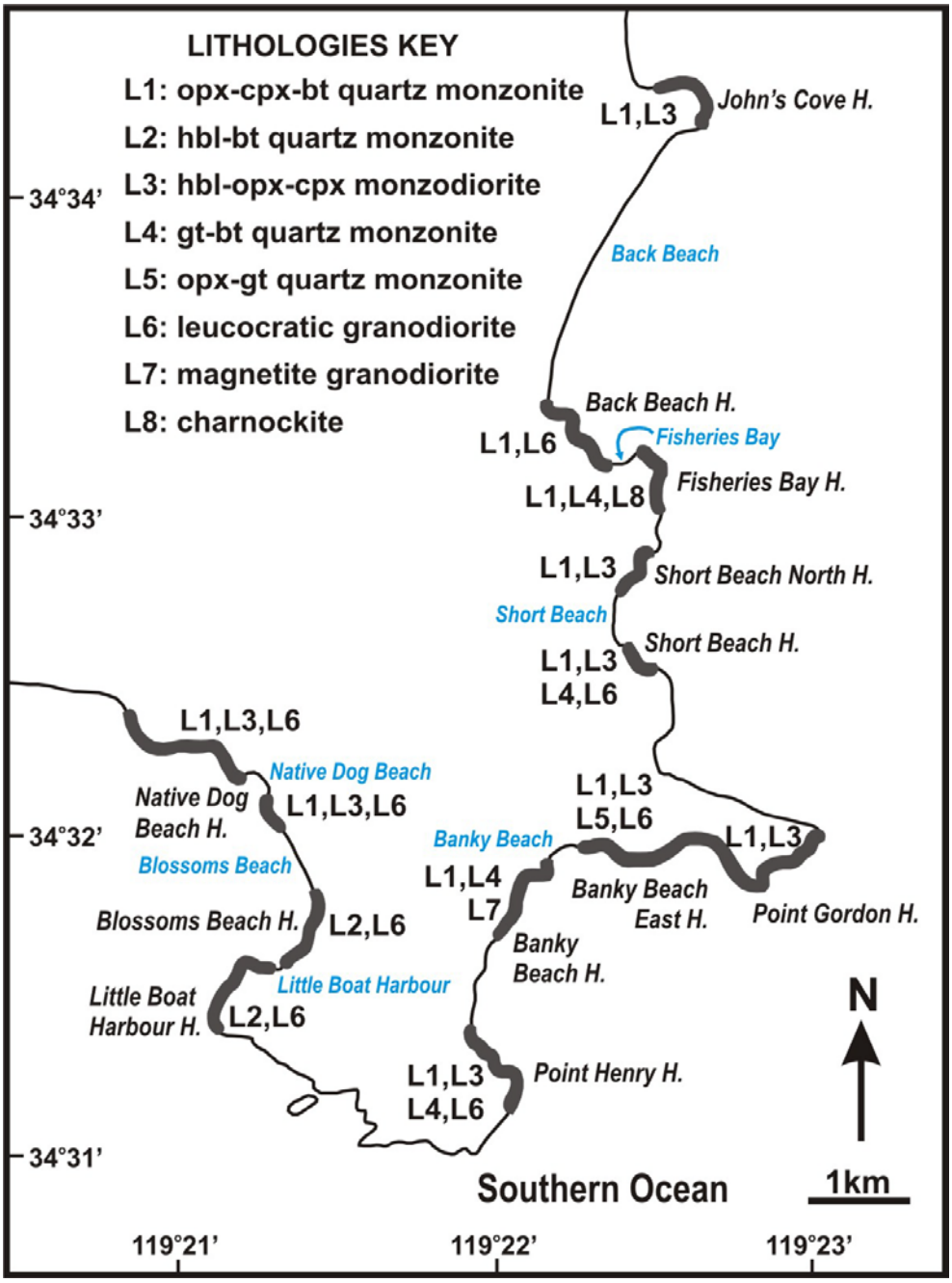

Figure 4.1. Map of the Bremer Bay peninsula, highlighting the 13 headlands mapped in this study, and the distribution of the main lithologies throughout the field area. The extent of the area mapped for each headland is highlighted in grey.

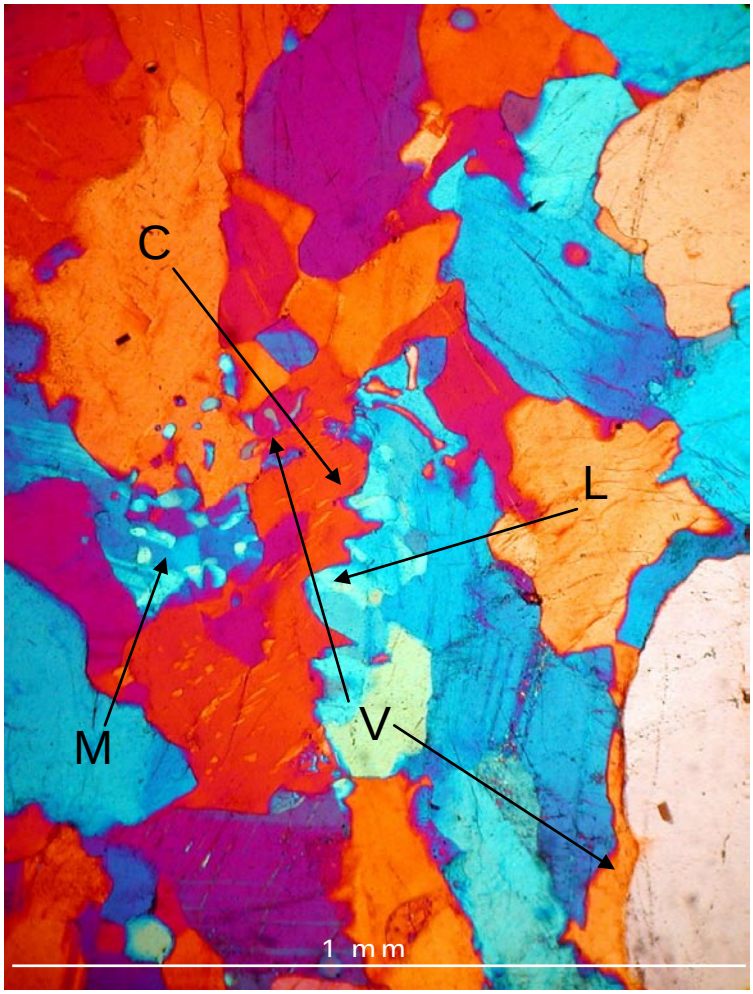

Figure 4.2. Partial melting textures preserved in leucosome band of quartz monzonitic orthogneiss from the Bremer Bay area. (**L)** Lobate grain boundaries. (**C**) Cuspate grain boundaries. (**V**) Former melt veinlets. (**M**) Myrmekite growths. Cross polarized light. Gypsum plate inserted to show mineral phases in optical continuity. Field of view is 1 millimeter wide. Sample NDBH5 (Native Dog Beach Headland, Plate 2).

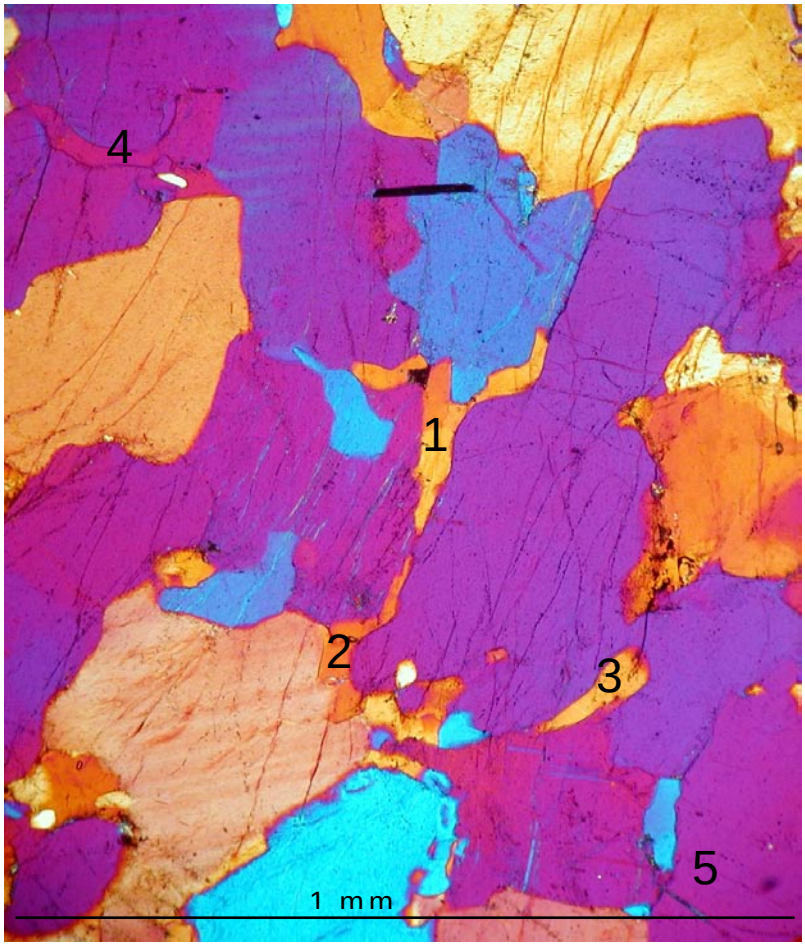

Figure 4.3. Former melt veinlets preserved in leucosome band of quartz monzonitic orthogneiss from the Bremer Bay area. Veinlets 1 through 3 are potassium feldspar, and have formed along plagioclase crystal boundaries. Veinlet 4 has also formed along plagioclase crystal boundaries, and it is most probably plagioclase in composition, as it shows optical continuity with the surrounding plagioclase crystals. Veinlet 5 appears to have intruded and later crystallized into a cleavage plane in a plagioclase crystal. Cross polarized light. Gypsum plate inserted to show mineral phases in optical continuity. Field of view is 1 millimeter wide. Sample NDBH5, Native Dog Beach Headland (Plate 2).

Figure 4.4. Mafic phases with rounded or lobate crystal faces (R) in leucosome band of quartz monzonitic orthogneiss from the Bremer Bay area. Cross polarized light. Gypsum plate inserted to show mineral phases in optical continuity. Field of view is 1.5 millimeter wide. Sample NDBH6, Native Dog Beach Headland (Plate 2).

Figure 4.5. Sheared centimeter-scale NW-trending boudins of a mafic layer in quartz monzonitic orthogneisses in Native Dog Beach Headland. Note the diatexitic texture in host orthogneisses surrounding the sheared mafic boudins. Pencil for scale is 12 cm long.

Figure 4.6. Plagioclase megacrystals (some highlighted in green) in Lithology 1B in Native Dog Beach Headland. Pencil (12 cm long) parallels the poorly developed foliation.

Figure 4.7. Tight, upright, NE-trending fold of the gneissic fabric, formed during the second folding phase recorded in the Bremer Bay area. Native Dog Beach Headland. Pencil for scale is 12 cm long.

Figure 4.8. Intermediate, bidirectional NE- and NW-trending boudins (corresponding to NE- and NW-directed extension respectively) of the migmatitic foliation and compositional layering formed during the second bidirectional phase in Bremer Bay. Yellow line indicates orientation of SE-trending and steeply SE-plunging boudin neck axes of boudins with NE-directed extension. Red line corresponds to orientation of NE-trending and sub-horizontal boudin neck axes of boudins with NW-directed extension. Boudins occur on NE-trending and steeply SE-dipping orthogneisses in Native Dog Beach Headland. Chisel for scale is 20 cm long.

Figure 4.9. Interlayered leucocratic granodiorite and melanocratic quartz-monzonite. Layers of leucocratic granodiorite, although somewhat wavy, show lateral continuity. Little Boat Harbour Headland.

Figure 4.10. Gradual contact between melanocratic quartz-monzonite and leucocratic granodiorite. Little Boat Harbour Headland. Field book for scale is 19 cm long.

Figure 4.11. Intermediate, NE-trending, meter-scale fold of the migmatitic fabric and compositional banding formed during the second folding phase in Bremer Bay. Little Boat Harbour Headland. Pencil for scale is 12 cm long.

Figure 4.12. Large NW- trending pegmatite, displaying a change in chemistry from quartz-potassium feldspar (pink in color) towards the edges to nearly pure quartz (white in color) towards the center. Little Boat Harbour Headland. Field book for scale is 19 cm long.

Figure 4.13. Decimeter-scale, NW-verging, SW-plunging tight folds of early centimeter-scale blocky boudins of foliation-parallel mafic layers, and compositional layering in Point Henry Headland. These folds formed during the second folding phase recorded in the rocks of the Bremer Bay area. Chisel for scale is 20 cm long.

Figure 4.14. Centimeter-scale torn, blocky, rectangular, NE- and NW-trending early bidirectional boudins of mafic layers parallel to the migmatitic foliation formed during the first bidirectional extension phase in Bremer Bay, Banky Beach Headland. This mafic layer has been reoriented subsequently to a subvertical orientation during regional folding. Field book for scale is 19 cm long.

Figure 4.15 Decimeter-scale folds of the migmatitic foliation, compositional banding, and early centimeter-scale boudins of foliation-parallel mafic layers formed during the second folding phase in Bremer Bay. Banky Beach Headland. Pencil for scale is 12 cm long.

Figure 4.16. NE-trending meter-sized boudins of the migmatitic foliation and compositional layering in Banky Beach Headland, formed during the second bidirectional extension phase in Bremer Bay. A boudin in the foreground (outlined green) contains an earlier tight fold of the foliation (outlined red) formed during the second phase of folding. Dip-slope exposure of compositional layering reveals NW-trending boudins of the same compositional layers, now subvertical due to later folding by regional-scale folds. Compass for scale is 12 cm long.

Figure 4.17. Late, NW-verging, SW-plunging meter-scale open fold of the migmatitic fabric and compositional layering formed during the last folding phase in the Bremer Bay area. Banky Beach Headland. Field book for scale is 19 cm long.

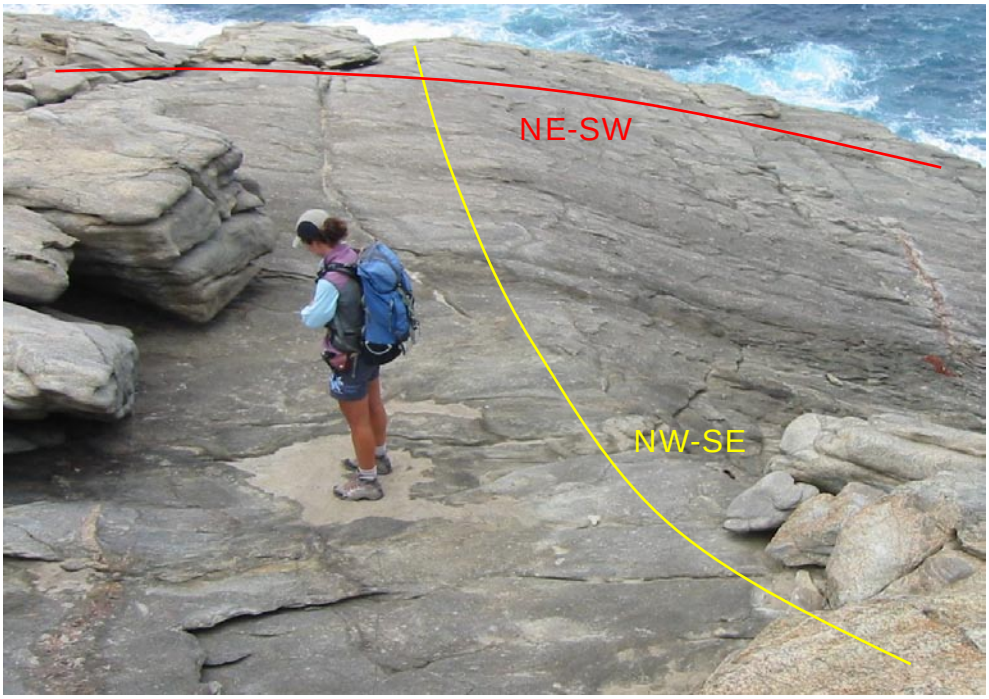

Figure 4.18. Dome and basin topography resulting from surface interference of NW- and NE-trending decameter scale boudins and boudin neck areas. Banky Beach East Headland.

Figure 4.19. Segregation into centimeter-wide, foliation parallel, felsic-enriched and mafic-enriched compositional bands displayed by orthopyroxene-clinopyroxene-hornblende-biotite quartz monzonite orthogneiss (lithology 1C) in Banky Beach East Headland. Field book for scale is 19 cm long.

Figure 4.20. Intermediate, meter-sized boudin of the migmatitic foliation and compositional layering (outlined green) that contains an earlier tight fold of the foliation (outlined red). Banky Beach East Headland. The extension direction for the now subvertical (after regional-scale folding) intermediate boudins is NW-SE, and they formed during the second bidirectional extension phase recorded in the Bremer Bay area. Pencil for scale is 12 cm long.

Figure 4.21. NE-trending (subhorizontal, outlined in green) and NW-trending (now subvertical, outlined in blue) meter-sized bidirectional boudins of the compositional layering and migmatitic foliation in Banky Beach Headland. Note boudinaged fold in Figure 4.26 is contained within outlined vertical NW-trending boudin.

Figure 4.22. Decimeter-scale SW-plunging recumbent refolded folds of the compositional layering and migmatitic foliation on Point Gordon Headland, formed during the second folding phase in the Bremer Bay area. A weak mineral lineation parallels the fold axes of some of these folds (see Figure 4.23), suggesting that the mineral lineation and the folds are coeval. Compass for scale is 20 cm long.

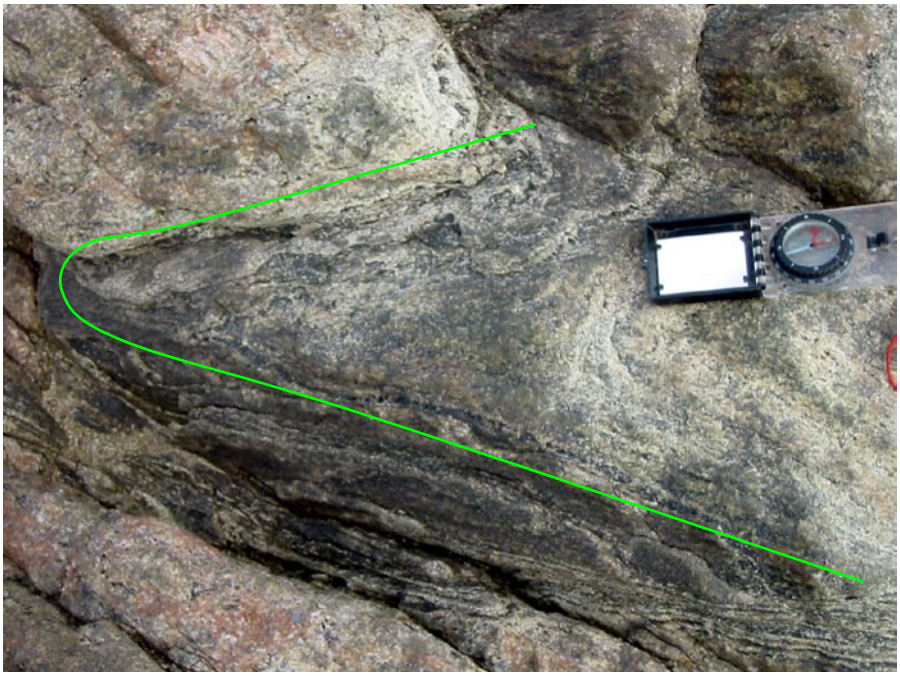

Figure 4.23. Fold hinge area of a decimeter-scale, SW-plunging, recumbent fold of the gneissic fabric and compositional layering (outlined green; view parallel to fold hinge line; see Figure 4.22) with a weak mineral grain lineation that parallels the fold axis, suggesting that the mineral lineation and the folds are coeval and formed during the second folding phase in the Bremer Bay area. Point Gordon Headland. Compass for scale is 20 cm long.

Figure 4.24. Meter-scale, sheared, NE-trending boudins of the migmatitic fabric and compositional layering formed during the second bidirectional extension phase in Bremer Bay. Point Gordon Headland.

Figure 4.25. Late, decimeter-wide felsic (quartz and potassium feldspar) pegmatitic vein that cuts through the neck of a set of NE-trending decameter-sized boudins of the migmatitic fabric and compositional layering. Point Gordon Headland. Field book for scale is 19 cm long.

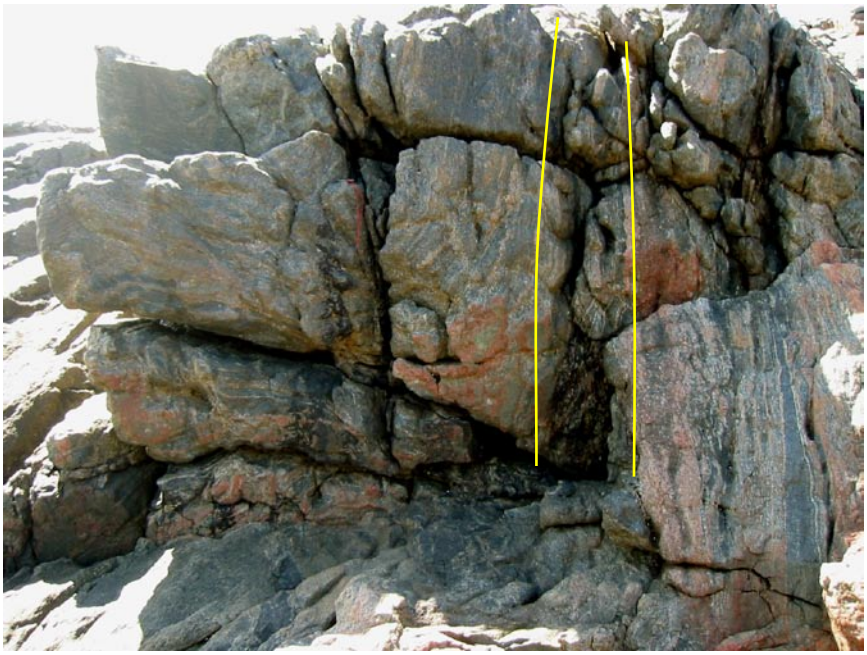

Figure 4.26. A sub-meter wide subvertical band of orthogneiss with diatexitic texture (outlined in yellow) transforms the dominant shallow-dipping compositional fabric (left of the band) so that it appears subvertical (right side of the band). Point Gordon Headland.

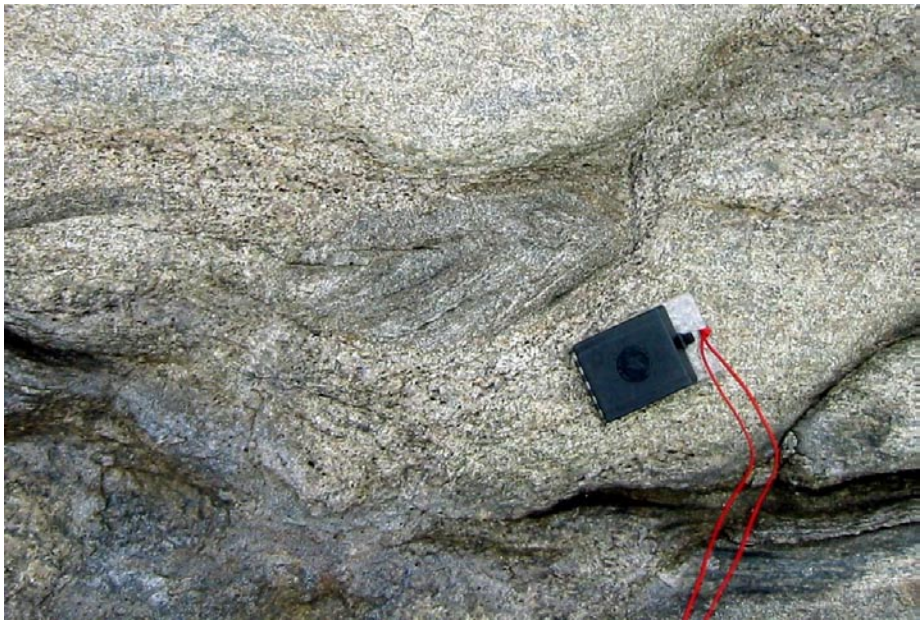

Figure 4.27. SW-trending decimeter-scale isoclinal fold of the migmatitic foliation and compositional banding formed during the first folding phase in the Bremer Bay area, and later disrupted by felsic leucosome. Short Beach Headland. Compass for scale is 10 cm long.

Figure 4.28. Steeply SW- to SE-plunging open folds of the migmatitic fabric and compositional layering, bounded by left-lateral shear bands with associated pegmatitic material in the shear plane. These folds could have been rotated due to motion between the shear couple. Short Beach Headland. Field book for scale is 19 cm long.

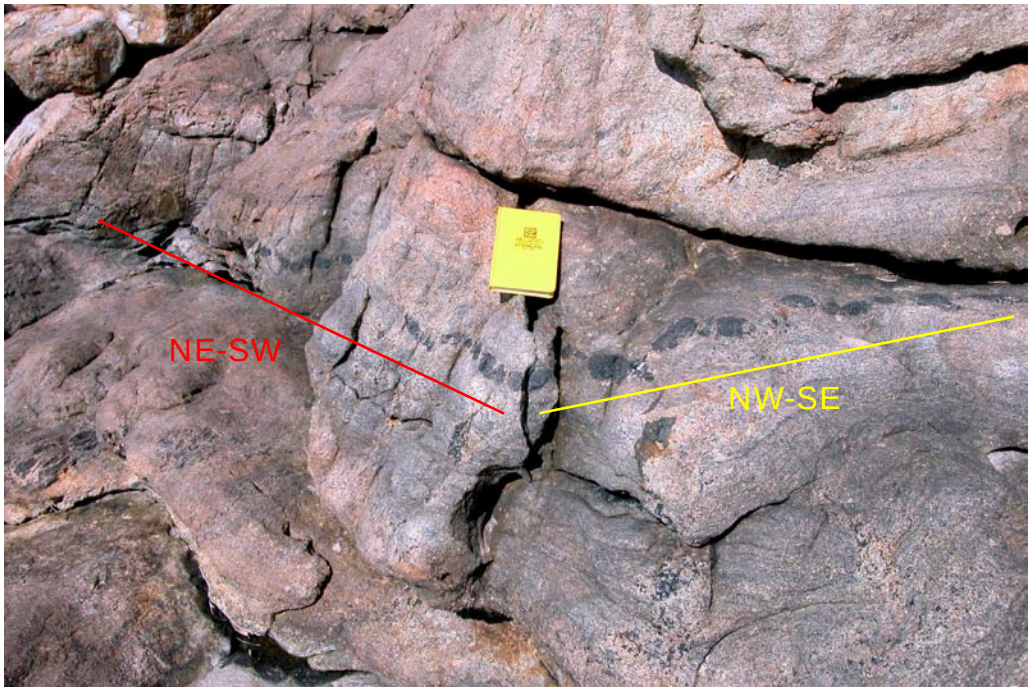

Figure 4.29. Centimeter-scale blocky bidirectional boudins of a mafic layer parallel to the compositional layering. Short Beach North Headland. Field book for scale is 19 cm long.

Figure 4.30. Decimeter-scale, NW-verging, SW-plunging, open to isoclinal folds that fold the migmatitic fabric, and boudinaged mafic layers parallel to the compositional banding. Short Beach North Headland. Field book for scale is 19 cm long.

Figure 4.31. Meter-scale bidirectional boudins of the migmatitic foliation and compositional layering. Short Beach North Headland. Field book for scale is 19 cm long.

Figure 4.32. N-trending “pull apart” pegmatite band, cutting migmatitic foliation, shows a change from intermediate to felsic melt composition from the outer portion to the interior, Short Beach North Headland. Open compass for scale is 18 cm long.

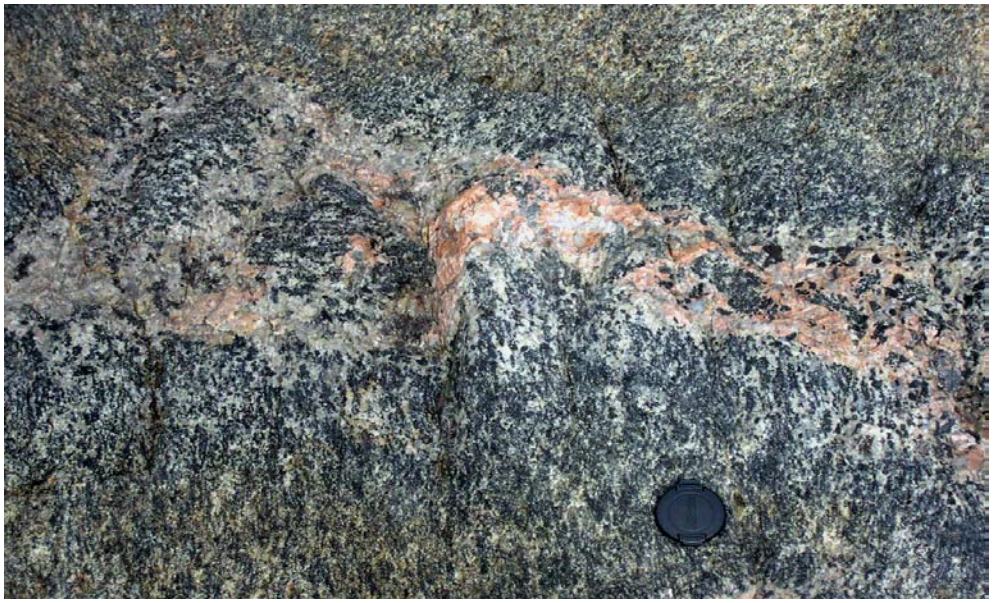

Figure 4.33. E-trending “pull apart” pegmatite band shows a change from intermediate (green) to felsic (pink) melt composition from the outer portion to the interior. Note the remnants of migmatitic foliation in coarser-grained intermediate part of the band. Short Beach North Headland. Lens cap for scale is 5 cm in diameter.

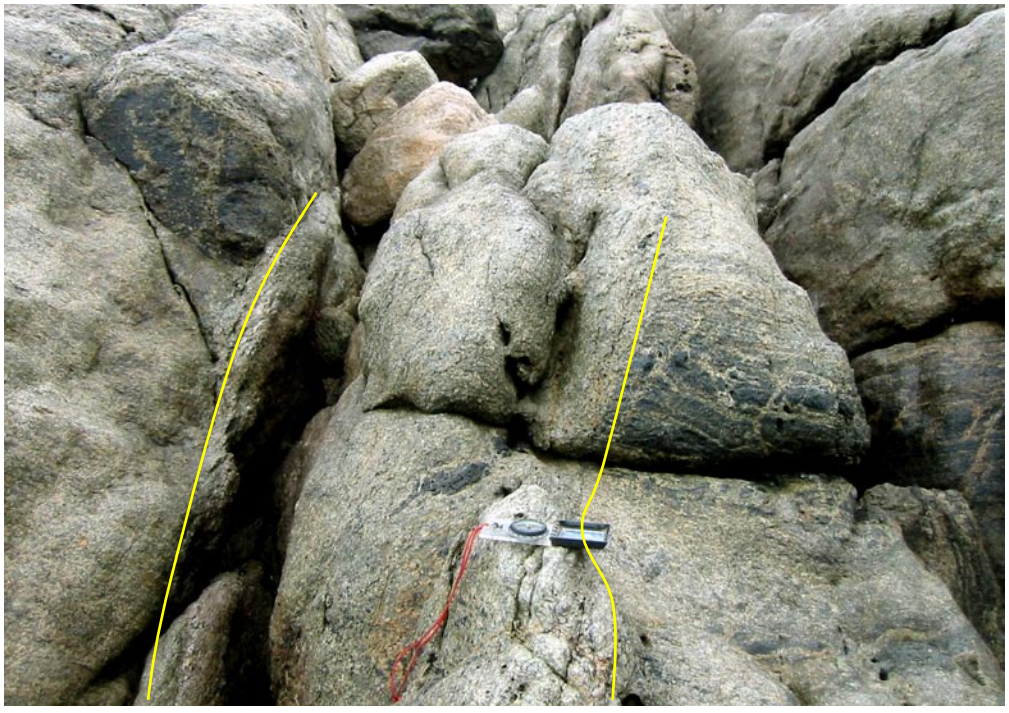

Figure 4.34. Meter-wide band of diatexitic texture (outlined in yellow) that cuts through shallowly dipping compositional banding and migmatitic foliation. Short Beach North Headland. Compass for scale is 20 cm long.

Figure 4.35. Jumbled centimeter- and one meter-scale mafic boudin blocks, parts of mafic layers and folds of compositional layering that behave as “rafters” surrounded by monzonitic leucosome. Short Beach North Headland.

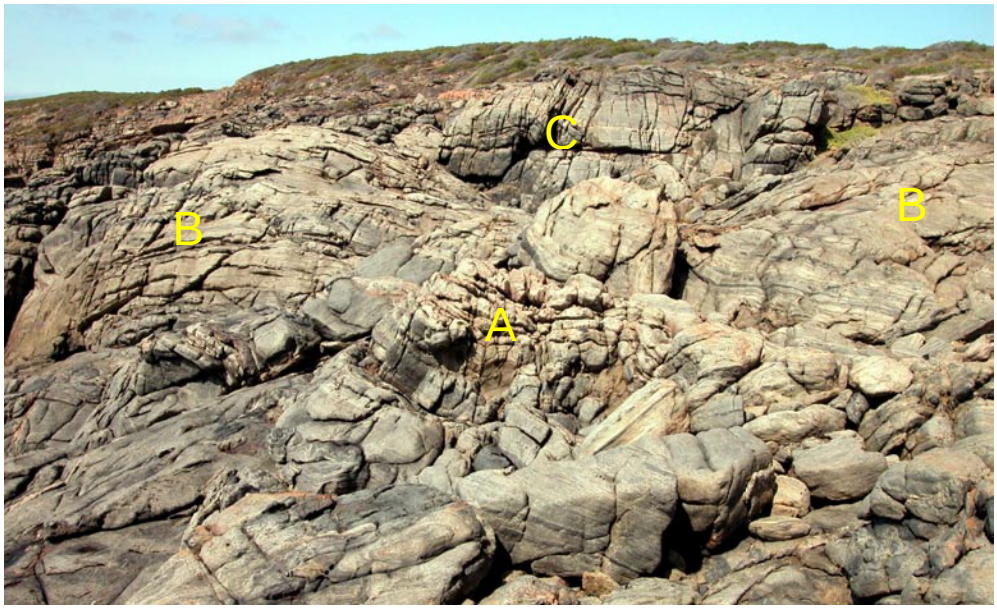

Figure 4.36. Hummocky topography resulting from the interference of NW and NE-trending boudin sets on the surface in Fisheries Bay Headland. Three different levels of nested boudins are seen (labeled A, B, C).

Figure 4.37. Meter-scale, recumbent, SW-plunging folds of the migmatitic foliation, compositional banding and early centimeter-scale boudins of a foliation-parallel mafic layer. Fold is later boudinaged by a large NW-trending boudin (outlined yellow). Fisheries Bay Headland. Field book for scale is 19 cm long.

Figure 4.38. Discrete pegmatitic vein intruded in the neck area between two NW-trending decameter-sized boudins. The pegmatitic vein displays zones of apparent different chemistry: felsic (white and pink) and intermediate (green). Fisheries Bay Headland. Sledge hammer for scale is 50 cm long.

Figure 4.39. Discrete melt zone of intermediate composition (hornblende-orthopyroxene-clinopyroxene monzodiorite orthogneiss, outlined yellow) intruded in the neck area between two NW-trending decameter-sized boudins. Fisheries Bay Headland. Field book for scale is 19 cm long.

Figure 4.40. NW-trending discrete “pull apart” pegmatite band showing a change from intermediate (green) to felsic (pink) melt composition from the outer portions to the interior. Fisheries Bay Headland. Field of view is approximately 1 meter wide.

Figure 4.41. Thin, intermediate (green) composition outer rims and tips of two late felsic (pink) NW-trending pegmatitic veins intruded in Fisheries Bay Headland. Field book for scale is 19 cm long.

Figure 4.42. Upright to recumbent, SW-plunging folds of a boudinaged mafic layer parallel to the compositional banding. Note asymmetrical offset of early rectangular boudin on one limb. Back Beach Headland. Field book for scale is 19 cm long.

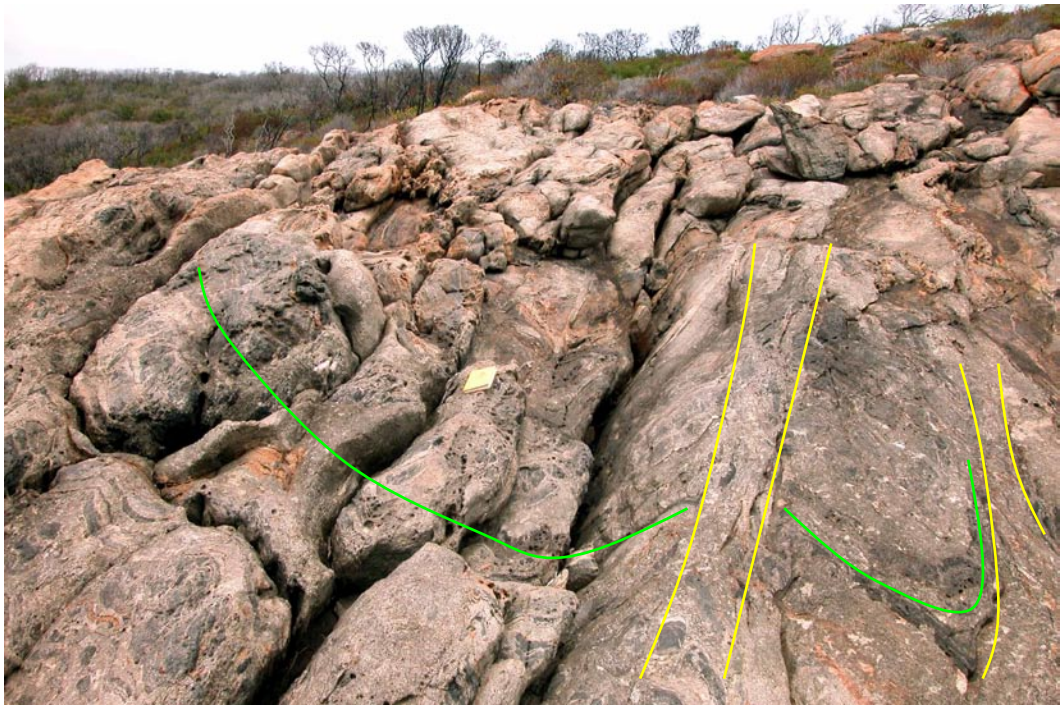

Figure 4.43. Two decimeter-wide zones of coarse-grained diatexitic texture in the orthogneisses (outlined yellow), clearly cut through the hinge-region of a several meter-wide fold of the compositional layering and migmatitic foliation (outlined green). Back Beach Headland. Field book for scale is 19 cm long.

Figure 4.44. NE-trending (sub-horizontal) and NW-trending (sub-vertical) blocky, bidirectional boudins of mafic layers parallel to the compositional layering. John's Cove Headland. Field book for scale is 19 cm long.

APPENDIX 1. Methods of structural mapping and petrographic work

Introduction

For this dissertation, I carried out detailed structural mapping of twelve different headlands along a peninsula surrounding the locality of Bremer Bay, in western Australia (Figure 4.1 in Chapter 4 and 2.7a in Chapter 2; Plate 1): Native Dog Beach, Blossoms Beach, Little Boat Harbour, Point Henry, Banky Beach, Banky Beach East, Point Gordon, Short Beach, Short Beach North, Fisheries Bay, Back Beach and John's Cove headlands. The names for the different headlands were given to them depending on the different local beaches, bays and capes that the headlands are adjacent to or constitute. The areas that were not mapped (Figure 4.1 in Chapter 4 and 2.7a in Chapter 2) are beaches or perilous coastal outcrops with limited surface exposure.

Rocks in the Bremer Bay area are granulite-facies migmatitic orthogneisses that record a very complex history of mid-crustal deformation. Rock outcrops are limited to a narrow coastal strip ranging averaging 50 meters in width, with inland outcrops being non-existent, as the vegetation cover is for the most part impenetrable. Owing to the limited outcrop exposure and the complexity of the structural deformation recorded by rocks in the Bremer Bay area, I constructed geologic maps of the different headlands at a scale of 1:500, and in the case of Fisheries Bay Headland (Figure 4.1 in Chapter 4) at a scale of 1:250. Plates 2 through 13 contain the geologic maps and corresponding geologic cross-sections for the twelve different headlands in the Bremer Bay area at a scale of 1:1000, because the original 1:500 and 1:250 geologic maps are too large to be reproduced on conventional printing equipment. A very limited amount of structural data, exclusively redundant migmatitic foliation measurements, was suppressed when converting the maps to a printable scale, but this process did not compromise integrity or interpretation of the remaining structural data on the maps. Plate 1 displays all the geologic maps for the twelve different headlands along the Bremer Bay peninsula, at a scale of 1:6666, the largest scale at which the entire peninsula could be printed. In this case, most structural data has been eliminated for clarity, as the purpose is to show the

mapped areas in their proper geographic position along the peninsula. Plate 1 also displays stereograms and rose diagrams for all the structural data collected for each of the headlands, which is plotted adjacent to the corresponding headland map, and combined data plots for the entire Bremer Bay area, which include all data from all twelve headlands.

Methodology

Construction of geologic maps in the field

Owing to the remote location of the field area, and my need for topographic base maps of relatively large scales, 1:500 and 1:250, no topographic maps, paper-based or digital, were available for this area. Consequently, as a first step towards the construction of detailed structural maps, I constructed my own topographic maps for each one of the headlands. A completed 1:500 or 1:250 scale geologic map for any given headland along the Bremer Bay peninsula is composed of a series of attached individual 11x17-inch sheets of paper. I started the construction of the topographic map for any given headland by drafting a UTM coordinate GPS grid system on each of the individual 11x17 inch sheets that would eventually become part of the overall headland map. Once on the outcrop, I carefully traced the width of the exposed outcrop between the ocean and the vegetation cover by walking those two boundaries with a hand-held GPS unit. I then proceeded to incorporate elevation information into the maps by again waking different topographic contours along the outcrop with the hand-held GPS unit. Once the base topography for each of the individual map sheets was completed, I moved on to the task of mapping geologic and structural features.

Construction of digital geologic maps

All the geologic maps for the twelve different headlands in Bremer Bay were fully completed while in the field. Upon returning to Austin, I converted all the individual map sheets into digital JPEG image files, which I then imported into drafting software (Corel Draw) to use as them as base layers from which to trace all the topographic,

geologic and structural information, effectively constructing digital structural maps. Once all the individual sheet maps for any one headland were transformed into digital files, I proceeded to assemble them to construct a complete 1:500 or 1:250 scale digital geologic map for that headland. Once all the digital geologic maps for all the headlands along the Bremer Bay peninsula were constructed, I assembled them into a single file according to their location along the Bremer Bay peninsula, constructing a completed digital geologic map for the entire area. The size of the final 1:500 scale digital geologic map for the entire Bremer Bay area is 15x20 meters, thus the need for reducing its scale so it can be accommodated into a printed medium.

Geologic cross-sections

I constructed paper-based 1:1000 scale, no vertical exaggeration, NW-SE oriented geologic cross-sections for each one of the twelve headlands I mapped along the Bremer Bay peninsula from printed versions of the 1:1000 scale digital geologic maps for each headland (Plates 2 through 13). I drew multiple, consecutive, NW-SE oriented cross-section lines covering the entire length of each of the twelve headlands I mapped in Bremer Bay. Once I completed the paper-based geologic cross-sections for all headlands, I converted all the individual cross-sections into digital JPEG image files. I followed the same digital drafting procedure I used to construct the geologic maps for all the headlands, where I utilized the digital JPEG image files from the manually-drafted, paper based cross-sections as base layers to digitally draft individual cross-sections for each of the headlands mapped.

The process of reducing the scale from 1:500 for the paper-based structural maps constructed in the field to a more convenient 1:1000 scale for printable digital maps eliminated only very small percentage of structural data, exclusively what I considered as redundant migmatitic foliation measurements. Therefore the 1:1000 scale geologic cross-sections reflect all the structural complexity of the different headlands, and their accuracy was in no way compromised by the re-scaling of the geologic maps.

While constructing geologic maps in the field, I simultaneously carried on a basic lithological description and correlation of the different units observed in the field area. I based my description on factors such as crystal size, mineral assemblage, weathering color, color of a freshly exposed surface, absence or presence of leucosomes (former melt), and leucosome textures. Nevertheless, the lithological characterization of the different units in the field was very challenging. The rocks in the area are relatively coarse grained, and the distribution of the mineral phases is very heterogeneous. Observed weathering and fresh exposure colors under the naked eye can dramatically change throughout the day, depending on the amount of direct sunlight on the outcrop.

To compile a much more accurate description of the lithologies present on coastal outcrops along the Bremer Bay peninsula, I carried out extensive sampling of the different lithologies observed in the field area. I collected a total of 85 rock samples from the Bremer Bay area, from each one of which I obtained anywhere from 1 to 3 petrographic thin sections. I conducted a detailed description for all the petrographic thin sections, and combined thin section petrographic descriptions and field observations to create an accurate depiction of all the lithologies present in the Bremer Bay area, and their map distribution.

Petrography

I had 178 oriented petrographic thin sections made from a total of 85 oriented rock samples collected from the field area, from which I intended to describe and measure potential microscopic shear sense indicators such as foliations, shear bands, S-C and C' structures, mica fish, mantled and winged porphyroblasts, quarter structures and lattice preferred orientation (LPO). My initial intention was to analyze LPO fabrics using the Scanning Electron Microprobe (SEM) Electron Backscattered Diffraction (EBSD) facilities in the Department Geological Sciences at The University of Texas at Austin. I was particularly interested in the study of LPO patters in petrographic thin sections from the orthogneisses in Bremer Bay because these fabrics can provide information about: 1) slip systems that were active on different minerals, which are related to the temperature

of deformation; 2) shape of the rock fabric, i.e. whether the rock has deformed under plane strain, flattening or constriction regimes; 3) finite strain, if deformation regime remains constant during deformation, as usually LPO patterns increase in strength and sharpness during deformation but undergo only slight changes in geometry; (4) kinematic vorticity number, which is related to the relative ratios of coaxial and non-coaxial deformation. I also intended to use oriented petrographic thin sections to determine the deformation and recrystallization mechanisms that were present for different deformation events in recorded in the Bremer Bay area, as they are dependent on external factors such as temperature, lithostatic pressure, differential stress, applied strain rate and fluid pressure.

In the field I collected oriented rock samples from all different lithologies recognized in the field area, as well as sampled structural features such as: a) migmatitic foliation, defined by alternating centimeter-wide leucosome and restitic bands; b) mineral grain lineation that locally grows on foliation planes in the field area; c) hinge areas of decimeter-scale folds of the migmatitic foliation and compositional banding formed during the second folding phase in Bremer Bay (Chapters 2 and 3 of this dissertation); d) small, centimeter-scale blocky boudins of foliation-parallel mafic layers formed during the first bidirectional extension event documented in Bremer Bay (Chapters 2 and 3 of this dissertation); and e) winged porphyroblasts, which appear locally in the field area. Many of the rock samples were collected from within intermediate, decimeter- to meter-scale boudins formed during the second (progressive) bidirectional extension event in Bremer Bay (Chapters 2 and 3 of this dissertation), and many others were collected in areas where all structures had been boudinaged by large, decameter-size boudins of the migmatitic foliation and compositional layering.

The criteria for preparing petrographic thin sections from rock samples were as follows: 1) I cut thin sections parallel and perpendicular to the migmatitic foliation in most rock samples that contained no other relevant structures such as folds or a mineral grain lineation; 2) in rock samples with a mineral grain lineation, which is always developed on foliation planes, I cut thin sections parallel and perpendicular to the

migmatitic foliation and parallel and perpendicular to the mineral grain lineation when present; 3) in rock samples from the hinge area of decimeter-scale folds of the migmatitic foliation and compositional banding; I cut thin sections parallel and perpendicular to the axial planes of the folds; 4) for rock samples containing centimeter-scale boudin blocks of mafic layers parallel to the migmatitic foliation, I cut thin sections that included both part of a boudin block and a boudin neck that were parallel and perpendicular to the boudin neck axis.

All rock samples and thin sections for this dissertation are housed in the core repository in the Department of Geological Sciences at The University of Texas at Austin.

References

Beaumont, C., Jamieson, R.A., Nguyen, M.H., and Lee, B. 2001, Himalayan tectonics explained by extrusion of a low-viscosity crustal channel coupled to focused surface denudation: Nature, 414, p. 738– 742, doi: 10.1038/414738a.Beeson, J., Delor, C.P., and Harris, L.P., 1988. A structural and metamorphic traverse across the Albany Mobile Belt, Western Australia. Precambrian Research, 40/41, 117-136.

Beeson, J., Harris, L.B., and Delor, C.P., 1995. Structure of the western Albany mobile belt (southwestern Australia); evidence for overprinting by Neoproterozoic shear zones of the Darling mobile belt. Precambrian Research, 75, 47-63.

Black, L. P., Harris, L. B., and Delor, C. P., 1992. Reworking of Archaean and Early Proterozoic components during a progressive, Middle Proterozoic tectonothermal event in the Albany Mobile Belt, Western Australia. Precambrian Research, 59, 95-123.

Blundy, J.D., and Holland, T.J.B., 1990. Calcic amphibole equilibria and a new amphibole-plagioclase geothermometer. Contributions to Mineralogy and Petrology, 104, 208-224.

Bodorkos, S., and Clark, D.J., 2004a. Evolution of a crustal-scale transpressive shear zone in the Albany-Fraser Orogen, SW Australia: 1. P-T conditions of Mesoproterozoic metamorphism in the Coramup Gneiss. Journal of Metamorphic Geology, 22, 691-711.

Bodorkos, S., and Clark, D.J., 2004b. Evolution of a crustal-scale transpressive shear zone in the Albany-Fraser Orogen, SW Australia: 2. Tectonic history of the Coramup Gneiss and a kinematic framework for Mesoproterozoic collision of the West Australian and Mawson cratons. Journal of Metamorphic Geology, 22, 713-731.

Bodorkos, S., and Wingate, M.T.D., 2008a. 184128: leucocratic tonalitic gneiss, Powell Point; Geochronology dataset 705, in Compilation of geochronology data: Geological Survey of Western Australia.

Bodorkos, S., and Wingate, M.T.D., 2008b. 184127: porphyritic monzodiorite, Powell Point; Geochronology dataset 704, in Compilation of geochronology data: Geological Survey of Western Australia.

Bodorkos, S., and Wingate, M.T.D., 2008c. 184123: garnet-bearing monzogranitic gneiss, Plum Pudding Rocks; Geochronology dataset 702, in Compilation of geochronology data: Geological Survey of Western Australia.

Bodorkos, S., and Wingate, M.T.D., 2008d. 184122: metamorphosed quartz sandstone, Plum Pudding Rocks; Geochronology dataset 701, in Compilation of geochronology data: Geological Survey of Western Australia.

Bodorkos, S, and Wingate, M.T.D., 2008e, 184119: monzogranitic gneiss, Point Henry; Geochronology dataset 699. In: Compilation of geochronology data: Geological Survey of Western Australia.

Bodorkos, S, and Wingate, M.T.D., 2008f, 184307: pegmatitic granodiorite, Point Henry Geochronology dataset 706. In: Compilation of geochronology data: Geological Survey of Western Australia.

Bodorkos, S, and Wingate, M.T.D., 2008g, 184310: leucocratic granodiorite, Fisheries Bay headland; Geochronology dataset 707. In: Compilation of geochronology data: Geological Survey of Western Australia.

Bodorkos, S, and Wingate, M.T.D., 2008h, 184311: orthopyroxene-clinopyroxene orthogneiss, Fisheries Bay headland; Geochronology dataset 708. In: Compilation of geochronology data: Geological Survey of Western Australia.

Bodorkos, S, and Wingate, M.T.D., 2008i, 184312: granodioritic gneiss, Short Beach headland; Geochronology dataset 709. In: Compilation of geochronology data: Geological Survey of Western Australia.

Bodorkos, S, and Wingate, M.T.D., 2008j, 184326: pegmatitic leucogranite, Short Beach headland; Geochronology dataset 711. In: Compilation of geochronology data: Geological Survey of Western Australia.

Boutilier, R.R., and Keen, C.E., 1994. Geodynamic models of fault-controlled extension: Tectonics, 13, 439-454.

Brun, J.P., and Tron, V., 1993. Development of the North Viking Graben: inferences from laboratory modeling. Sedimentary Geology, 86, 31-51.

Burg, J.P, and Ford, M., 1997. Orogeny through time: an overview. In Burg, J.P., and Ford, M., eds.: Orogeny through Time. Geological Society of London, 121, 1-17.

Cassidy, K.F., Champion, D.C., McNaughton, N.J., Fletcher, I.R., Whitaker, A.J., Bastrakova, I.V., and Budd, A.R., 2002. Characterisation and metallogenic significance of Archean granitoids of the Yilgarn Craton, Western Australia: Amira International Limited, AMIRA project no. P482/MERIWA Project M281, Report no. 222 (unpublished).

Chauvet, A., and Séranne, M., 1994. Extension-parallel folding in the Scandinavian Caledonides: implications for late-orogenic processes. Tectonophysics, 238, 31-54.

Clark, D.J., 1999. Thermo-tectonic evolution of the Albany–Fraser Orogen, Western Australia: University of New South Wales, Australia, PhD thesis (unpublished).

Clark, D. J., Hensen, B. J. & Kinny, P. D., 2000. Geochronological constraints for a two-stage history of the Albany–Fraser Orogen, Western Australia. Precambrian Research, 102, 155–183.

Clark, D. J., Kinny, P. D., Post, N.J., and Hensen, B. J., 1999. Relationships between magmatism, metamorphism and deformation in the Fraser Complex, Western Australia: constraints from new SHRIMP U-Pb zircon geochronology. Australian Journal of Earth Sciences, 46, 923-932.

Clark, W. C, 1995. Granite petrogenesis, metamorphism and geochronology of the western Albany-Fraser Orogen, Albany, Western Australia. Curtin University of Technology, Australia, BSc (Honours) thesis (unpublished).

Collins, W. J., 1994. Upper- and middle-crustal response to delamination: an example for the Lachlan fold belt, eastern Australia. Tectonophysics, 235, 249-275.

Condie, K. C., and Myers, J. S., 1999. Mesoproterozoic Fraser Complex: geochemical evidence for multiple subduction-related sources of lower crustal rocks in the Albany-Fraser Orogen, Western Australia. Australian Journal of Earth Sciences, 46, 875-882.

Coney, P. J., and Harms, T. A., 1984. Cordilleran metamorphic core complexes: Cenozoic extensional relics of Mesozoic compression. Geology, 12, 550-554.

Cruse, T., 1991. The sedimentology, depositional environment and Ediacaran fauna of Mondurup and Barnett Peaks, Stirling Range Formation, Western Australia: University of Western Australia, BSc (Honours) thesis (unpublished).

Cruse, T., and Harris, L.B., 1994. Ediacaran fossils from the Stirling Range Formation, Western Australia. Precambrian Research, 67, 1–10.

Davies, J. H., and von Blankenburg, F., 1995. Slab breakoff: a model of lithosphere detachment and its tests in the magmatism and deformation of collisional orogens. Earth and Planetary Science Letters, 129, 85-102.

Davis, G.H., and Coney, P.J., 1979. Development of the Cordilleran metamorphic core complexes: Geology, 7, p. 120-124.

Davis, G.H., Lister, G.S., and Reynolds, S.J., 1986. Structural evolution of the Whipple and South mountains shear zones, southwestern United States. Geology, 14, 7-10.

Dawson, G. C., Krapež, B., Fletcher, I. R., McNaughton, N. J., and Rasmussen, B., 2002. Did late paleoproterozoic assembly of proto-Australia involve collision between the Pilbara, Yilgarn and Gawler Cratons? Geochronological evidence from the Mount Barren Group in the Albany-Fraser Orogen, Western Australia. Precambrian Research, 118, 195-220.

Dawson, G.C., Krapež, B., Fletcher, I.R., McNaughton, N.J., and Rasmussen, B., 2003. 1.2 Ga thermal metamorphism in the Albany-Fraser Orogen of Western Australia: consequence of collision or regional heating by dyke swarms?. Journal of the Geological Society, London, 160, 29-37.

Dewey, J. F., 1988. Extensional collapse of orogens. Tectonics, 7, (6), 1123-1139.

De Waele, B., and Pisarevsky, S.A., 2008. Geochronology, paleomagnetism and magnetic fabric of metamorphic rocks in the northeast Fraser Belt, Western Australia. Australian Journal of Earth Sciences, 55, 605–621.

Doepel, J.J.G., and Lowry, D.C., 1970. Zanthus, W.A.: Western Australia Geological Survey, 1:250 000 Geological Series Explanatory Notes, 19p.

Duebendorfer, E. M., 2002. Regional correlation of Mesoproterozoic structures and deformational events in the Albany-Fraser orogen, Western Australia. Precambrian Research, 116, 129-154.

Eaton, D.W., Hynes, A., Indares, A., and Rivers, T., 1995. Seismic images of eclogites, crustal-scale extension, and Moho relief in the eastern Grenville Province, Quebec. Geology, 23, 855-858.

England, P. C., and Houseman, G. A., 1989. Extension during continental convergence, with application to the Tibetan Plateau. Journal of Geophysical Research 94, 17561–17579.

Evans, T., 1999. Extent and nature of the 1200 Ma Wheatbelt dyke swarm, southwestern Australia. BSc Honours Thesis, University of Western Australia, Perth (unpublished).

Fitzsimons, I. C. W., 2003. Proterozoic basement provinces of southern and southwestern Australia, and their correlation with Antarctica. In: Yoshida, W., Windley, B. F., and Dasgupta, S. (Eds.), Proterozoic East Gondwana: Supercontinent Assembly and Breakup. Geological Society of London Special Publication, 206, 93-130.

Fitzsimons, I.C.W., and Buchan, C., 2005. Geology of the western Albany-Fraser Orogen, Western Australia-a field guide. Western Australia Geological Survey, Record 2005/11, 32 p.

Fletcher, I.R., Myers., J.S., and Ahmat, A.L., 1991. Isotopic evidence on the age and origin of the Fraser Complex, Western Australia: A sample of Mid-Proterozoic lower crust. Chemical Geology, 87, 197-216.

Fletcher, J.M., and Bartley, J.M, 1994. Constrictional strain in a noncoaxial shear zone; implications for fold and rock fabric development, central Mojave core complex, California. Journal of Structural Geology, 16, 555-570.

Geological Survey of Western Australia, 2007. South Yilgarn Geological Exploration Package: Western Australia Geological Survey Record, 2007/13.

Geological Survey of Western Australia, 2008, Compilation of geochronology data, 2008 update: Geological Survey of Western Australia.

Giles, D., Betts, P. G. & Lister, G. S., 2004. 1.8–1.5-Ga links between the North and South Australian Cratons and the early-middle Proterozoic configuration of Australia. Tectonophysics, 380, 27–41.

Hall, C.E., Jones, S.A., and Bodorkos, S., 2008. Sedimentology, structure and SHRIMP zircon provenance of the Woodline Formation, Western Australia: implications for the tectonic setting of the West Australian Craton during the Paleoproterozoic. Precambrian Research, 162, 577–598.

Harris, L.B., 2003. Folding in high-grade rocks due to back-rotation between shear zones. Journal of Structural Geology, 25, 223-240.

Harris, L.B., Koyi, H.A., and Fossen, H., 2002. Mechanisms for folding of high-grade rocks in extensional tectonic settings. Earth-Science Reviews, 59, 163-210.

Harris, L.B., and Koyi, H.A., 2003. Centrifuge modeling of folding in high-grade rocks during rifting. Journal of Structural Geology, 25, 291-305.

Hopper, J.R., and Buck, W.R., 1996. The Effect of Lower Crustal Flow on Continental Extension and Passive margin Formation. Journal of Geophysical Research, 101, A10, 20175-20194

Huismans, R.S., Buiter, S.J.H., and Beaumont, C., 2005. Effect of plastic-viscous layering and strain softening on mode selection during lithospheric extension. Journal of Geophysical Research, 10, B02406, doi:10.1029/2004JB003114.

Jones, S.A., 2006. Mesoproterozoic Albany–Fraser Orogen-related deformation along the southeastern margin of the Yilgarn Craton. Australian Journal of Earth Sciences, 53, 213–234.

Korja, A., and Heikkinen, P.J., 1995. Proterozoic extensional tectonics of the Fennonscandian Shield: results from the Baltic and Bothnian Echoes from the Lithosphere experiment. Tectonics, 14, 504-517.

Koyi, H.A., Milnes, A.G., Schmeling, H., Talbot, C.J., Juhlin, C., and Zeyen, H., 1999. Numerical models of ductile rebound of crustal roots beneath mountain belts. Geophysics Journal International, 139, 556-562.

Kruger, J.M., and Johnson, R.A., 1994. Raft model of crustal extension: evidence from seismic reflection data in Southeast Arizona. Geology, 22, 351-354.

Kurtz, W., 2005. Constriction during exhumation: evidence from eclogite microstructures. Geology, 33, 37-40.

Lindsley, D. H., 1983. Pyroxene thermometry. American Mineralogist, 68, 477-493.

Lister, G.S., and Davis, G.A., 1989. The origin of metamorphic core complexes and detachment faults formed during Tertiary continental extension in the northern Colorado River region. Journal of Structural Geology, 21, 607-610.

Lister, G.S., and Baldwin, S.L., 1993. Plutonism and the origin of metamorphic core complexes. Geology, 21, 607-610.

Love, G.J., 1999. A study of wall-rock contamination in tonalitic gneiss from King Point, near Albany, Western Australia. BSc Honours Thesis, Curtin University of Technology, Perth (unpublished).

MacCready, T., Snoke, A.W., Wright, J.E., and Howard, K.A., 1997. Mid-crustal flow during Tertiary extension in the Ruby Mountains core complex, Nevada. Geological Society of America Bulletin, 109, 1576-1594.

Molnar, P., England, P, and Martinod, J., 1993. Mantle dynamics, uplift of the Tibetan Plateau, and the Indian monsoon. Reviews of Geophysics, 31, 357-396.

Muhnling, P. C., and Brakel, A. T., 1985. Mount Barker-Albany W. A.: Western Australia Geological Survey, 1:250 000 Geological Series Explanatory Notes, 21pp.

Müntener, O., Hermann, J., and Trommsdorff, V., 2000. Cooling history and exhumation of lower-crustal granulite and upper mantle (Malenco, East central Alps). Journal of Petrology, 41, 175-200.

Myers, J. S., 1985. The Fraser Complex -a major layered intrusion in Western Australia. Western Australia Geological Survey, Report 14, 57–66.

Myers, J. S., 1990. Albany-Fraser Orogen, *in* Geology and Mineral Resources of Western Australia. Memoir 3, Geological Survey of Western Australia, Perth, WA, 255-264.

Myers, J.S., 1995a. Geology of the Albany 1:1 000 000 sheet: Western Australia Geological Survey, 1:1 000 000 Geological Series Explanatory Notes, 10 p.

Myers, J.S., 1995b. Geology of the Esperance 1:1 000 000 sheet: Western Australia Geological Survey, 1:1 000 000 Geological Series Explanatory Notes, 10 p.

Myers, J. S., Shaw, R. D., and Tyler, I. M., 1996. Tectonic evolution of Proterozoic Australia. Tectonics, 15, 1431–1446.

Nelson, D.R., 1995a. 83696A: biotite monzogranite gneiss, Powell Point, in Compilation of SHRIMP U–Pb zircon geochronology data, 1994: Geological Survey of Western Australia, Record 1995/3, 23–25.

Nelson, D.R., 1995b. 83659: recrystallised leucogranite, Observatory Point, in Compilation of SHRIMP U–Pb zircon geochronology data, 1994. Geological Survey of Western Australia, Record 1995/3, 59–62.

Nelson, D.R., 1996a. 112168: fine-grained sandstone, No tree Hill, in Compilation of SHIRIMP U-Pb zircon geochronology data, 1996. Geological Survey of Western Australia, Record 1996/5, p. 80-83.

Nelson, D.R., 1996b. 112170: metasandstone, Barrens Beach, in Compilation of SHRIMP U-Pb zircon geochronology data, 1996. Geological Survey of Western Australia, Record 1996/5, p. 84-86.

Nelson, D. R., Myers, J. S., and Nutman, A. P., 1995. Chronology and evolution of the middle Proterozoic Albany-Fraser Orogen, Western Australia. Australian Journal of Earth Sciences, 42, 481-495.

Osmundsen, P.T., Eide, E.A., Haabesland, N.E., Roberts, D., Andersen, T.B., Kendrick, M., Bingen, B., Braathen, A., and Redfield, T.F., 2006. Kinematics of the Hoybakken detachment zone and the More-Trondelag Fault Complex, central Norway. Journal of the Geological Society, London, 163, 303-318.

Perry, E.R., 2005. Field and petrographic analysis of mylonitic fabrics: implications for tectonic corrugation development, Tanque Verde Ridge, Arizona, USA, M.S. Thesis, The University of Texas at Austin, 201 p.

Pidgeon, R. T., 1990. Timing of plutonism in the Proterozoic Albany Mobile belt, southwestern Australia. Precambrian Research, 47, 157-167.

Pisarevsky, S., and Harris, L.B., 2001. Determination of magnetic anisotropy and ca. 1.2. Ga paleomagnetic pole from the Bremer Bay area, Albany Mobile Belt, Western Australia. Australian Journal of Earth Sciences, 48, 101-112

Platt, J. P., and England, P. C., 1994. Convective removal of lithosphere beneath mountain belts: Thermal and mechanical consequences. American Journal of Science, 293, 307-336.

Rasmussen, B., Bengtson, S., Fletcher, I.R., and McNaughton, N.J., 2002. Discoidal impression and trace-like fossils more than 1200 million years old. Science, 296, 1112-1115.

Rasmussen, B., Fletcher, I.R., Bengtson, S., and McNaughton, N.J., 2004. SHRIMP U-Pb dating of diagenetic xenotime in the Stirling Range Formation, Western Australia: 1.8 billion year minimum age for the Stirling biota. Precambrian Research, 133, 329-337.

Rasmussen, B., and Fletcher, I.R., 2004. Zirconolite; a new U-Pb chronometer for mafic igneous rocks. Geology, 32, 785-788.

Ruppel, C., 1995. Extensional processes in continental lithosphere. Journal of Geophysical Research, 100, B12, 24187-24216.

Ryan, P.D., and Soper, N.J., 2001. Modeling anatexis in intra-cratonic rift basins: an example from the Neoproterozoic rocks of Scottish Highlands. Geological Magazine, 138, 577-588.

Sacks, P. E., and Secor, D. T., 1990. Delamination in collisional orogens. Geology, 18, 999-1002.

Schott, B., and Schmeling, H., 1998. Delamination and detachment of a lithospheric root. Tectonophysics, 296, 225-247.

Sofoulis, J., 1958. The geology of the Phillips River Goldfield, W.A. Geological Survey of Western Australia Bulletin, 110, 240 p.

Spaggiari, C. V., Bodorkos, S., Tyler, I. M., and Barquero-Molina, M. 2008. The *c*. 1680 Ma Dalyup Gneiss of the Albany–Fraser Orogen, Western Australia: What is it, and where did it come from? Geological Society of Australia, Abstracts, 89, 232–233.

Spaggiari, C.V., Bodorkos, S., Barquero-Molina, M., and Tyler, I.M., (in press). Interpreted Bedrock Geology of the South Yilgarn and central Albany–Fraser Orogen, Western Australia. Western Australia Geological Survey, Record 2009/??, 77pp.

Terry, M.P., and Robinson, P., 2003. Evolution of amphibolite-facies structural features and boundary conditions for deformation during exhumation of high- and ultrahigh- pressure rocks, Nordøyane, Western Gneiss Region, Norway. Tectonics, 22, (4), 1036, doi:10.1029/2001TC001349.

Thom, R., Chin, R.J., and Hickman, A.H., 1984. Newdegate, W.A.: Western Australia Geological Survey 1:250 000 Geological Series Explanatory Notes, 24 p.

Thom, R., Lipple, S.L., and Sanders, C.C., 1977. Ravensthorpe, W.A.: Western Australia Geological Survey 1:250 000 Geological Series Explanatory Notes, 40 p.

Vallini, D.A., Rasmussen, B., Krapež, B., Fletcher, I.R., and McNaughton, N.J., 2002. Obtaining diagenetic ages from metamorphosed sedimentary rocks: U–Pb dating of unusually coarse xenotime cement in phosphatic sandstone. Geology, 30, 1083–1086.

Vallini, D.A., Rasmussen, B., Krapež, B., Fletcher, I.R., and McNaughton, N.J., 2005. Microtextures, geochemistry and geochronology of authigenic xenotime

constraining the cementation history of a Paleoproterozoic metasedimentary sequence. Sedimentology, 52, 101–122.

Vanderhaeghe, O., and Teyssier, C., 2001. Crustal-scale rheological transitions during late-orogenic collapse. Tectonophysics, 335, 211-228.

Wernicke, B., 1990. The fluid crustal layer and its implications for continental dynamics, In: Salisbury, M.H., Fountain, D.M., eds., Exposed Cross-sections of the Continental Crust. Kluwer Academic, 509-544.

Westaway, R., 1998. Dependence if active normal fault dips on lower-crustal flow regimes. Journal of the Geological Society of London, 155, 233-253.

Wetherley, S., 1998. Tectonic evolution of the Mount Barren Group, Albany-Fraser Province, Western Australia. Ph.D. Thesis, University of Western Australia, Perth, 269 pp.

Whitaker, A.J., 1992. Albany Magnetic and Gravity Interpretation (1: 1 000 000 scale map). Bureau of Mineral Resources, Geology and Geophysics, Canberra.

Whitaker, A.J., 1993. Esperance Magnetic and Gravity Interpretation (1: 1 000 000 scale map). Australian Geological Survey Organisation, Canberra.

Wilson, A.F., 1969. The pyroxene granulites and associated gabbros of the Fraser Range, Western Australia, and their economic significance. Australian Institute of Mining and Metallurgy, Proceedings, 231, 47–57.

Wingate, M.T.D. and Bodorkos, S., 2007. 177910: metamorphosed quartz sandstone, Peter's Dam; Geochronology dataset 660, in Compilation of geochronology data: Western Australia Geological Survey.

Wingate, M.T.D., Campbell, I. H., and Harris, L. B., 2000. SHRIMP baddeleyite age for the Fraser dyke swarm, southeast Yilgarn Craton, Western Australia. Australian Journal of Earth Sciences 47, 309-313.

Wingate, M.T.D. & Evans, D. A. D., 2003. Palaeomagnetic constraints on the Proterozoic tectonic evolution of Australia. In: Yoshida, M., Windley, B. F. & Dasgupta, S. (Eds.), Proterozoic East Gondwana: Supercontinent Assembly and Breakup. Geological Society of London Special Publication, 206, 77–91.

Witt, W.K., 1997. Geology of the Ravensthorpe and Cocanarup 1:100 000 sheets: Western Australia Geological Survey, 1:100 000 Geological Series Explanatory Notes, 26 p.

Witt, W.K., 1998. Geology and mineral resources of the Ravensthorpe and Cocanarup 1:100 000 sheets: Western Australia Geological Survey, Report 54, 152 p.

VITA

Miriam Barquero-Molina attended Colegio Salesiano Santo Angel in Aviles, Asturias (Spain) during her four years of high school education. In 1996 she entered the Universidad de Oviedo in Asturias (Spain). For the academic year 2000-2001 she attended National University of Ireland-Galway as an exchange student in the Department of Geology, under the auspices of the European student-exchange program ERASMUS. She received a Bachelor of Science in Geological Sciences from the Universidad de Oviedo in June, 2001. In September, 2001, she entered the Graduate School at the University of Wisconsin-Madison. She received a Masters of Science in Geology from the University of Wisconsin-Madison in December, 2003. During her graduate work in the Department of Geology and Geophysics at the University of Wisconsin-Madison, her research focused on the geochronology of Pliocene pyroclastic deposits and lava flows from Central and South America. In September, 2004, she entered the Graduate School at The University of Texas at Austin. During her graduate work in the Department of Geological Sciences at The University of Texas at Austin, her research focused on the kinematics of extension and shortening in the Grenville-aged Albany-Fraser Orogen, in southwestern Australia.

Permanent address: C/ Puerto de Leitariegos, n. 12, Corvera de Asturias, C. P. 33470, Principado de Asturias, SPAIN

This manuscript was typed by the author.